University of Adelaide

THE UNIVERSITY of ADELAIDE

Doctoral Thesis

Beryllium oxide (BeO) ceramic fibre-coupled luminescence dosimetry

Alexandre Manuel Caraça Santos

Supervisors:
Dr. Mohammad Mohammadi, A/Prof Shahraam Afshar V.
and Prof Eva Bezak

A thesis submitted in fulfilment of the requirements for the degree of Doctor of Philosophy

in the

School of Physical Sciences
University of Adelaide

January 2016

Declaration of Authorship

I, Alexandre Manuel Caraça Santos, certify that this thesis titled, 'Beryllium oxide (BeO) ceramic fibre-coupled luminescence dosimetry' and the work presented in it are my own. I confirm that:

- I certify that this work contains no material which has been accepted for the award of any other degree or diploma in my name, in any university or other tertiary institution and, to the best of my knowledge and belief, contains no material previously published or written by another person, except where due reference has been made in the text. In addition, I certify that no part of this work will, in the future, be used in a submission in my name, for any other degree or diploma in any university or other tertiary institution without the prior approval of the University of Adelaide and where applicable, any partner institution responsible for the joint-award of this degree.
- I give consent to this copy of my thesis when deposited in the University Library, being made available for loan and photocopying, subject to the provisions of the Copyright Act 1968.
- The author acknowledges that copyright of published works contained within this thesis resides with the copyright holder(s) of those works.
- I also give permission for the digital version of my thesis to be made available on the web, via the University's digital research repository, the Library Search and also through web search engines, unless permission has been granted by the University to restrict access for a period of time.

Signed:

Date:

Publications Contained Within Thesis

Published

P1. Alexandre M. C. Santos, Mohammad Mohammadi and Shahraam Afshar V., Optimal light collection from diffuse sources: application to optical fibre-coupled luminescence dosimetry, *OPTICS EXPRESS*, 22 (4), 2014.

P2. Alexandre M. Caraça Santos, Mohammad Mohammadi, Johan Asp, Tanya M. Monro and Shahraam Afshar V., Characterisation of a real-time fibre-coupled beryllium oxide (BeO) luminescence dosimeter in X-ray beams, *Radiation Measurements* 53-54, 2013.

P3. Alexandre M. Caraça Santos, Mohammad Mohammadi and Shahraam Afshar V., Investigation of a fibre-coupled beryllium oxide (BeO) ceramic luminescence dosimetry system, *Radiation Measurements* 52-58, 2014.

P4. Alexandre M. Caraça Santos, Mohammad Mohammadi and Shahraam Afshar V., Energy dependency of a water-equivalent fibre-coupled beryllium oxide (BeO) dosimetry system, *Radiation Measurements* 1-6, 2015.

P5. Alexandre M. C. Santos, Mohammad Mohammadi and Shahraam Afshar V., Evaluation of a real-time beryllium oxide (BeO) ceramic fibre-coupled luminescence dosimetry system for dose verification of high dose rate brachytherapy, *Medical Physics* 42 (11), 2015.

These publications are included within this thesis. When referred to in the text the reference number is prefixed by a 'P'. For example, the first publication in this list is referred to as [P1].

Grants and Scholarships

- Co-recipient of a small-grant ($10K value) for the construction of a Beyllium oxide (BeO) ceramic fibre-coupled luminescence dosimeter.
- ACPSEM EPSM 2011 Scholarship.

Conference Presentations

- Santos A., Mohammadi M., Asp J., Afshar S., *Beryllium Oxide (BeO) Fibre Optic Dosimeter*, EPSM-ABEC, 2011, Darwin, Australia.
- Santos A., Mohammadi M., Afshar S., *Light Collection Simulations in BeO Fibre Optic Dosimetry*, EPSM-ABEC, 2011, Darwin, Australia.
- Santos A., Mohammadi M., Afshar S., *Optimal Light Collection in BeO Fiber Optic Dosimetry*, CLEO Pacific Rim, 2011, Sydney, Australia.
- Santos A., Mohammadi M., Afshar S., *Fibre optic dosimetry with beryllium oxide (BeO) ceramics*, Radiation, 2012, Sydney, Australia.
- Santos A., Mohammadi M., Afshar S., *Characterisation of an RL/OSL beryllium oxide (BeO) ceramic fibre-coupled luminescence dosimeter in 6MV x-ray beams*, EPSM-ABEC, 2012, Gold Coast, Australia.
- Santos A., Mohammadi M., Afshar S., *A real-time beryllium oxide (BeO) ceramic fibre-coupled luminescence dosimetry system for high dose rate brachytherapy dosimetry*, Australasian Brachytherapy Group Conference, 2014, Adelaide, Australia.
- Santos A., Mohammadi M., Afshar S., *A beryllium oxide (BeO) fibre-coupled luminescence dosimeter for high dose rate brachytherapy*, AAPM Annual Meeting, 2014, Austin, Texas, USA
- Santos A., Mohammadi M., Afshar S., *A near water equivalent beryllium oxide ceramic dosimetry system for high dose rate brachytherapy*, Australasian Brachytherapy Group Conference, 2015, Sydney, New South Wales, Australia

Other Presentations

- Santos A., Mohammadi M., Afshar S., *The optimal light collection in Fiber Optic Dosimetry, The 2010 student paper night*, ACPSEM - Student Night, 2010, Adelaide, Australia
- Santos A., Mohammadi M., Afshar S., *Beryllium Oxide (BeO) Fibre Optic Dosimetry – a versatile in-vivo dosimeter*, ACPSEM - Student Night, 2011, Adelaide, Australia [Second Prize]

- Santos A., Mohammadi M., Afshar S., *A beryllium oxide (BeO) fibre-coupled luminescence dosimeter for high dose rate brachytherapy*, ACPSEM - Student Night, 2014, Adelaide, Australia [First Prize]
- Santos A., Mohammadi M., Afshar S., *A beryllium oxide (BeO) fibre-coupled luminescence dosimeter for high dose rate brachytherapy*, ARPS - Gerald Laurence Student Award, 2014, Adelaide, Australia [Second Prize]

"Se não receio o erro, é porque estou sempre disposto a corrigi-lo."
"If I don't fear the error, it simply is because I'm always willing to amend it."

Bento de Jesus Caraça

Abstract

Brachytherapy treatments are becoming more complex and generally high doses per fractions are prescribed. Therefore there is a need for a real-time dosimeter which is able to accurately verify the dose delivered to a patient during treatment. Beryllium oxide (BeO) ceramics are a near water-equivalent material capable of radioluminescence (RL) and optically stimulated luminescence (OSL). A low energy dependence is expected from BeO ceramics since it has an effective atomic number similar to water. In this thesis the feasibility of using BeO ceramic as the probe for a fibre-coupled luminescence dosimetry system is demonstrated.

In order to maximise the sensitivity of the fibre-coupled luminescence dosimetry system, the light collection from the probe material into the optical fibre was simulated. Since BeO ceramics are self optically attenuating, a range of probe designs were investigated including: a reflective wall surrounding the BeO ceramic and the potential use of another optically transparent layer to provide a less attenuating optical path into the optical fibre. A model was developed using ray tracing through the BeO ceramic until reaching the optical fibre. It was found that for a 1 mm diameter BeO ceramic probe coupled directly to an optical fibre, that there is no increase in light collection beyond 1 mm length of BeO ceramic.

An RL/OSL reader system was developed which could be connected to an optical fibre with a 1 mm diameter, 1 mm long BeO ceramic coupled to the fibres tip. The dosimetry system was capable of real-time dose rate measurements by reading the RL signal, and post exposure accumulated dose measurements by stimulating and integrating the OSL. The dosimetry system was characterised with high energy 6 MV and 18 MV x-ray beams, an ^{192}Ir source, and a range of superficial x-ray beam energies.

The OSL dose response was shown to be supralinear to doses greater than 10 Gy, and independent to dose rate. The RL is shown to be linear to dose rates from 100 cGy/min to 600 cGy/min, and that the integral of the RL responded linearly to doses from 30 cGy to 15 Gy. The RL from BeO ceramics was observed to be insensitive to the accumulated dose, making dose rate measurements easily obtained. Energy dependency measurements showed that there is a different energy response for the OSL and RL signals. The RL shows little energy dependency for x-ray energies above a superficial 50 kVp beam, while the OSL response differs from the RL response for x-ray energies above a superficial 150 kVp beam.

Finally the system was evaluated for use in high dose rate (HDR) brachytherapy applications. The reproducibility, energy dependence, angular dependence and probe temperature dependence were evaluated for an ^{192}Ir HDR source. An overall uncertainty of 7.9% and 10.1% for the RL and OSL, respectively, was estimated.

This work has shown that BeO ceramics have the potential to be a very useful material for dosimetry in radiotherapy. Especially for dosimetry in brachytherapy where its low energy dependency may be of use.

Acknowledgements

I have many people to acknowledge for their contribution and support throughout my PhD experience, both professionally and personally.

First acknowledgements must go to my supervisors, Mohammad Mohammadi, Shahraam Afshar and Eva Bezak. Without your support and guidance this thesis would not have been possible. Thank you Mohammad for taking me on as a student and for always offering your support. Thank you Shahraam for everything; your enthusiasm was always motivating and continually pushed this project forward.

Thanks to Nigel Spooner for all of the early discussions into optically stimulated luminescence and BeO ceramics. Thank you for your help with the preliminary measurements which we performed.

Thanks to Johan Asp for the initial help in getting the experimental measurements setup. Thanks to John Schneider for his help and work in the construction of some of the detector components.

Thank you to all the current and previous, staff and students of the Medical Physics department at the Royal Adelaide Hospital. All of you have had to listen to, debate with and put up with me at different stages of my journey. Thank you to Joshua Moorrees, Mathew Jennings, Daniel Ramm, Thomas Rutten and Michael Douglass. You have all helped me through this project and for that I will always be grateful.

I am highly indebted to Eva Bezak. Her enthusiasm and ability was what made me take interest in Medical Physics so many years ago. Thank you for all your great lectures and guidance. The time and effort that you have put into so many of the students, including myself, is unbelievable. This PhD is thanks to your belief in me, and giving me a chance to pursue my dreams and turn them into a reality.

A special thank you to my work colleague, course coordinator, close friend and mentor Scott Penfold. You have helped and guided me through all stages of my studies and training and I simply could not have done this without you.

A big thank you to all of my friends and family. You have all given me so much support through the years. Thank you to my father Jose and my sister Joanna in Portugal, for their support from afar.

A special thank you to my Mum, Maria. All of the love and support which you have given me always made me believe that I could do anything. This would certainly not be possible without you. A big thank you to my big brother, Tony, who has always been the most important role model in my life. Thank you for all of your support and always being there for me.

To my fiancé, Jessie, thank you for being so supportive and always understanding of my late nights, early mornings and work on the weekends. You gave me the strength to complete this work.

Contents

List of Figures

List of Tables

To my family and my fiance.

Chapter 1

Introduction

In 2010, one in three and one in four Australian men and women respectively, were diagnosed with caner by the age of 75 (Australian Institute of Health and Welfare, 2014). Various methods of treatment are available including surgery, chemotherapy, radiotherapy, immunotherapy and targeted therapies, many of which are often used in conjunction with each other. Approximately 50% of all cancer patients will have radiotherapy during their course of illness (Baskar et al., 2012).

1.1 Radiation therapy

Radiotherapy is the use of radiation in the treatment of a disease. The key of radiotherapy is to deliver the necessary dose to the target volume, while sparing any healthy tissue from damage as much as possible. There are many different types of treatment in radiotherapy which can be classified as external beam radiotherapy and brachytherapy.

1.1.1 External beam radiotherapy

External beam radiotherapy (EBRT) or teletherapy, is where the source of radiation is located a distance from the surface of the patient. EBRT is generally performed using either kilovoltage x-ray units, megavoltage linear accelerators, or cobalt-60 machines.

Though kilovoltage x-ray units may still be useful for the treatment of superficial lesions, they were superseded by Cobalt-60 machines in the 1950s in order to treat deeper targets. In modern radiotherapy centres today, the majority of treatments now utilise either megavoltage x-rays or electrons produced by linear electron accelerators (Mayles et al., 2007).

1.1.2 Brachytherapy

Brachytherapy is where the source of ionising radiation is near or within the treatment volume, this is commonly achieved with the use of radioisotopes. With this therapy, a high radiation dose can be delivered locally to the target with rapid dose fall-off in the surrounding normal tissue. Brachytherapy is separated into three modalities; low dose rate is where the dose rate is between 0.4-2 Gy/hr, medium dose rate is between 2-12 Gy/hr and high dose rate is where the dose rate is greater than 12 Gy/hr (Podgoršak and Agency, 2005).

Some of the most common radioactive sources in brachytherapy are ^{125}I, ^{103}Pd, ^{192}Ir, ^{198}Au, ^{137}Cs, ^{60}Co and ^{90}Sr. Usually gamma rays are used for treatment, but beta rays are sometimes used in situations where the target volume is closer to organs at risk (OAR).

Sources can be loaded into the patient with the use of needles and applicators. There are many different types of applicators for different treatments. Remote afterloading systems are systems which are capable of holding the sources, and then remotely delivering the sources through the applicators. This helps with the radiation protection of the staff, since the radiation will be shielded from them when they are preparing the patient for treatment, and they will be out of the treatment room during loading since there is no need for manual loading.

A recent review investigated the total uncertainties associated with brachytherapy treatments, through all of the patient procedures (Kirisits et al., 2014). These included uncertainties due to:

- Source strength - i.e. uncertainties due to the calibration of the brachytherapy source.
- Treatment planning system - i.e. uncertainties associated with the use of AAPM TG-43 dose calculation formalism (Nath et al., 1995, Rivard et al., 2004).
- Dose delivery - i.e. the accuracy of the source position and dwell times. Also the transit dose of the source which is not accounted for by the treatment planning system.
- Imaging accuracy - i.e. uncertainties resulting from computational limitations and assumptions due to the finite slice thickness.
- Target contouring accuracy - i.e. uncertainties due to inter- and intra-observer variability in target and OAR contouring
- Anatomy changes between dose delivery and post-implant imaging.

By making estimates on uncertainties from literature, and in discussion with experts, they reported on the overall dosimetry uncertainties associated with various treatment sites. In the case of ^{192}Ir HDR brachytherapy they report a typical total dosimetry uncertainty of 8%, 12%, 13%, and 5%, for vaginal cylinder applicator, image-guided cervical cancer, breast balloon applicator and prostate treatments, respectively (Kirisits et al., 2014).

Brachytherapy treatments are becoming more complex and generally high doses per fractions being prescribed. However, brachytherapy still typically involves more manual procedures during catheter/applicator insertion, treatment planning and treatment delivery than does EBRT. Also, treatment delivery verification is less advanced in brachytherapy than in EBRT. Therefore, brachytherapy may be more prone to errors than EBRT (Kertzscher et al., 2014). As a result it is desirable to conduct *in-vivo* dosimetry as a useful final check to the final treatment dose delivered.

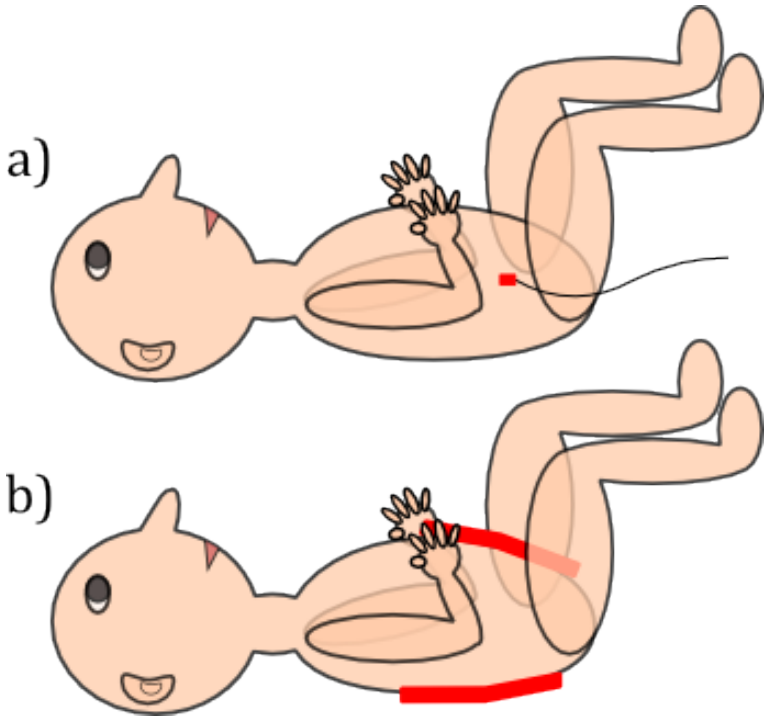

FIGURE 1.1: The two approaches to *in-vivo* dosimetry, either a) where dose measurement is performed from within the patient, or b) where dose measurement is perform on the patient's surface.

1.2 *In-vivo* dosimetry in brachytherapy

In-vivo dosimetry is where a dose measurement is performed during the patient's actual treatment. Due to the various uncertainties associated with the many steps required before and during a patient's treatment, an ultimate check is of use. Especially for specific patient groups and for unusual treatment conditions.

There are two approaches toward *in-vivo* dosimetry either internal dosimetry or surface dosimetry, shown in figure 1.1 (Podgoršak and Agency, 2005). Internal dosimetry is where the dosimetry system is placed inside of the patient, either in the target volume or in one of the critical OAR, shown in figure 1.1 (a). Surface dosimetry is where the dosimetry system in placed on the surface of the patient and records the dose exiting and entering the patient, shown in figure 1.1 (b).

A recent review of *in-vivo* dosimetry in brachytherapy highlighted the need for *in-vivo* dosimetry due to the number of uncertainties and potential errors during brachytherapy

treatments (Tanderup et al., 2013). The energy dependence and small size of the dosimeters were highlighted as key characteristic requirements for an ideal *in-vivo* dosimetry system for brachytherapy compared to dosimeters used in megavoltage EBRT.

The purpose of this section is to provide an overview of the various radiation dosimeters commonly used for *in-vivo* dosimetry in brachytherapy. Here their advantages and disadvantages are discussed.

1.2.1 Point detectors

One-dimensional or point dosimeters make up the majority of detectors which are routinely utilised. A key characteristic to the use of point detectors is that they may be small enough to be inserted within either intraluminal catheters or special applicators inserted into patients.

1.2.1.1 Ionisation chambers

The most routinely utilised dosimetry system in a radiation oncology department, used as a reference dosimeter to calibrate other relative dosimeters. In the case of brachytherapy their use for *in-vivo* dosimetry is limited due to their current sizes not allowing for patient implantation (Ismail et al., 2009). Also the voltage required to operate an ionisation chamber may make implantation difficult.

1.2.1.2 Semiconductor diodes

Semiconductor diodes are commonly used for *in-vivo* dosimetry in brachytherapy and EBRT. Diodes have been shown to provide real-time readout systems, have a high sensitivity and a small size. However, they do require corrections for angular dependence, energy dependence, temperature dependence, dose and dose-rate dependence. One of the major drawbacks of in the use of diodes is that they exhibit changes in response overtime due to radiation damage (Piermattei et al., 1995, Waldhäusl et al., 2005).

Diode detectors have been utilised for *in-vivo* dose verification of gynaecological HDR brachytherapy treatments (Waldhäusl et al., 2005, Alecu and Alecu, 1999). A commercially available diode detector, PTW probe type 9112 (PTW, Germany), consisting of five diodes positioned with 15 mm separation, has routinely be used for rectal dose measurements (Zaman et al., 2014, Seymour et al., 2011, Waldhäusl et al., 2005). An estimate of the overall uncertainty in these systems ranging from 7% to 10% has been reported (Waldhäusl et al., 2005, Seymour et al., 2011).

1.2.1.3 Metal oxide semiconductor field effect transistor (MOSFET)

Similar to diodes, MOSFETs are semiconductors which provide real-time readout systems, have a high sensitivity and a small size. The major drawbacks exhibited by MOSFETs are that they are not energy independent and that they have a limited lifetime due to radiation damage. Various micro-MOSFETs have been commonly utilised for *in-vivo* dose verification due to its small size (Cygler et al., 2006, Qi et al., 2012, Hardcastle et al., 2010, Gambarini et al., 2014, Tenconi et al., 2014).

Recently a new system called RADPOS developed by Best Medical Canada (Ottawa, Canada) couples a micro-MOSFET with a 3D-Guidance medSAFE electromagnetic positioning tracker (Ascension Technology Corporation, Burlington, VT). The system was shown to have a positional accuracy of within 0.5 mm, and an estimated dose uncertainty of 3%. The system was shown to significantly over-respond at depth by approximately 60% at 10 cm depth, hence an energy correction was required. Only integrated dose measurement were reported, making dwell time error detection difficult (Reniers et al., 2012).

1.2.1.4 Diamond detectors

Diamond detectors are capable of real-time readout systems, a small detector size and have a high sensitivity. One of their major advantages are their near water-equivalent composition, and therefore little energy dependence. However, the use of diamond detectors has been limited, primarily due to high cost (Rustgi, 1998).

Lambert et al. (2007) performed a phantom study where they compared a diamond detector, MOSFET, TLD and a scintillation detector. They noted that out of the commercial detectors, that the diamond detector was the most accurate but had a large physical size. While there have been some phantom studies with diamond detectors for dose verification using brachytherapy sources (Rustgi, 1998, Nakano et al., 2003, Lambert et al., 2007), to our knowledge *in-vivo* dose verification in brachytherapy has not yet been reported.

1.2.1.5 Thermoluminescent dosimeters (TLD)

TLDs have been routinely used for *in-vivo* dose verification. This is primarily due to the versatility of the dosimetry system, with TLDs being available in a variety of forms: powder, chips and rods. Therefore these detectors can be easily placed on the surface of patients for skin dose verification, or inserted into special applicators.

TLDs have been available in a variety of different base materials, such as; lithium fluoride (LiF), lithium borate ($Li_2B_4O_7$), magnesium borate (MgB_4O_7), magnesium orthosilicate (Mg_2SiO_4), calcium sulphate ($CaSO_4$), calcium fluoride (CaF_2), beryllium oxide (BeO), and aluminium oxide (Al_2O_3) (McKeever, 1988). Lithium fluoride (LiF) has been the most commonly used, clinically they have been used for dose verification of the skin, urethra and rectum (Toye et al., 2009, Raffi et al., 2010, Kapp et al., 1992, Anagnostopoulos et al., 2003, Brezovich et al., 2000, Das et al., 2007, Gambarini et al., 2012). The uncertainty in the TLDs for skin, urethra and rectum dose measurements has been reported to be 5.6%, 9% and 8%, respectively (Toye et al., 2009, Raffi et al., 2010).

The drawbacks associated with TLDs are they require careful handling, annealing after use, and if using chips or rods then individual calibrations are required. The primary drawback is that they are not capable of real-time information and hence the *in-vivo* dosimetry results are only available some time after exposure (Tanderup et al., 2013).

1.2.1.6 Optically stimulated luminescent dosimeters (OSLD) and radiophotoluminescent glass dosimeters (RPLGD)

OSLDs are similar to TLDs except that they are not stimulated with heat but instead optical light. These detectors are available in a range of size chips and base materials, such as; aluminium oxide (Al_2O_3) and beryllium oxide (BeO). They do still come with the drawback of no real-time capability.

Carbon-doped aluminium oxide (Al_2O_3:C) has certainly been the most commonly utilised OSLD in medical applications, being the only system commercially available for some time (Landauer Inc., USA). The use of BeO is increasing due to it's effective atomic number (Z_{eff}=7.2) being close to that of water (Z_{eff}=7.5). This is an attractive alternative to Al_2O_3:C which has a higher effective atomic number (Z_{eff}=11.3) (Yukihara et al., 2014). Recently, BeO ceramic OSLD dosimetry systems have become available (Dosimetrics, Germany).

RPLGDs use an ultra-violet light source to read the detectors (Hsu et al., 2008). In a phantom study the mean difference between RPLGDs measurements and that calculated for clinical prostate treatment plans was less than 5% (Hsu et al., 2008). These dosimeters have been used for *in-vivo* dosimetry in head and neck and pelvic high dose rate brachytherapy interstitial treatments (Nose et al., 2005, 2008).

1.2.1.7 Alanine/electron paramagnetic resonance dosimetry system

Alanine detectors are capable of small sizes and are not read in a destructive manner, hence any one alanine detector can be read more than once. Alanine detectors are also near water equivalent and have been shown to have little energy dependence (Anton et al., 2015, Waldeland et al., 2010). In a phantom study the uncertainty for measurements inside the urethra was estimated to be 3.6% for prostate treatments (Anton et al., 2009). These detectors have been used for *in-vivo* dose verification in gynaecological LDR brachytherapy treatments (Schultka et al., 2006).

1.2.1.8 Fibre-coupled luminescence dosimetry systems

Organic plastic scintillation detectors are capable of real-time dose rate measurements, have a small size and have been shown to have a linear dose and dose rate response. Plastic scintillation detectors have also be shown to be near water equivalent. One major disadvantage of plastic scintillation detectors is the "stem effect" which produces unwanted light in the system (Beddar et al., 1992a,b).

Plastic scintillation detectors have been used for *in-vivo* dose verification of urethral dose (Suchowerska et al., 2011) and rectal dose (Wootton et al., 2014) in HDR prostate treatments. Recently, a commercial plastic scintillation system designed for *in-vivo* dose verification has been developed called OARtrac (RadiaDyne, LLC., Houston, TX) (Klawikowski et al., 2014).

Carbon-doped aluminium oxide (Al_2O_3:C) crystals have also been investigated for similar fibre-coupled detectors. Though since they are OSL materials, then these detectors have the added advantage of not only have the real-time dose rate measurements from the radioluminescence (RL) signal but they also can be stimulated post exposure for an OSL accumulated dose measurement. The major disadvantages of Al_2O_3:C crystals are that they are not as water equivalent as plastic scintillators and that the RL has been shown to be sensitive to dose, and hence is not constant for a constant dose rate (Andersen et al., 2009a, Kertzscher et al., 2011). Al_2O_3:C dosimetry systems have been used for *in-vivo* dose verification of cervix treatments (Andersen et al., 2009b).

1.2.2 Two dimensional dosimeters

Two dimensional dosimetry systems are an important quality assurance tool in radiation oncology departments. They can provide high resolution dose maps and hence can provide greater information that point detectors.

1.2.2.1 Film

Both radiographic and radiochromic film provide high spatial resolution and a large dynamic range. Radiographic films have the disadvantage of having a high effective atomic number, requiring processing of the film post exposure, and must also be keep in a light-tight package. However, radiochromic film are near water equivalent, are self-processing and can be exposed to visible light for short periods.

Radiochromic films have been shown to be useful for characterising HDR ^{192}Ir sources (Poon et al., 2006, Palmer et al., 2013a, Aldelaijan et al., 2011, Palmer et al., 2013b), and LDR ^{125}I seeds (Chiu-Tsao et al., 1994, 2008). Radiochromic film has been used for *in-vivo* dose verification of vaginal cylinder HDR treatments (Pai et al., 1998). *In-vivo* dosimetry was performed for eight patients with 3-4 fraction treatments, and with the exception of two fractions the film measurements agreed with the calculated dose to within 10% (Pai et al., 1998).

1.2.2.2 Electronic portal imaging devices

Electronic portal imaging devices (EPIDs) have been extensively utilised for patient position verification in EBRT. EPIDs are capable of providing high resolution, real-time 2D dose maps. However, EPIDs have been shown to over-respond to low energy photons and are quite costly (Smith et al., 2013). No use of EPIDs for *in-vivo* dosimetry in brachytherapy has yet been reported.

1.2.2.3 Semiconductor arrays

Two dimensional semiconductor arrays may be a useful tool for pre-treatment dose verification. A 2D 11 x 11 diode array detection system has been developed called "magic phantom" which is capable of accurately measuring the dwell positions and times and compare them directly to the treatment plan. This may one day play a role in determining potential errors in treatment delivery before patient treatment (Espinoza et al., 2015, 2013).

Recently, a new 256 x 1024 pixel silicon detector system has been developed for prostate brachytherapy dose verification, named *BrachyView*. This devise is capable of being inserted into the rectum and taking images of the sources in real-time (Safavi-Naeini et al., 2013).

1.2.3 Three dimensional dosimeters

Fricke gel dosimetry systems are capable of providing 3D dose information. Recently, fricke gel dosimetric catheters (FGDC) have been developed. These have not been used clinically yet, but show promise to being inserted into a patient and providing 3D dose verification information (Gambarini et al., 2010).

A cylindrical (4 mm × 20 mm) *in-vivo* PRESAGE dosimetry system (PRESAGE-IV) has been investigated and shown to be promising. This system is capable of providing a line profile for *in-vivo* dose verification (Vidovic et al., 2014).

1.2.4 Summary

Table 1.1 shows a summary of the characteristics of the small 1D dosimetry systems which have been utilised for *in-vivo* dose verification in brachytherapy. While there are only a couple of commercially available dosimetry systems for the purpose of *in-vivo* dose verification of brachytherapy treatments, there are a large range of dosimetry systems being investigated. Each of these systems have pros and cons to their use.

From the systems which can be placed into an applicator and inserted into a patient, only the diode, MOSFET and fibre-coupled systems can provide real-time online dose information. However, diodes and MOSFETs have been shown to have a high energy and angular dependence, and exhibit changes in response due to radiation damage. Therefore fibre-coupled dosimetry systems show great promise in providing a robust dosimetry system for *in-vivo* dose verification.

TABLE 1.1: Summary of the characteristics of the small 1D dosimetry systems which have been utilised for *in-vivo* dose verification in brachytherapy. Rated as advantageous (✓✓), good (✓), and inconvenient (✗). Based on (Tanderup et al., 2013) with the inclusion of OSLD.

	TLD	OSLD	MOSFET	Diode	Alanine	Fibre systems
Size	✓	✓	✓✓	✓	✓	✓✓
Cables	✓✓	✓✓	✗	✗	✓✓	✗
Sensitivity	✓	✓	✓	✓✓	✗	✓✓
Radiation damage/reuse	✓✓	✓✓	✗	✓	✗	✓✓
Energy dependence	✓	✗	✗	✗	✓	✓✓
Angular dependence	✓✓	✓✓	✓	✗	✓	✓✓
Commercially available	✓✓	✓✓	✓✓	✓✓	✓✓	✓
Online dosimetry	✗	✗	✓	✓✓	✗	✓✓

1.3 Beryllium oxide (BeO) ceramics

BeO ceramics has been known to exhibit both OSL and TL since the 1950's (Albrecht and Mandeville, 1956, Tochilin et al., 1969, Rhyner and Miller, 1970, Scarpa, 1970). Because of its near tissue equivalence, Z_{eff}=7.2, low cost and commercial availability, BeO was an attractive material for passive dosimetry. It was investigated for use in personal dosimetry as a TLD (Busuoli et al., 1977, 1983). From the late 1990's there has been increased interest in the use of the OSL from BeO ceramic for medical dosimetry (Bulur and Göksu, 1998).

The OSL emission spectrum was assumed to be the same as the TL emission, though it has been shown that the OSL emission spectrum of BeO consists of two bands at ≈310 nm and ≈370 nm (Yukihara, 2011). The stimulation spectrum of the OSL signal was thought to be a broad peak ranging from 420 to 550 nm with a maximum near 435 nm, which is temperature independent (Bulur and Göksu, 1998). However, recently it has been shown that the OSL stimulation spectrum shows a continuous increase in OSL intensity with decreasing stimulation wavelength (Yukihara, 2011, Bulur, 2014).

The OSL signal has a linear response to dose over 6 orders of magnitude, from doses less than 5 µGy to 5 Gy (Bulur and Göksu, 1998, Sommer and Henniger, 2006, Sommer et al., 2007, 2008). The OSL from BeO has also been shown to weakly under respond to low energy radiation doses (Sommer and Henniger, 2006, Sommer et al., 2007, Jahn et al., 2013, 2014). Measurements of the fading of the OSL signal for BeO show that there is some short term fading, where 6% of the OSL fades 10 hours after exposure. Whereas the long term fading is negligible, being less than 1% over 6 months (Sommer et al., 2007), similar to that of its TL (Scarpa, 1970).

Other than the continuous wave (CW) OSL method which has been discussed BeO ceramics have also been investigated with a linearly modulated (LM) OSL method and frequency-modulated pulsed OSL. These techniques linearly increase the stimulation light intensity, which allows for the possibility to distinguish the signal resulting from different traps (Bulur et al., 2001b,a, Bulur and Yeltik, 2010).

Recently, the OSL from BeO has also been investigated for its use as a 2D dosimeter, where a sheet of BeO is exposed and read using a point-by-point measurement technique (Sommer et al., 2008, Jahn et al., 2010, 2011).

The RL emission of BeO has had very limited reporting in literature. It has been shown to have an emission peak around 370 nm, and that it may be more intense than that from TLD-500 (Al_2O_3:C) (Erfurt and R. Krbetschek, 2002, Marcazzó et al., 2007).

A review of the properties of various OSL materials noted that BeO ceramics may be a potential alternative to the use of Al_2O_3:C crystals for OSL dosimetry because of it's near water equivalence (Pradhan et al., 2008).

1.4 Motivation and thesis structure

1.4.1 Motivation

From the large range of dosimetry systems discussed in the previous section, fibre-coupled luminescence dosimetry systems have shown great promise to provide a dosimetry system

suitable of *in-vivo* dosimetry verification for brachytherapy treatments. Plastic scintillation detectors have been the first to become commercially available. Their near water equivalence makes them a clear choice for a brachytherapy dosimeter.

As briefly discussed, the stem effect is one major issue for plastic scintillation detectors. This is light produced in the optical fibre when exposed to ionising radiation. One approach around the stem effect issue, has been to use a probe material which is also capable of an OSL reading after exposure. In this method the OSL reading is unaffected by the stem effect since the optical fibre is not being exposed to ionising radiation when the OSL is read.

Al_2O_3:C crystals have been the most commonly investigated OSL material for this approach. However, Al_2O_3:C has a higher effective atomic number compared to water. BeO ceramics are an OSL material which are near water equivalent, and could hence provide a near water equivalent RL and OSL fibre-coupled luminescence dosimeter.

1.4.2 Project objectives

The objective of this work was to investigate the feasibility and development of the first BeO ceramic fibre-coupled luminescence dosimeter. The final goal was to construct and characterise a near water equivalent, real-time dosimeter suitable for *in-vivo* dose verification of HDR brachytherapy treatments.

1.4.3 Thesis outline

This thesis is comprised of the five publications listed on page ii. These publications form a clear structure, such as the modelling and optimisation of the probe design to the construction and characterisation of the BeO ceramic dosimeter.

Chapter 2 contains an overview of fibre-coupled luminescence dosimeters. Research conducted into real-time scintillation and OSL based fibre-coupled luminescence dosimetry systems will be reviewed. The advantages and disadvantages, along with some of the issues faced in the dosimetry systems will be discussed.

Chapter 3 contains the modelling of the light collection from a scintillating probe coupled to an optical fibre. The model allowed for the optimisation of a variety of different probe designs, in order to determine which would provide the best light collection into the system [P1]. An example of the Matlab code developed for one of the probe designs is given in App. A.

Chapter 4 contains details on the development of the first RL fibre-coupled luminescent dosimeter using a BeO ceramic probe, named RL BeO FOD. In addition the characterisation of the RL BeO FOD using a 6 MV x-ray beam and superficial x-rays is discussed. An (Al_2O_3:C) RL probe was also developed for comparison [P2].

Chapter 5 contains details on the development of the first RL/OSL fibre-coupled luminescence dosimeter using a BeO ceramic probe, named RL/OSL BeO FOD. In addition the characterisation of the RL/OSL BeO FOD using a 6 MV x-ray beam is discussed [P3].

Chapter 6 contains details on the energy dependence of the RL/OSL BeO FOD. Details on the absorbed dose energy dependence estimated with use of the Burlin cavity theory is discussed. In addition the experiments involved to evaluate the energy dependence of the RL/OSL BeO FOD using 6 MV and 18 MV high energy x-ray beams, an ^{192}Ir source and various kV x-ray beams from a superficial x-ray unit are discussed [P4]. The Matlab code used to calculated the effective atomic number and Burlin cavity theory is given in App. B.

Chapter 7 contains details on the characterised of the RL/OSL BeO for HDR dose verification using an ^{192}Ir source. The experiments involved to evaluated the RL/OSL BeO FOD response are discussed [P5].

Chapter 8 contains a conclusion and summary of the thesis. A discussion of the future work which would improve the system is also given.

Chapter 2

Fibre-coupled luminescence dosimetry systems

2.1 Introduction

Since the early 1990s fibre-coupled luminescence dosimetry systems have been investigated for their application to medical radiation dosimetry (Beddar et al., 1992a,b). The principles of these dosimeters are to have a phosphor optically coupled to an optical fibre. When exposed to ionising radiation, the phosphor probe emits light via scintillation or RL with an intensity ideally proportional to the dose rate which the probe is exposed to. A portion of the emitted light can then be collected by the optical fibre, and guided to a photosensitive reader commonly located outside of the treatment suite.

Some of these dosimetry systems are based on probe materials which are also capable of OSL. During the probes exposure to ionising radiation, some charge is trapped in defects within the crystalline structure of the probes. After the exposure, this charge can then be stimulated with a light source resulting in light being emitted, known as OSL. Again a portion of this light can be collected by the optical fibre and guided to a reader located outside of the treatment suite. Integration of the measured OSL signal ideally is proportional to the accumulated dose by the probe material.

The purpose of this chapter is to present an overview of fibre-coupled luminescence dosimetry systems. This review mostly focuses of the physical principles of these detectors, the different approaches and probe materials previously reported.

2.2 Theory of optical fibres

Figure 2.1 shows light incident upon an interface dividing two transparent media of different refractive indices, n. The angle of the transmitted ray through the interface is related to the angle of incidence by the Law of Refraction (Snell's Law), shown in Eq 2.1:

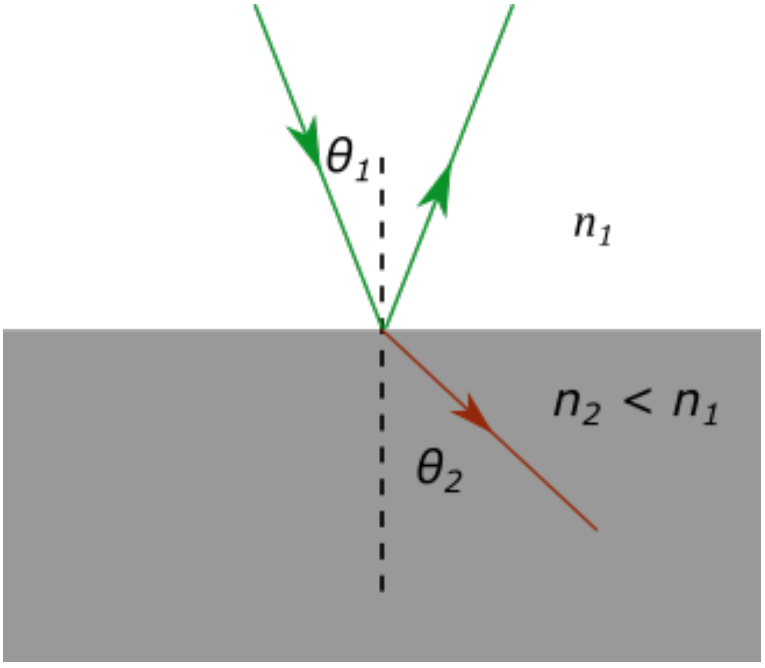

FIGURE 2.1: Light incident on an interface dividing two transparent media of refractive indices n_1 and n_2, with an incident angle θ_1 and transmitted angle θ_2.

Via Snells law:

$$n_1 sin(\theta_1) = n_2 sin(\theta_2). \tag{2.1}$$

Therefore as the incident angle increases, so does the angle of the transmitted light. At a critical angle, θ_c, the angle of the transmitted light reaches 90^o, where θ_c is given by Eq 2.2.

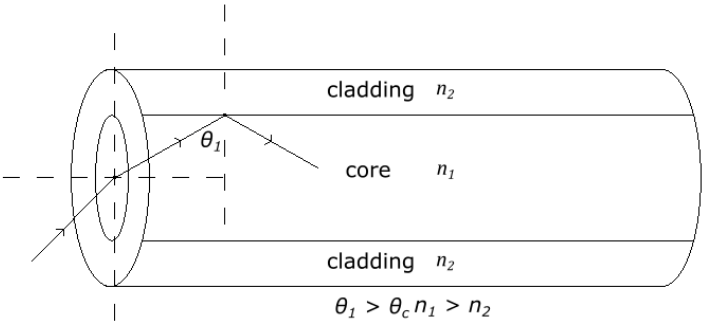

FIGURE 2.2: Total internal reflection of an optical fibre.

$$\theta_c = sin^{-1}(\frac{n_2}{n_1}). \tag{2.2}$$

Hence for any incident angle greater than the critical angle, the light will experience total internal reflection within the optical fibre when $n_1 > n_2$, shown in Figure 2.2.

2.2.1 Stem effect

The "stem effect" is light produced within the optical fibre when exposed to high energy ionising radiation. The stem effect has two contributions, the luminescence from the optical fibre itself and Cerenkov emissions generated in the core of the fibre. Cerenkov radiation has the main contribution to the stem effect and is emitted when a charged particle is travelling faster than the speed of light within the medium.

As a charged particle with velocity v, transverses a medium of refractive index n, such that v is greater than the speed of light in the medium c/n, Cerenkov radiation is emitted. This is due to excited atoms near the particle become polarized, and a part of the excitation energy is emitted as radiation, with an angle Θ to the direction of motion of the particle, given by Eq 2.3:

$$cos(\Theta) = \frac{1}{\beta n}, \tag{2.3}$$

where $\beta = v/c$. The Cerenkov radiation is a continuous spectrum, where the intensity is most intense at lower wavelengths.

The radioluminescence emitted from different optical fibres when exposed to ionising radiation was investigated by (Nowotny, 2007). This is very important since Cerenkov emission within an optical fibre is insignificant for photon energies up to 150 keV, except that the radioluminescence within the fibre may still be of importance. The results of this study showed that polymethyl methacrylate (PMMA) was the best optic fibre for dosimetric applications, generating the lowest amount of light within the fibre.

Many techniques have been investigated for correcting the stem effect from the optical fibres. The first of which was conducted by (Beddar et al., 1992b), where a second (background) optical fibre without any scintillator coupled to it is placed along side the scintillator coupled fibre. This background optical fibre hence measures only the stem effect which is then able to be removed from the scintillator coupled fibre signal. This method has the major drawback that it increases the size of the dosimeter system.

More recently a similar approach using twisted optical fibres was investigated (Liu et al., 2013). In this work the two optical fibres were twisted to form a double helix, such that the two optical fibres are exposed to the same conditions. They reported a maximum stem effect difference between the two optical fibres of 3.59%. This is an improvement on the parallel approach which has been reported to have a stem effect difference between the two optical fibres of up to 25% (Liu et al., 2011).

de Boer et al. (1993) and Clift et al. (2000) investigated the use of a longer-wavelength scintillator such that there is a spectral difference between the scintillator emissions and that of the stem effect from the optical fibre. Optical absorption filters were chosen such that their band pass region was situated directly over the emission of the scintillators spectrum. They were able to show that with the use of optical filters, that the scintillator signal was reduced by 56%, while that of the Cerenkov and fluorescence was reduced by 82%. Therefore successfully removing a significant amount of the stem effect but also removing large portion of the scintillator signal.

A chromatic removal technique has since been developed (Fontbonne et al., 2002, Archambault et al., 2006). This approach takes advantage of the fact that the scintillation and Cerenkov light have different spectra of emission. The dose can then be assessed by measuring the light in the blue (M_{Blue}) and green (M_{Green}) wavelength regions, shown in Eq 2.4:

$$Dose = A \times M_{Green} + B \times M_{Blue}, \tag{2.4}$$

where A and B are calibration factors. This approach has been shown to successfully correct for the stem effect (Archambault et al., 2006).

Clift et al. (2002) investigated the use of a long decay constant plastic scintillator (BC-444G) such that its signal can be time resolved from the Cerenkov radiation signal, for a 16 MeV electron beam. This method utilizes the fact that the linear accelerator emits pulsed radiation, and that the Cerenkov radiation is prompt and short-lived. Hence the scintillator signal can be resolved by choosing the time interval by which to sample the signal to be after the termination of the Cerenkov radiation and before the termination of the longer-living scintillation signal. They were able to show that within this time interval there was a 44% loss of scintillator signal, while a 99% loss of Cerenkov signal, hence successfully correcting for the Cerenkov induced within the fibre. This method has the disadvantage of only being applicable to pulsed radiation and not to brachytherapy where the radiation is continuous.

The stem effect generated in an air-core fibre was investigated by (Lambert et al., 2008, 2010, Liu et al., 2011). The use of an air-core fibre means that no Cerenkov is generated within the optical fibre. This study used a plastic scintillator (Bicron BC400) glued inside of the fibre, and characterised using photon beams of 6 MV and 18 MV and electron beams of 6 MeV and 20 MeV. The air core fibre was only used within the radiation beam. It was coupled to a polymethyl methacrylate (PMMA) fibre which then transports the light outside of the radiotherapy bunker. The dosimeter was successful in measuring the depth dose of the 6 MV and 18 MV photon beams to within 1.6% of ion chamber measurements

and to within 3.6% and 4.5% for the 6 MeV and 20 MeV electron beams, respectively. They were also successful in measuring no stem effect present in the dosimeter.

2.3 Organic plastic scintillators

Plastic scintillators have been extensively investigated for their use in fibre-coupled luminescence dosimetry because of their small size, near tissue equivalence and high sensitivity. The near water equivalence and high sensitivity make the use of plastic scintillators very attractive, but plastic scintillators under respond at low energies (Williamson et al., 1999), also the stem effect produced by the optical fibre makes their use difficult in some situations.

2.3.1 Theory of scintillation

There are two types of light emission, fluorescence and phosphorescence. Fluorescence corresponds to prompt light emission and is temperature independent, whereas phosphorescence corresponds to longer-living light emission and is temperature dependent. A good scintillator should convert as much of the incident radiation energy as possible to fluorescence and as little as possible to phosphorescence (Leroy and Rancoita, 2009).

Plastic scintillators are organic scintillators which has been dissolved in a solvent and then polymerized such that a solid solution is produced. Light emission in organic scintillators is produced by a molecular effect, where excitation of molecular levels in a primary fluorescent material, emits ultra-violet light upon de-excitation. The light signal can then be extracted by introducing a second fluorescent material which is a wavelength shifter and convert the UV light into visible light (Knoll, 2000).

The relation between the emitted light and the energy deposited by the ionising radiation can be non-linear, and is dependent of the type of particle. A relation first suggested by Birk's, assumed that a high ionization density along the track of the particle leads to quenching from damaged molecules and a lowering of the scintillation efficiency (Birks, 1964).

2.3.2 Plastic scintillators use in fibre-coupled luminescence dosimeters

Beddar et al. (1992b,a) first investigated the properties of a plastic scintillator for its use as a fibre-coupled optical dosimeter. The system was investigated for photon and electron beams in the radiotherapy beam energy range. It was found that plastic scintillators are very tissue equivalent such that the energy dependency is better than most commonly used dosimeters, e.g. ionisation chamber, LiF TLDs, film and Si diodes. Plastic scintillators were also shown to not be affected by temperature variations. It was also shown that for an accumulated dose of 10 kGy, the plastic scintillator exhibited a decrease in its response of 2.8%, whereas a photon and electron diode showed a decrease in response of 9% and 25% respectively. Hence the plastic scintillator is much less susceptible to radiation damage than diodes.

Since then plastic scintillators have been applied to various areas of medical radiation dosimetry, such as small field dosimetry (Beddar et al., 2001, Archambault et al., 2007, Klein et al., 2010b, Lambert et al., 2010, Létourneau et al., 1999) and brachytherapy dosimetry (Cartwright et al., 2010, Lambert et al., 2007, 2006, Suchowerska et al., 2011). More recently a multi-point plastic scintillator fibre-coupled system has been developed (Therriault-Proulx et al., 2013, 2012, Archambault et al., 2012). This system is based on the use of multiple plastic scintillators of different emission spectra coupled at various distances along the same optical fibre. This way one optical fibre could be used to measure the dose at various points along its length simultaneously.

Plastic scintillators have however been shown to have a reduced response at low energies. Williamson et al. (1999) investigated the response of plastic scintillators to x-rays of energy 20 keV to 57 keV, as well as photons emitted by ^{99m}Tc, ^{192}Ir and ^{137}Cs sources. It was found that there was a significant decrease in plastic scintillator response for energies below 133 keV, and that the quenching model of Birks and Brooks does not properly account for this decrease in response. To correct for this reduction in response, Cl was loaded into the scintillators and a 4% Cl loading was found to significantly reduce the loss of sensitivity of the plastic scintillator to low-energy photons.

Nowotny and Taubeck (2009) attempted to account for the drop in response of plastic scintillators to low energy photons by incorporating inorganic scintillator powder to the polystyrene-based plastic scintillator. It was found that the optimum inorganic scintillator additive was CaF2:Eu giving the flattest energy response and the lowest temperature dependence.

Lambert et al. (2006) characterised the response of a plastic scintillator fibre-coupled luminescence dosimeter, named *Brachy*FOD for HDR brachytherapy dosimetry using an ^{192}Ir source. An energy dependence measurement using an orthovoltage x-ray beam showed that the response reduced by 100% over a 50–125 kVp energy range. While the *Brachy*FOD was shown to be adequate for dose verification of HDR brachytherapy treatments, the energy dependence may be an issue when considering lower energy brachytherapy sources.

2.4 Inorganic scinillators

Inorganic scintillators such as aliox (Al_2O_3:C) have been widely used in fibre-coupled luminescence dosimeters. The major advantage of the use of these materials are that they have a high sensitivity and hence small size sensitive volumes are possible. Inorganic scintillators may exhibit OSL properties, which is advantageous since the OSL measurements are unaffected by the stem effect from the optical fibres. Hence allowing for the possibility of two dose measurements to be conducted, one via the RL signal measuring the dose rate and the other via OSL measuring the accumulated dose within the crystal. A major drawback has been that inorganic materials tend to not be water-equivalent.

2.4.1 Theory of Radioluminescence

RL is the prompt light emitted by inorganic scintillators when exposed to ionising radiation. The RL process can be explained by considering the available energy levels and transitions of electrons in crystalline insulator and semiconductor materials. Figure 2.3 depicts the RL process when the inorganic scintillator is exposed to ionising radiation.

The dose deposited to the material causes ionisations and excitations, promoting electrons to the conduction band and leaving behind holes in the valence band. The electrons and holes may become trapped at defects in the crystal lattice, or the prompt recombination of the electron and hole pairs may occur. If recombination occurs then optical photons, RL, are emitted (Yukihara and McKeever, 2011).

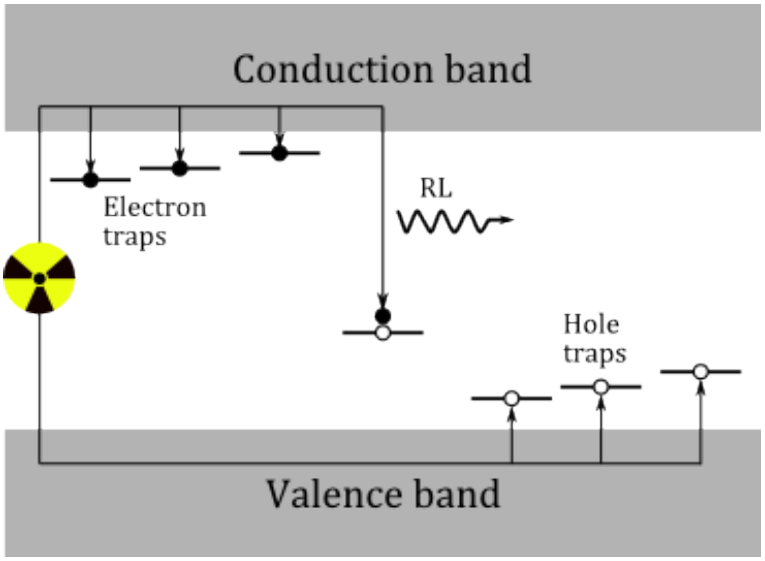

FIGURE 2.3: Depiction of the electron/hole pairs created when exposed to ionising radiation, and the radioluminescence resulting from the recombination of the electron/hole pairs.

2.4.2 Theory of optically stimulated luminescence

To understand how OSL works we need to begin with the energy levels in the crystalline structure of the dosimeter are delocalized energy bands, where we are interested in the valence and conduction bands. Between the valence and conduction bands is a band gap, where only localized energy levels due to defects in the crystalline structure can exist. When the structure is exposed to ionizing radiation, electrons from the valence band can be excited to the conduction band, leaving behind holes in the valence band.

Electrons in the conduction band and holes in the valence band are able to move freely until they recombine (RL) or are trapped in the localized energy levels. This trapped charge provides information about the total accumulated absorbed dose by the crystal. This trapped charge can be released or 'read' via optical light stimulation, which excites

the trapped charge to the conduction band, allowing for electron-hole recombination and luminescence is emitted, known as OSL. These processes are shown in Figure 2.4.

The valence and conduction bands can be represented by three electron traps: shallow traps, dosimetric traps and deep traps. Shallow traps can be exited by room temperatures, while deep traps can capture charges released during the readout stage. The luminescence from the dosimetric traps is what we are interested in for dosimetry (Yukihara and McKeever, 2011, Bøtter-Jensen et al., 2003).

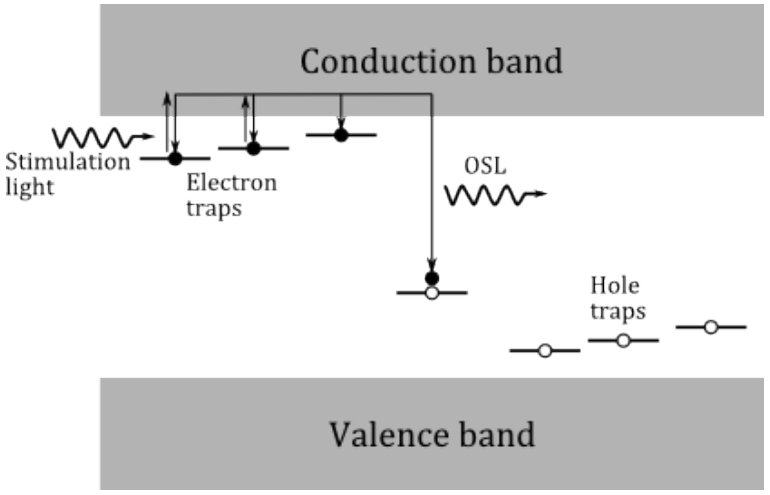

FIGURE 2.4: Electron transitions between the dosimeters energy levels during optical stimulation.

2.4.3 Inorganic scintillators use in fibre-coupled luminescence dosimeters

Various inorganic scintillators have been investigated for use in fibre-coupled luminescence dosimetry systems. One attractive feature that they bring is that two dose measurements are possible via the RL and OSL signals. Therefore when exposed to ionising radiation, a real-time dose rate measurement is possible from the RL signal. After irradiation, a measurement of the accumulated dose within the crystal is possible via OSL stimulated by a laser, shown in Figure 2.5. Unlike the RL measurement, the OSL measurement is unaffected by the stem effect since it is read post exposure.

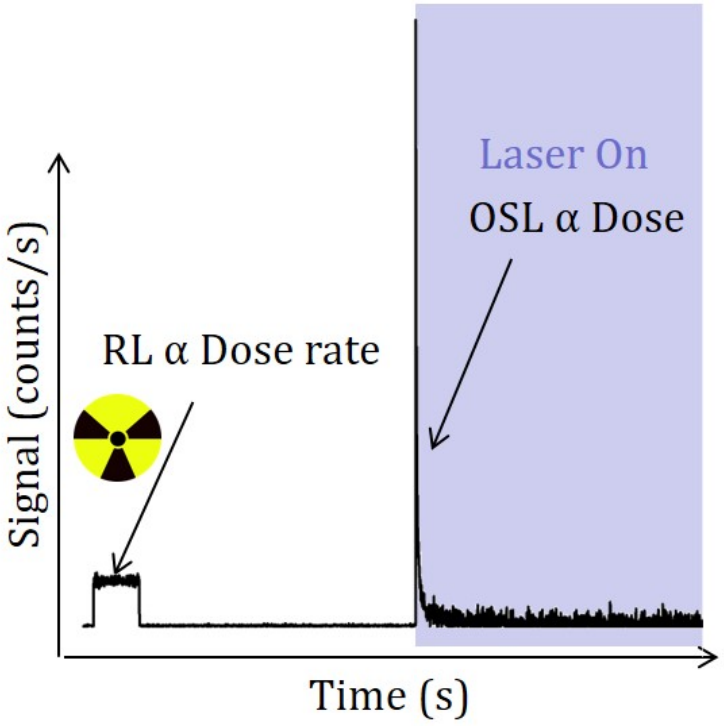

FIGURE 2.5: RL signal measured during irradiation to ionising radiation, after irradiation a laser is used to stimulate crystal allowing for measurements of the OSL signal.

Al_2O_3:C has been a common material studied for RL/OSL based fibre-coupled dosimetry systems. An initial Al_2O_3:C OSL system was presented by (C. Polf et al., 2002, Polf et al., 2004), where a Al_2O_3:C crystals were coupled to the end of a bifurcated fused silica fibre optic cable. Stimulation was provided via a 40 mW Nd:YAG laser coupled to one end of the bifurcated fibre, measurement of the 420 nm emission was conducted via a photomultiplier tube, with two one-half inch thick 420 nm interference filters, at the other end of the bifurcated fibre. OSL measurements were conducted after irradiation and a linear dose response was found from approximately 0.05 Gy to above 100 Gy.

Aznar et al. (2004) and Andersen et al. (2003) reported on what is now the most common RL/OSL reader which uses only one optical fibre. In this set up a green laser (532 nm, 20 mW) is focused through a dichroic color beamsplitter into the optical fibre to stimulate the Al_2O_3:C. The OSL emission is then carried back through the same optical fibre, where it is reflected by the beamsplitter into a PMT. To better remove any of the green laser signal from the OSL signal, a set of filters are placed in front of the PMT.

An analysis of the OSL signal, looking at the effect of pre-dose, background subtraction, bleaching time and integration times was performed by (Edmund et al., 2006). It was found that a pre-dose significantly improved the reproducibility of the integrated OSL, where the necessary pre-dose is different for different crystals. Increasing the integration time of the OSL signal was observed to improve the linearity and reproducibility.

The temperature dependence was investigated by (Marckmann et al., 2006). This is important since the OSL measurements taken from within the patient are compared to a calibration curve taken at room temperature for dose comparison. Various temperatures were investigated from 0 to 45^{0}C, and it was observed that the temperature dependence was significant for integrated times <100 s, but that they were negligible for integrated times >100 s.

A novel approach using multiple probes was investigated by (Magne et al., 2008). A multichannel dosimetry system was developed, where only one detector is read at any one time via the use of an optical switch. The optical switch allows the OSL reader to switch between the optic fibres and read each independently. This approach may be of use in *in-vivo* dosimetry such that many probes can be used.

Andersen et al. (2009b,a) investigated the use of an Al_2O_3:C fibre-coupled dosimeter for *in-vivo* dose verification of pulsed dose rate (PDR) brachytherapy, with a 1 s time resolution. It was reported that there was a good reproducibility of both RL and OSL of 1.3%, and that measured depth doses agreed well with Monte-Carlo simulations for depths of 2-50 mm, suggesting that the energy dependency is less than 6%. A total uncertainty budget of 8% and 5% for the RL and OSL, respectively, was reported.

Ideally the RL signal should be proportional to the dose rate. However, in the case of Al_2O_3:C the RL has been shown to be sensitive to the accumulated dose. Hence for a constant dose rate, the RL signal does not stay constant but increases with the accumulated dose. This is a major drawback since it makes dose rate measurements using the RL difficult. Andersen et al. (2006) showed the significance of the RL dose sensitivity, where for a delivered dose of 1.5 Gy at a constant dose rate of 3 Gy min^{-1} the RL signal was observed to double.

Andersen et al. (2006) and Damkjaer et al. (2008) reported on correction algorithms in order to correct for the RL dose sensitivity. The algorithm was experimentally tested against an ion chamber for a 6 MV photon beam and found that there was a good agreement with ion chamber measurements, with a standard deviation of 2%, including the phantom positioning errors.

In order to overcome the RL dose sensitivity issue, more recently a dose saturation protocol has been developed (Andersen et al., 2011). In this approach the Al_2O_3:C is pre-dosed by ∼20 Gy before use, such that the OSL is saturated. This saturates both the deep and dosimetry traps prior to the measurements and results in the RL becoming constant for a constant dose rate. The RL sensitivity was observed to be -0.45%± 0.03% per 100 Gy. Unfortunately, this approach does result in the OSL being of no use due to saturation.

The energy dependence of a Al_2O_3:C fibre-coupled luminescence dosimeter has been investigated using a mammography unit (Aznar et al., 2005). Due to the effective atomic number of Al_2O_3:C, it was found that there was an 18% increase in the dosimeter's response when the tube potential was increased form 23 kV to 35 kV. This energy dependence is a drawback in the use of Al_2O_3:C, especially when considering low energy brachytherapy sources.

Various other inorganic scintillator materials have been investigated as fibre-coupled luminescence dosimeter probe materials. A Ce^{3+} doped SiO_2 RL fibre-coupled dosimeter has shown promising results (Carrara et al., 2013, 2014b,a, Caretto et al., 2010). Because of the high effective atomic number (Z_{eff}=12.3) an increase in RL response was observed for low energy x-rays (Caretto et al., 2010). Unlike Al_2O_3:C, the Ce^{3+} doped SiO_2 detectors do not have the added OSL dose measurement.

There have been some reports on gallium nitride (GaN) probes used for RL fibre-coupled dosimeters (Pittet et al., 2015, Wang et al., 2014, Ismail et al., 2011). Results have shown a linear dose rate response and high reproducibility. However similar to the Ce^{3+} doped SiO_2 detectors, there is no OSL dose measurement, and the high effective atomic number of GaN results in an over-response to low energy photons (Pittet et al., 2015).

KBr:Eu probe materials have also been reported as OSL only fibre-coupled dosimeters (Klein and McKeever, 2008, Klein et al., 2010a, Gaza and McKeever, 2006). Characterisation of this system is still early but results have shown a linear dose response. Again, the high effective atomic number of KBR:Eu results in an over-response to low energy photons (Klein et al., 2010a). Currently one drawback of this system is that the RL is not used, and hence no real-time dose rate measurements are performed.

Other inorganic materials which have been used in fibre-coupled dosimeters include SrS:Ce,Sm (Benoit et al., 2008b,a) and Y_2O_3:Eu (Molina et al., 2013). However, these systems are still at early stages of development and require further characterisation.

2.5 Summary

The current status of fibre-coupled luminescence dosimetry systems has been reviewed. Plastic scintillators being near water equivalent have been extensively investigated and characterised, and clinically applied to *in-vivo* dosimetry in brachytherapy. However, plastic scintillators are not capable of OSL and have been shown to have a reduced response to low energy x-rays.

Inorganic Al_2O_3:C crystals have similarly been extensively investigated and characterised. The advantage of being capable of OSL measurements provides these systems with the added post exposure accumulated dose measurement which are not affected by the stem effect. However, the RL is sensitive to accumulated dose making dose rate measurements difficult. Also, all of the inorganic scintillators used in fibre-coupled dosimetry systems have a high effective atomic number resulting in an over-response to low energy x-rays.

As discussed in Section 1.3 beryllium oxide (BeO) ceramics are an inorganic material which exhibit both RL and OSL, and have an effective atomic number comparable to that of water. Therefore BeO ceramic may be an energy independent alternative to Al_2O_3:C crystals and will be investigated in this thesis.

Chapter 3

Fibre-coupled luminescence light collection modelling

The publication [P1] forms the basis of this chapter.

Alexandre M. C. Santos, Mohammad Mohammadi and Shahraam Afshar V., Optimal light collection from diffuse sources: application to optical fibre-coupled luminescence dosimetry, *OPTICS EXPRESS*, 22 (4), 2014.

3.1 Introduction and motivation

The light collection from a plastic scintillator into an optical fibre has been investigated previously (Beddar et al., 2003, Elsey et al., 2007), involving transparent plastic scintillator probes. Figure 3.1 shows the different transparencies between BeO ceramic, Al_2O_3:C and plastic scintillators. Therefore when considering the light collection from a BeO ceramic probe, the self optical attenuation must be accounted for.

In this chapter, simulation of the light collection from a diffuse source into an optical fibre will be discussed. The model which was developed, ray traces skew and meridional rays through a scintillating probe to an optical fibre for various designs of scintillating probes. This approach allows the optical attenuation of the material to be accounted for.

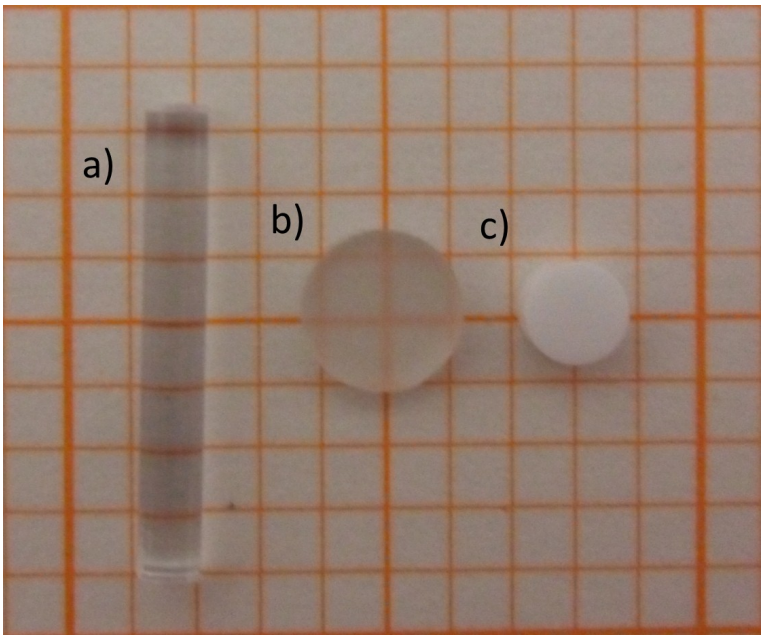

FIGURE 3.1: A depicting of the differences in transparency between (a) Plastic scintillator, (b) Al_2O_3:C and (c) BeO ceramic

3.2 Statement of Contribution

3.2.1 Conception

The idea to develop a model for the light collection from a scintillating probe into an optical fibre was first conceptualised by Shahraam Afshar V. The method by which to achieve this, and also the probe designs to investigate were conceptualised by Alexandre M. Caraça Santos and Shahraam Afshar V.

3.2.2 Realisation

The theory was developed by Alexandre M. Caraça Santos. The model was then checked by Shahraam Afshar V. Matlab coding of the model was performed by Alexandre M. Caraça Santos. An example of the Matlab code used for the more complicated cladding coupled design is given in App. A.

3.2.3 Documentation

This paper was primarily written by Alexandre M. Caraça Santos. Editing was performed by all authors.

Statement of Authorship

Title of Paper	Optimal light collection from diffuse sources: application to optical fibre-coupled luminescence dosimetry
Publication Status	☑ Published ☐ Accepted for Publication ☐ Submitted for Publication ☐ Publication Style
Publication Details	Alexandre M. C. Santos, Mohammad Mohammadi and Shahraam Afshar V., Optimal light collection from diffuse sources: application to optical fibre-coupled luminescence dosimetry, OPTICS EXPRESS, 22 (4), 2014.

Principal Author

Name of Principal Author (Candidate)	Alexandre Santos
Contribution to the Paper	Developed the entire model in Matlab and performed all of the validation experiments. Wrote the manuscript and acted as corresponding author.
Overall percentage (%)	85%
Signature	Date 12/1/2016

Co-Author Contributions

By signing the Statement of Authorship, each author certifies that:

i. the candidate's stated contribution to the publication is accurate (as detailed above);

ii. permission is granted for the candidate in include the publication in the thesis; and

iii. the sum of all co-author contributions is equal to 100% less the candidate's stated contribution.

Name of Co-Author	Mohammad Mohammadi
Contribution to the Paper	Supervised development of work and manuscript evaluation.
Signature	Date 12/01/2016

Name of Co-Author	Shahraam Afshar V.
Contribution to the Paper	Supervised development of work, helped in data interpretation and manuscript evaluation.
Signature	Date 6/01/2016.

Optimal light collection from diffuse sources: application to optical fibre-coupled luminescence dosimetry

Alexandre M. C. Santos,[1,2,*] Mohammad Mohammadi,[2] and Shahraam Afshar V.[1]

[1]*Institute for Photonics and Advanced Sensing and School of Chemistry and Physics, University of Adelaide, Australia*

[2]*Department of Medical Physics, Royal Adelaide Hospital, Australia*

[*]*alexandre.santos@adelaide.edu.au*

Abstract: A model is developed to evaluate the light collection of a diffuse light source located at the tip of an optical fibre. The model is confirmed experimentally and used to evaluate and compare the light collection efficiency of different fibre-coupled luminescence dosimeter probe designs. The model includes contributions from both meridional and skew rays, and considers the light collection from an optically attenuating scintillator. Hence the model enables the optimisation of different, but useful and new probe materials such as BeO ceramic. Four different dosimeter architectures are considered, including previously investigated probe designs; the butt-coupled and reflective wall, along with two novel designs. The novel designs utilise a combination of the scintillating material and transparent media to increase the light collection. Simulations indicate that the novel probes are more efficient in light collection for applications in which it is necessary to minimise the volume of the scintillating material.

OCIS codes: (040.0040) Detectors; (280.4788) Optical sensing and sensors; (260.3800) Luminescence.

References and links

1. S. Afshar V., S. C. Warren-Smith, and T. M. Monro, "Enhancement of fluorescence-based sensing using microstructured optical fibres," Opt. Express **15**(26), 17891–17901 (2007).
2. S. C. Warren-Smith, S. Afshar, and T. M. Monro, "Fluorescence-based sensing with optical nanowires: a generalized model and experimental validation," Opt. Express **18**(9), 9474–9485 (2010).
3. M. Jianjun and W. J. Bock, "Addressing factors affecting fluorescent signal collection of a multimode photonic crystal fiber fluorometer," IEEE Trans. Instrum. Meas. **57**(12), 2813–2818 (2008).
4. U. Utzinger and R. R. Richards-Kortum, "Fiber optic probes for biomedical optical spectroscopy," J. Biomed. Opt. **8**(1), 121–147 (2003).
5. A. S. Beddar, T. R. Mackie, and F. H. Attix, "Water-equivalent plastic scintillation detectors for high-energy beam dosimetry: I. Physical characteristics and theoretical consideration," Phys. Med. Biol. **37**(10), 1883–1900 (1992).
6. A. S. Beddar, T. R. Mackie, and F. H. Attix, "Water-equivalent plastic scintillation detectors for high-energy beam dosimetry: II. Properties and measurements," Phys. Med. Biol. **37**(10), 1901–1913 (1992).
7. N. Suchowerska, J. Lambert, T. Nakano, S. Law, J. Elsey, and D. R. McKenzie, "A fibre optic dosimeter customised for brachytherapy," Radiat. Meas. **42**(4–5), 929–932 (2007).
8. C. E. Andersen, S. K. Nielsen, S. Greilich, J. Helt-Hansen, J. C. Lindegaard, and K. Tanderup, "Characterization of a fiber-coupled Al_2O_3:C luminescence dosimetry system for online in vivo dose verification during 192Ir brachytherapy," Med. Phys. **36**(3), 708–718 (2009).
9. C. E. Andersen, S. K. Nielsen, J. C. Lindegaard, and K. Tanderup, "Time-resolved in vivo luminescence dosimetry for online error detection in pulsed dose-rate brachytherapy," Med. Phys. **36**(11), 5033–5043 (2009).
10. J. Lambert, D. R. McKenzie, S. Law, J. Elsey, and N. Suchowerska, "A plastic scintillation dosimeter for high dose rate brachytherapy," Phys. Med. Biol. **51**(21), 5505–5516 (2006).
11. J. Lambert, Y. Yin, D. R. McKenzie, S. H. Law, A. Ralston, and N. Suchowerska, "A prototype scintillation dosimeter customized for small and dynamic megavoltage radiation fields," Phys. Med. Biol. **55**(4), 1115–1126 (2010).

#201721 - $15.00 USD Received 21 Nov 2013; revised 22 Jan 2014; accepted 22 Jan 2014; published 20 Feb 2014

12. A. F. Fernandez, B. Brichard, S. O'Keeffe, C. Fitzpatrick, E. Lewis, J. R. Vaille, L. Dusseau, D. A. Jackson, F. Ravotti, M. Glaser, and H. El-Rabii, "Real-time fibre optic radiation dosimeters for nuclear environment monitoring around thermonuclear reactors," Fusion Eng. Des. **83**(1), 50–59 (2008).
13. A. S. Beddar, N. Suchowerska, and S. H. Law, "Plastic scintillation dosimetry for radiation therapy: minimizing capture of Cerenkov radiation noise," Phys. Med. Biol. **49**(5), 783–790 (2004).
14. A. S. Beddar, S. Law, N. Suchowerska, and T. R. Mackie, "Plastic scintillation dosimetry: optimization of light collection efficiency," Phys. Med. Biol. **48**(9), 1141–1152 (2003).
15. J. Elsey, D. R. McKenzie, J. Lambert, N. Suchowerska, S. L. Law, and S. C. Fleming, "Optimal coupling of light from a cylindrical scintillator into an optical fiber," Appl. Opt. **46**(3), 397–404 (2007).
16. L. Lembo, M. Pimpinella, and B. Mukherjee, "Self optical attenuation coefficient of TL glow in BeO detectors," Radiat. Prot. Dosimetry **33**, 43–45 (1990).
17. A. M. C. Santos, M. Mohammadi, J. Asp, T. M. Monro, and S. Afshar V, "Characterisation of a real-time fibre-coupled beryllium oxide (BeO) luminescence dosimeter in X-ray beams," Radiat. Meas. **53–54**, 1–7 (2013).
18. A. W. Snyder and J. D. Love, *Optical Waveguide Theory* (Chapman and Hall, 1983).
19. A. Snyder, "Leaky-ray theory of optical waveguides of circular cross section," Appl. Phys. A Mater. **4**, 273–298 (1974).

1. Introduction

Collection of the emission of point sources at the tip of an optical fibre is conceptually important since it can be employed in various applications, such as fluorescence-based sensing [1, 2], fluorometers [3], chemical and biological optical spectroscopy [4], and radiation detection and dosimetry [5–12]. Thus it is important to identify the parameter regime for optimum collection of light emitted by point sources.

Optical fibre-coupled luminescence dosimetry has been an increasingly investigated topic due to its attractive attributes for dosimetry in radiation oncology [5–11] and in the general detection of ionising radiation [12]. In general, this is where a phosphor probe is attached to an optical fibre. When exposed to ionising radiation, light is emitted from the probe, known as radioluminescence (RL) or scintillation. A portion of this light can then be collected by the optical fibre and guided to a reader [5]. Plastic scintillators have been the most common probe material. Another branch of fibre-coupled luminescence dosimetry has been the use of a light source to stimulate charges stored in some probes due to the exposure to ionising radiation. Upon stimulation of the stored or trapped charges, light is emitted. This process is known as optically stimulated luminescence (OSL). In fibre-coupled luminescence dosimetry a portion of the OSL can be collected by the optical fibre [8, 9]. Among available detectors, Al_2O_3:C crystals have been the most common probes for OSL. Both RL and OSL have been shown to be able to potentially satisfy the need for a small and sensitive dosimeter in radiation oncology for such applications as the dosimetry of small field sizes [11] and *in-vivo* brachytherapy dose verification [7–10].

Optimisation of the light collection, either RL or OSL, by the optical fibre is of great importance in fibre-coupled luminescence dosimetry in order to increase the sensitivity of the dosimeter. A very important phenomenon in fibre-coupled luminescence dosimetry is the "stem effect", which is the term given for light produced within the optical fibre when it is exposed to ionising radiation. This produces unwanted signal in the reader, hence reducing the signal-to-noise ratio [13]. Therefore, increasing the light collected from the phosphor probe reduces the effect of the stem effect.

The light collection of optically transparent, plastic scintillator coupled fibre optic dosimeters has been modelled for a number of designs using ray optics [14, 15]. Modelling of the light coupled from a cylindrical scintillator into an optical fibre has shown that the addition of reflections from the scintillator wall improves the light collection from a butt-coupled geometry. The use of a reflective coating on the end face of the scintillator effectively doubles the length of the scintillator. The use of optical elements such as lens between the scintillator and optical fibre can also improve the performance, though in some cases the improvement is marginal [15].

The purpose of this study is to investigate the light collection of different phosphor probe designs, for an optically attenuating phosphor, in order to maximise the light collection for a

#201721 - $15.00 USD Received 21 Nov 2013; revised 22 Jan 2014; accepted 22 Jan 2014; published 20 Feb 2014

given probe design. The light collection is modelled by the use of ray tracing. We include skew rays in the model since they make up the majority of rays in an optical fibre. Also by explicitly including the attenuation of phosphor probes in our models, we have investigated the collection efficiency of different probe designs in the presence of optically attenuating scintillating materials such as beryllium oxide (BeO) ceramics [16]. Recently BeO ceramics have been investigated for their use in fibre-coupled luminescence dosimetry because of their attractive properties; near tissue equivalence, exhibiting RL and OSL [17].

2. Theory

The theory for the light collection modelling was developed by the consideration of multimode optical fibres with comparatively large cores. Hence a ray optics approach is valid and used in the modelling of the light collection from the different probes. Rays in a multimode fibre are either meridional or skew. Meridional rays, depicted in Fig. 1(a) pass through the optical axis after every reflection from the core-cladding boundary, whereas skew rays, depicted in Fig. 1(b) spiral down the fibre, never passing through the optical axis. Meridional rays are defined by a single angle, the longitudinal propagation angle, ϕ_z, which is the angle between the ray and the fibre optical axis. Skew rays are defined by two angles; similarly to meridional rays, the longitudinal propagation angle, ϕ_z, and the azimuthal propagation angle, ϕ_{az} [18]. This is the angle that the projection of the ray onto the fibre cross section, makes with the tangent to the fibre core at the point of incidence. The total angle of incidence for a skew ray, α, depicted in Fig. 1(c) is given by $\cos\alpha = \sin\phi_z \sin\phi_{az}$.

The rays in a multimode fibre can be categorized into; bound, refracting and tunnelling. Bound rays are able to propagate in the core of the fibre and are dependent on the longitudinal propagation angle, ϕ_z. These are confined within the critical angle, φ_c, defined by $\cos\varphi_c = n_{cl}/n_{co}$. The range of longitudinal propagation angles for which the rays are bound is hence given by; $0 \leq \phi_z \leq \phi_c$.

Refracting rays, unlike bound rays, are lost at the core-cladding boundary. They are defined on their total incidence angle, α, with ranges: $0 \leq \alpha < \alpha_c$. Where α_c, the critical incident angle is defined by $\sin\alpha_c = n_{cl}/n_{co}$.

Tunnelling rays are skew rays which are not bound rays but are still able to propagate significant distances along a fibre. Their longitudinal propagation and total incident angles are confined within the ranges given by $\phi_c \leq \phi_z \leq \pi/2$ and $\alpha_c \leq \alpha \leq \pi/2$. Whereas Tunnelling rays are due to the curvature of the optical fibre, and thus as an example a slab waveguide would not have tunnelling rays [19].

#201721 - $15.00 USD Received 21 Nov 2013; revised 22 Jan 2014; accepted 22 Jan 2014; published 20 Feb 2014

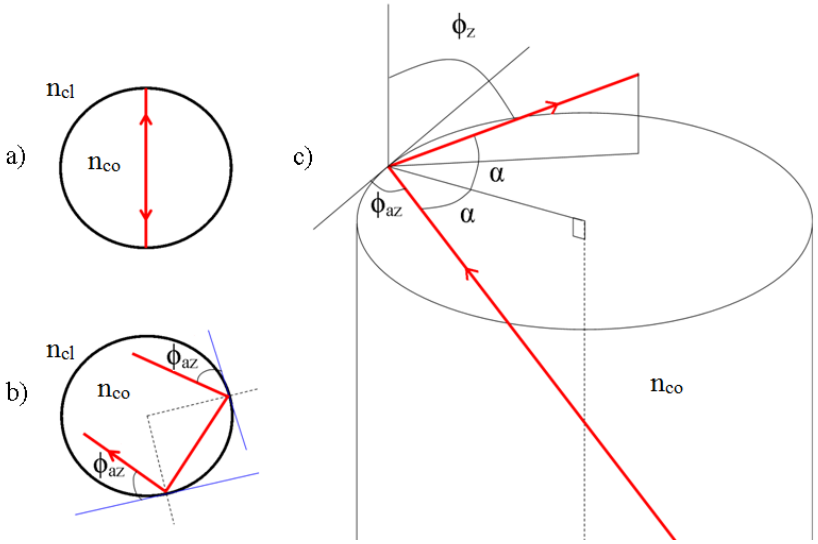

Fig. 1. Ray paths within a step-index fibre of core refractive index, n_{co}, and cladding refractive index, n_{cl}, a) a meridional ray and b) a skew ray showing the azimuthal angle, ϕ_{az}, and c) a skew ray showing all angles including the total angle of incidence, α.

In the current model, the scintillator is treated as many point sources. Due to the symmetry of the cylindrical scintillators, any source point of the same distance from the optical fibre and the optical axis will contain identical light collection properties. Therefore an entire annulus of points with the same distance from the optical fibre and the optical axis, can simply be modelled by a single point, as depicted in Fig. 2.

The parameter t, R_1 and R_2 shown in Fig. 2(a), determine the resolution of the number of diffuse source points modelled. The total power of either bound, refracted or tunnelling rays is given by Eq. (1):

$$P_b=\sum_i^{N_b}\frac{I_i}{N_b}\Omega_b V,\quad P_r=\sum_i^{N_r}\frac{I_i}{N_r}\Omega_r V,\quad P_t=\sum_i^{N_t}\frac{I_i}{N_t}\Omega_t V, \tag{1}$$

Where I_i, is the intensity of the i^{th} ray. N_b, N_r, and N_t are the total number of bound, refracting and tunnelling rays respectively. V is the volume of the annulus of which the source point represents, and is given by:

$$V=\pi t\left(R_2^2-R_1^2\right). \tag{2}$$

Here, Ω_b, Ω_r, and Ω_t are the solid angles produced by the bound, refracting and tunnelling rays, respectively. They are determined by the fraction of each class of rays from the total rays modelled, given by Eq. (3).

$$\Omega_b=2\pi\frac{N_b}{N_s},\Omega_r=2\pi\frac{N_r}{N_s},\Omega_t=2\pi\frac{N_t}{N_s}, \tag{3}$$

where N_s is the total number of rays modelled.

Therefore the total power of a slice of the scintillator is calculated by the summation of all annuli of the same distance from the optical fibre.

#201721 - $15.00 USD Received 21 Nov 2013; revised 22 Jan 2014; accepted 22 Jan 2014; published 20 Feb 2014

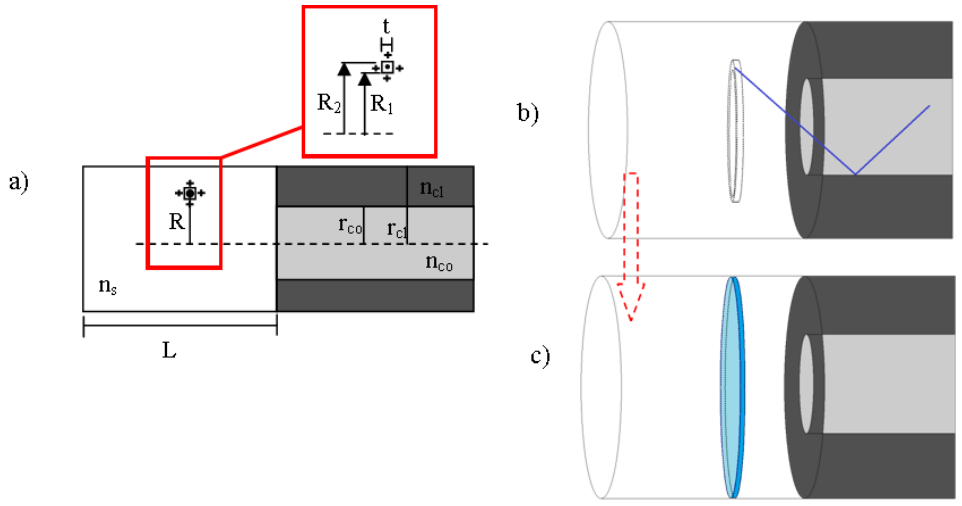

Fig. 2. Due to the symmetry of the system, a) the light collection by a point source, represents an area between the other modelled point sources, where the parameters t, R_1 and R_2 are defined by the number of point sources modelled and hence the pixel size, b) where the light collection of each point source represents an annulus, c) the summation of all the represents a slice of the scintillator.

Figure 3 shows the probe arrangements investigated here. The butt-coupled and reflective wall configurations, shown in Figs. 3(a) and 3(b) respectively, have been previously investigated for transparent plastic scintillators but without considering skew rays [15]. Two novel arrangements are modelled here; named double-cladding and cladding-coupled, shown in Figs. 3(c) and 3(d) respectively. These novel designs utilise a combination of the scintillating material and a transparent media to increase the light collection.

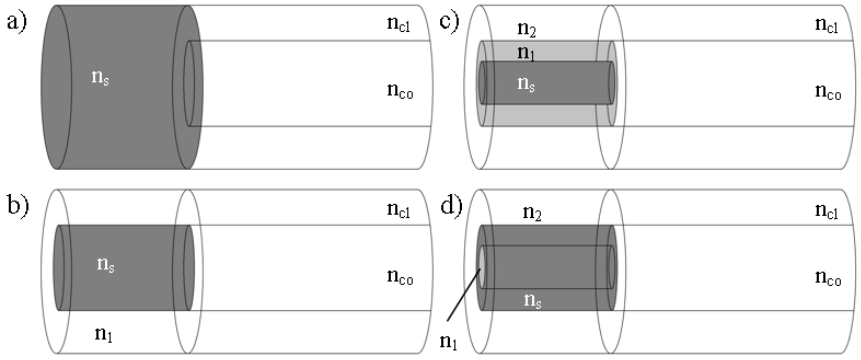

Fig. 3. The BeO probe arrangements a) butt-coupled, b) reflective wall, c) cladding-coupled and d) double-cladding. The dark grey shaded region is the scintillating material and the lower refractive index layer, shaded in a light grey.

2.1 Butt-coupled

The butt-coupled design shown in Fig. 3(a), is where a cylindrical scintillator is simply coupled directly to the optical fibre. In modelling the light collection from the butt-coupled architecture, only rays which are directly incident on the optical fibre core can be collected. All longitudinal propagation angles within the range; $0 \leq \phi_z \leq \pi/2$ are modelled, along with the cross sectional angle, ϕ_a , depicted in Fig. 4, with range; $0 \leq \phi_a \leq \pi$. This will model all forward propagating rays towards the optical fibre. All backward propagating rays are not modelled since they will not be incident on the optical fibre. With these two angles, the Cartesian

#201721 - $15.00 USD Received 21 Nov 2013; revised 22 Jan 2014; accepted 22 Jan 2014; published 20 Feb 2014

coordinates of the ray path can now be described by Eqs. (4)–(6), where r is the ray path length.

$$x = r\cos\phi_a \sin\phi_z, \tag{4}$$

$$y = r\sin\phi_a \sin\phi_z, \tag{5}$$

$$z = r\cos\phi_z. \tag{6}$$

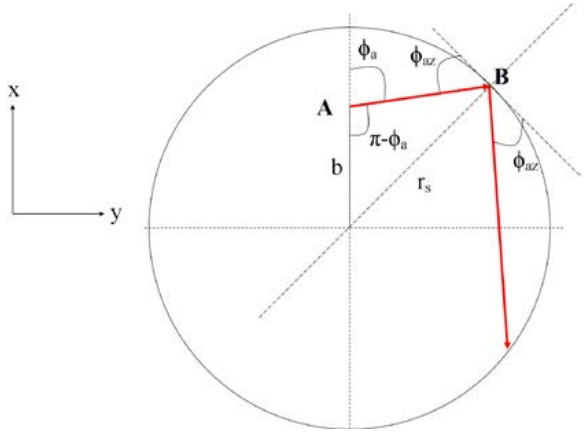

Fig. 4. A cross-section of the scintillator depicting the azimuthal angle, ϕ_{az}, the simulated cross sectional angle utilized in model, ϕ_a. Where b is the distance of the emitting source at point A from the optical axis, point B is the project of the ray onto the scintillator of radius r_s.

The azimuthal angle, ϕ_{az}, can be calculated from the modelled cross sectional angle, ϕ_a, shown in Fig. 4, where b is the distance of the emitting source at point A from the optical axis, and r_s is the radius of the scintillator, by using the sine rule:

$$\frac{\sin\left(\frac{\pi}{2}-\phi_{az}\right)}{b} = \frac{\sin(\pi-\phi_a)}{r_s}. \tag{7}$$

Hence

$$\phi_{az} = \frac{\pi}{2} - \sin^{-1}\left\{\frac{b}{r_s}\sin[\pi-\phi_a]\right\}. \tag{8}$$

The total incidence angle can hence be calculated. Rays incident on the core of the optical axis can be determined by using the ray path Eqs. (4)–(6), those rays not incident on the core of the fibre can be rejected since they will not contribute to collected light. The rays can then be characterised as following:

(1) If $\phi_z < \phi_m$ then the ray is a bound ray within the optical fibre. ϕ_m is the maximum acceptance angle of the fibre, determined from the complement of the critical angle of the fibre and given by Eq. (9).

$$\phi_m = \sin^{-1}\left\{\frac{1}{n_s}\sqrt{n_{co}^2 - n_{cl}^2}\right\}. \tag{9}$$

(2) If $\alpha_c < \alpha_m$ then the ray is a refracted ray in the optical fibre. α_m is the maximum total incidence angle, determined from the critical angle and given by Eq. (10).

#201721 - $15.00 USD Received 21 Nov 2013; revised 22 Jan 2014; accepted 22 Jan 2014; published 20 Feb 2014

$$\alpha_m = \cos^{-1}\left\{\frac{1}{n_s}\sqrt{n_{co}^2 - n_{cl}^2}\right\}. \quad (10)$$

(3) Any other ray which is not either bound or refracting is thus a tunnelling ray within the optical fibre.

Any optical attenuation of the ray can then be applied to the intensity collected as follows:

$$I = I_0 e^{-\mu r}, \quad (11)$$

where μ is the optical attenuation coefficient and r is the path length travelled within the scintillator.

2.2 Reflective wall

In the case of the reflective wall design shown in Fig. 3(b), a reflective interface surrounds the scintillator, produced by a lower refractive index medium, n_1. For the modelling of the reflective wall architecture, there are two possibilities for rays to be incident on the core of the optical fibre.

(1) Rays directly incident on the optical fibre core, which are modelled in the same way as for the butt-coupled design.

(2) Rays reflected off the wall of the scintillator.

In tracing the rays after reflection after incidence on a reflective interface, as long as $r_s \leq r_{co}$ all rays reflected off the scintillator wall will be incident on the fibre core. For the purpose of increasing the light collection, this is optimal. Since the propagation properties of the ray, i.e. the longitudinal propagation angle and azimuthal angle do not change after multiple reflections, then all rays that satisfy the condition that their propagation angle, ϕ_z, is less than the complement of the critical angle, ϕ_c, of the n_s, n_1 interface, given by Eq. (12), will be incident of the fibre core.

$$\phi_z < \phi_c. \quad (12)$$

Here the complement of the critical angle, ϕ_c, is given by Eq. (13).

$$\phi_c = \sqrt{1 - \left(\frac{n_1}{n_s}\right)^2}. \quad (13)$$

For proper ray tracing through the probe, the ray path equations are used, previously discussed in Eqs. (4)–(6). Once a ray is incident upon the scintillator wall, it will incur a reflection which will rotate the modelled cross-sectional angle, given in Eq. (14).

$$\phi_c' = \phi_c + 2\phi_{az}. \quad (14)$$

2.3 Double-cladding

The double-cladding design shown in Fig. 3(c), consists of a scintillator surrounded by a lower refractive index, transparent layer, n_1, which itself is surrounded by a reflective layer, n_2. Hence $n_2 < n_1 < n_s$, where the purpose of this probe design is for when the scintillating material is optically attenuating, an optically transparent layer surrounding the scintillator may significantly increase the light collection.

For modelling the double-cladding design, the following are the possibilities for ray incidence on the fibre core;

#201721 - $15.00 USD Received 21 Nov 2013; revised 22 Jan 2014; accepted 22 Jan 2014; published 20 Feb 2014

(1) Rays directly incident on the optical fibre core, which are modelled in the same way as for the butt-coupled design.

(2) Rays reflected off the wall of the scintillator, at the n_s, n_1 interface, modelled in the same way as for the reflective wall design.

(3) Rays incident on the fibre core after refraction into n_1.

Once rays are refracted in n_1 there are many scenarios which can occur on fibre core incidence, i.e.

(1) Reflections off n_2, n_1 interface.

(2) Further refractions into the scintillator, n_s.

This results in two possibilities for incidence; either via the scintillator, n_s, or via the optically transparent layer, n_1. If the scintillator has a higher refractive index then the transparent layer, refraction will result in a smaller propagation angle in the transparent layer, ϕ_{r1}, then the initial propagation angle, ϕ_i, in the scintillator. Hence with some optimisation there could be a significant increase in light collection with an appropriate choice of n_1. This is depicted in 2D in Fig. 5, where via n_1 a lower propagation angle is incident on the fibre core, due to the refraction into n_1. With a closely matched lower refractive index, n_1, and fibre core refractive index, then effectively a larger acceptance angle of rays incident from n_1 is obtained.

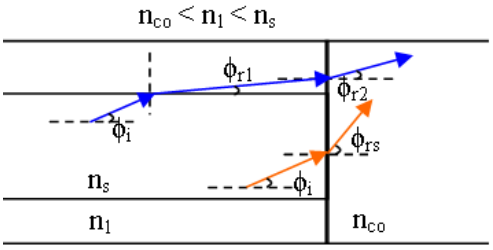

Fig. 5. The benefit of the use of a lower refractive index surrounding the scintillator, for identical rays with longitudinal propagation angles, φ_i, there is a smaller longitudinal propagation angle for rays incident from n_1 than from n_s, hence $\varphi_{r2} < \varphi_{rs}$.

In modelling the double-cladding design, rays directly incident on the fibre core, or via reflections off the n_1, n_s interface have been previously discussed in the butt-coupled and reflective wall probes. If rays are incident upon the n_1, n_s interface and the total incidence angle of the ray is less that the critical angle, α_c, given in Eq. (15), then the ray will be refracted into n_1.

$$\alpha_c = \sin^{-1}\left\{\frac{n_1}{n_s}\right\}. \tag{15}$$

The ray invariants, given in Eqs. (16)–(18), are solved to calculate the properties of the ray after each refraction and reflection. These are based on the fact that the longitudinal propagation angle and azimuthal angle are constant along a particular ray path.

$$\bar{\beta} = n\cos\phi_z, \tag{16}$$

$$\bar{1} = n\sin\phi_z\cos\phi_{az}, \tag{17}$$

$$\bar{\beta}^2 + \bar{1}^2 = n^2\sin^2\alpha. \tag{18}$$

#201721 - $15.00 USD Received 21 Nov 2013; revised 22 Jan 2014; accepted 22 Jan 2014; published 20 Feb 2014

Therefore rearranging the ray invariants, the longitudinal propagation angle, azimuthal angle and total incidence angle after refraction, ϕ_z', ϕ_{az}', α' respectively, can be calculated, given in Eqs. (19)–(21).

$$\phi_z' = \cos^{-1}\left\{\frac{n_s}{n_1}\cos\phi_z\right\}, \tag{19}$$

$$\phi_{az}' = \cos^{-1}\left\{\frac{n_s \sin\phi_z}{n_1 \sin\phi_z'}\cos\phi_{az}\right\}, \tag{20}$$

$$\alpha' = \sin^{-1}\left\{\frac{n_s}{n_1}\sin\alpha\right\}, \tag{21}$$

The modelled cross sectional angle also changes after refraction into n_1, shown in Fig. 6, which can be easily calculated using Eq. (22).

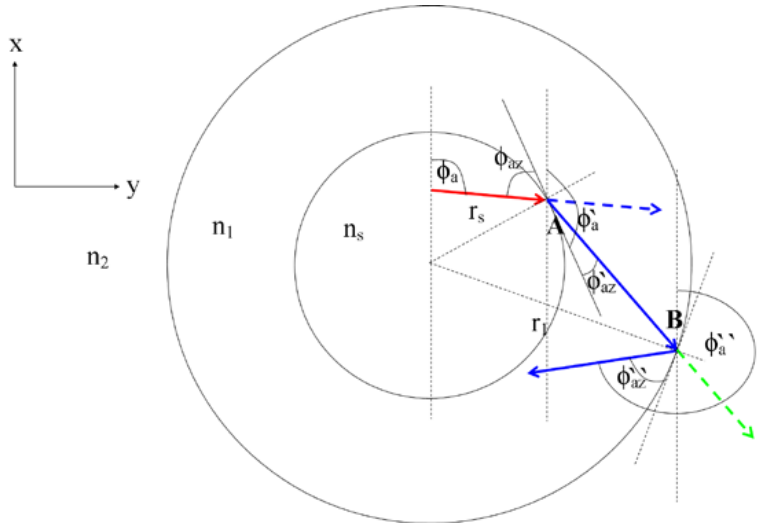

Fig. 6. A cross section of the double-cladding probe showing the change in the azimuthal angle and the modelled cross sectional angle after refraction and a following reflection.

$$\phi_a' = \phi_a + \left(\phi_{az} - \phi_{az}'\right). \tag{22}$$

The calculated longitudinal propagation angle and cross sectional angle can be substituted into the ray path equations to determine the path of the ray within n_1.

If the ray is also incident on the n_1, n_2 interface before reaching the fibre core then a reflection can also occur, which has been previously discussed in the reflective wall design. Unlike the reflective wall situation, the azimuthal angle that the ray makes with the n_2, n_1 interface is different to that it makes with the n_1, n_s interface. This is due to the difference in radii and hence curvature of the two interfaces, which has been depicted in Fig. 6. The azimuthal angle which is made with the n_2 interface, ϕ_{az}'', is calculated using the law of cosines, as:

$$\phi_{az}'' = \frac{\pi}{2} - \cos^{-1}\left\{\frac{R^2 + r_1^2 - r_2^2}{2Rr_1}\right\}, \tag{23}$$

where R is the distance between the two points A = (x_1, y_1) and B = (x_2, y_2), hence $R = \sqrt{\left(x_2^2 - x_1^2\right)^2 + \left(y_2^2 - y_1^2\right)^2}$.

#201721 - $15.00 USD Received 21 Nov 2013; revised 22 Jan 2014; accepted 22 Jan 2014; published 20 Feb 2014

This method is then continually applied to any refractions and reflections until the ray reaches the optical fibre core. Depending on whether the ray is incident on the fibre core from the scintillator or the transparent layer, then the appropriate refractive index must be applied, n_s or n_1 respectively.

2.4 Cladding coupled

In the case of the cladding coupled design shown in Fig. 3(d), the probe consists of a hollow cylinder scintillator surrounded by a reflective layer, n_2, and filled with a lower refractive index, transparent material, n_1. The purpose of this probe design is similar to that of the double-cladding, when the scintillating material is optically attenuating, an optically transparent central region may significantly improve the light collection efficiency.

The modelling of the light collection is similar to that of the double-cladding.

2.5 Probe design comparison

An in-house Matlab code was developed to simulate the models discussed. Figure 7 shows the two probe scenarios that have been modelled in order to compare the different probe designs, these are:

(1) Figure 7(a) shows the scenario where the overall size of the probes are kept constant, corresponding to a radius, r, of 0.4 mm. Therefore all probes are evaluated with the same physical size, though this may correspond to the probes having different scintillator volumes. This is important for applications where the size of the detector needs to be minimised.

(2) Figure 7(b) shows the scenario where the volumes of the scintillating materials are kept constant, V_s, such that in each case the same volume of scintillating material is investigated. This is important for applications where the sensitive volume of the detector needs to be minimised.

The optical fibre parameters, which have been used in the simulations are given in Table 1. For all probe designs the refractive index of the scintillating material was 1.73, corresponding to that of BeO ceramic, and a unit value is assumed for the power emitted per unit volume per steradian of the scintillator, I_0. In the case of the novel architectures, PMMA of the same refractive index as the cladding of the optical fibre, n_{cl}, was used as the transparent medium in the probe, n_1. The dimensions used for simulating the different probe designs are given in Table 2.

Table 1. Simulated Optical Fibre Parameters

Parameter	Value
r_{co}	0.4 mm
n_{co}	1.47
NA	0.22

Table 2. Simulation Parameters for the Comparison of the Different Probe Designs

	Butt-coupled		Reflective wall		Double-cladding		Cladding coupled	
	Parameter	Value	Parameter	Value	Parameter	Value	Parameter	Value
Size constrained	r_s	0.4 mm	r_s	0.4 mm	r_s	0.2 mm	r_s	0.4 mm
					r_1	0.4 mm	r_1	0.2 mm
Volume constrained	r_s	0.1 mm	r_s	0.1 mm	r_s	0.1 mm	r_s	0.4 mm
					r_1	0.4 mm	r_1	0.387 mm

#201721 - $15.00 USD Received 21 Nov 2013; revised 22 Jan 2014; accepted 22 Jan 2014; published 20 Feb 2014

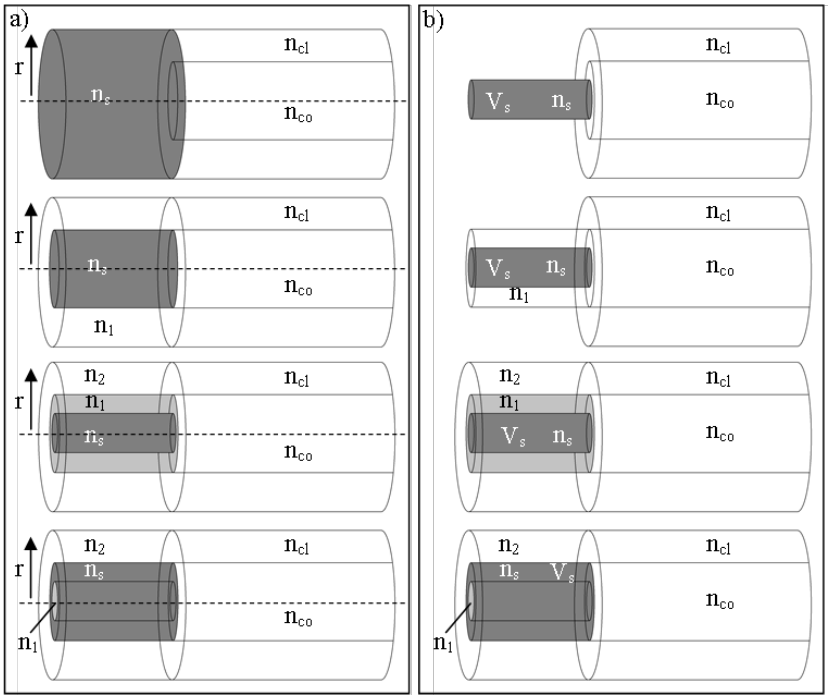

Fig. 7. The two scenarios modelled: a) where the overall size of the different probe designs are kept constant, and b) where the volume of the scintillating material in the different probe designs are kept constant.

3. Experimental validation

In order to validate the model discussed above, it was compared to experimentally measured data from commercially available scintillators. These included:

(1) The butt-coupled design using a ~1.2 mm × 2 mm × 200 mm BC-400 plastic scintillator (Bicron), cut from a thick sheet of BC-400.

(2) The reflective wall design using a 1.5 mm diameter BCF-10 plastic scintillating fibre (Bicron).

(3) An optically attenuating butt-coupled design using eight 1 mm diameter × 1 length BeO ceramic cylinders (Thermalox 995, Materion).

These scintillators were placed at the tip of a 20 m long polymethyl methacrylate (PMMA) optical fibre, ESKA Ck-20 with ~0.5 mm core diameter and ~1.0 mm outer jacket diameter (Mitsubishi Rayon Co., LTD, Tokyo, Japan) and the scintillation intensity measured using a photomultiplier tube, Burle 8575 (Burle Technologies, Inc., USA). A light tight heat shrink was used to encapsulate the scintillator and the optical fibre. This jacket was not modelled in the simulations as it was assumed that all light which reaches the jacket is lost.

A superficial x-ray unit (SXR), Gulmay D3150 (Gulmay Medical LTD., UK), was used to expose the scintillators to ionising radiation. A 3 mm thick lead plate was used to shield the scintillators such that length of the scintillator exposed to x-rays could be controlled, as shown in Fig. 8. In the case of the BeO ceramic cylinders, they were simply placed against each other one by one to control the length of scintillator exposed.

#201721 - $15.00 USD Received 21 Nov 2013; revised 22 Jan 2014; accepted 22 Jan 2014; published 20 Feb 2014

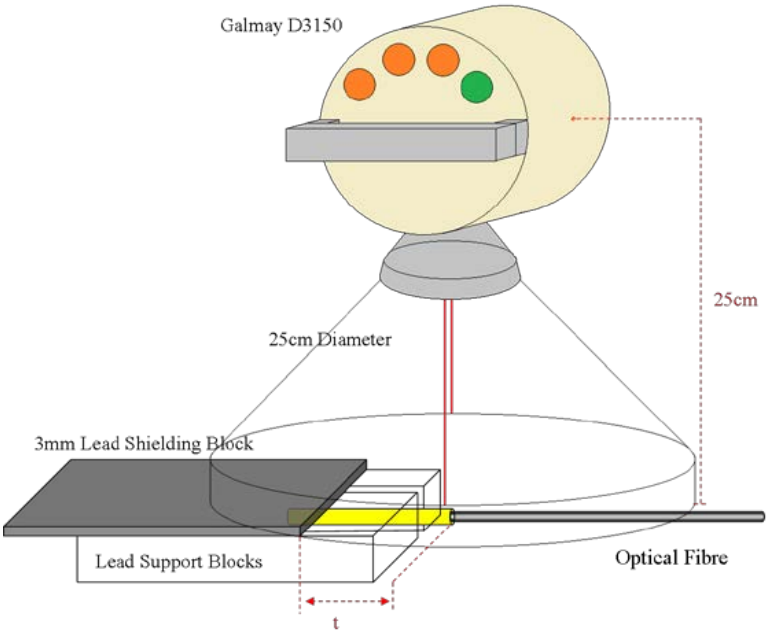

Fig. 8. The experimental setup used to validate the model. An SXR unit was used to expose various lengths of the scintillators, controlled by a 3 mm lead shielding block.

The simulated probe parameters are given in Table 3, and optical fibre parameters in Table 1. An power emitted per unit volume per steradian, I_0, of 1.25 was modelled for the butt-coupled design to account for the higher light output of BC-400 compared to BCF-10.

Table 3. Probe Parameters Simulated for the Experimental Validation

Transparent Scintillator			
Butt-coupled		Reflective wall	
Parameter	Value	Parameter	Value
r_s	0.6 mm	r_s	0.75 mm
n_s	1.58	n_s	1.6
I_0	1.25	n_1	1.49
		I_0	1

Optically Attenuating Scintillator	
BeO Butt-coupled	
Parameter	Value
r_s	0.5 mm
n_s	1.73
μ	2.69×10^{-3} m^{-1}
I_0	1

4. Results and discussion

4.1 Transparent scintillators

In order to verify the model, we compare the results found for the bound ray light collection of the butt coupled and reflective wall designs with those experimentally measured. The results shown in Fig. 9 are comparing both the modelled and measured normalised to the highest power. The uncertainties graphed for the measured data is for two standard deviations from the mean readings, and a 0.25 mm uncertainty on the placement of the lead plate.

These results agree with that previously reported [15], where the bound light collection from the butt-coupled increases linearly with scintillator length, until a point, beyond which it increases to an asymptotic limit. The bound light collection from the reflective wall on the other hand continually increases linearly with scintillator length, due to the reflections occurring from the wall.

#201721 - $15.00 USD Received 21 Nov 2013; revised 22 Jan 2014; accepted 22 Jan 2014; published 20 Feb 2014

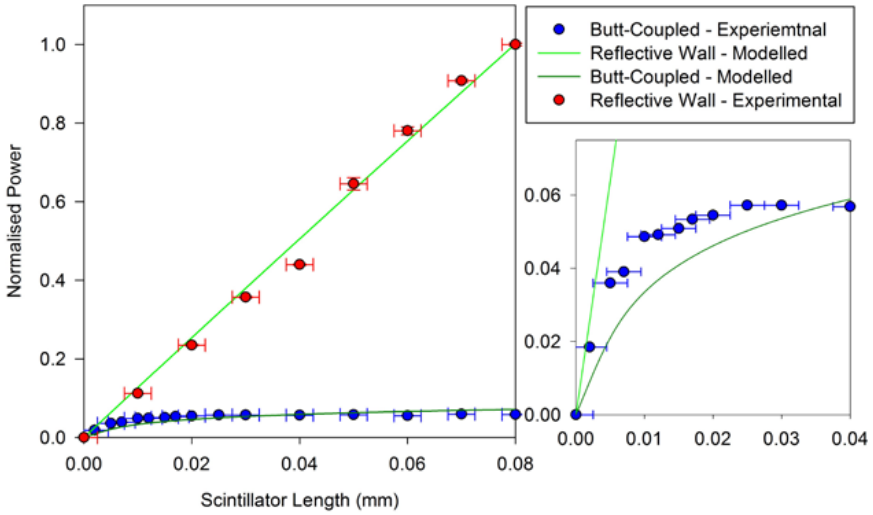

Fig. 9. Comparison between the modelled butt-coupled and reflective wall and corresponding measurements.

Both the reflective wall and butt-coupled measured and modelled results have an average relative agreement to each other of within 5% and 12.5%, respectively. With this partial validation, the model is now used to compare the performance of the various investigated probes.

Figures 10(a) and 10(b) depict the modelling results for a cladding-coupled and double-cladding architecture, respectively. Both bound and tunnelling rays' power within the fibre is shown. Results show that not only is there a significant bound power collected via the transparent medium, n_1, but that there is also a significant amount of tunnelling power collected via n_1.

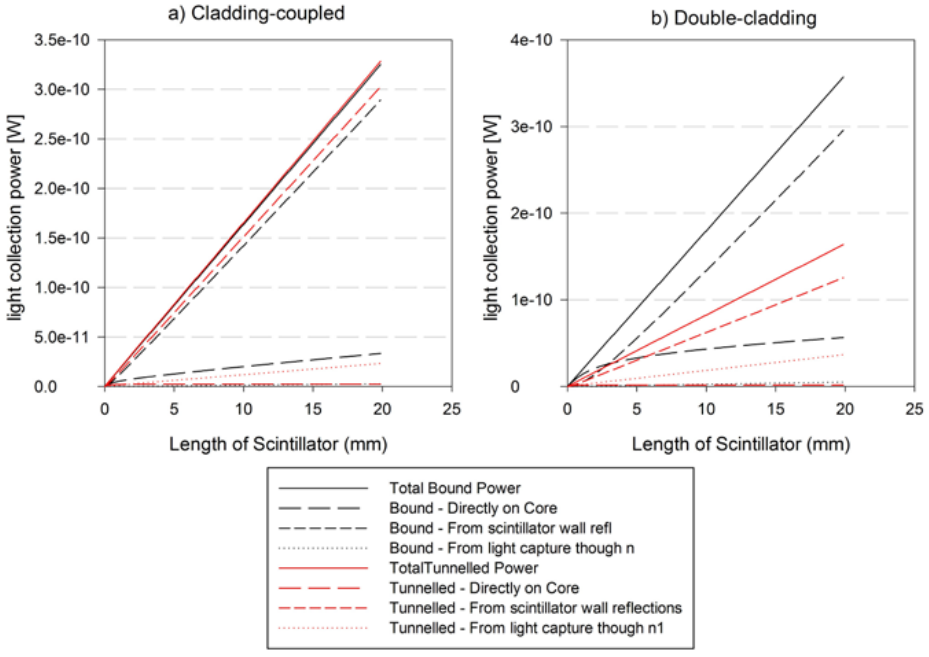

Fig. 10. Modelling results of the novel probes, a) cladding-coupled and b) double-cladding.

#201721 - $15.00 USD Received 21 Nov 2013; revised 22 Jan 2014; accepted 22 Jan 2014; published 20 Feb 2014

Figure 11(a) shows the comparison of the total light collection of the four probes designs when constraining the overall size of the probe. It is clear that the reflective wall achieves the most light collection over the novel probes. This is due to the fact that when simply constraining the overall size of the probe, that there is more emitting scintillator possible for the reflective wall over the novel. In fact, as the volume of scintillator in the novel probes is increased, the light collection increases until reaching the reflective wall situation.

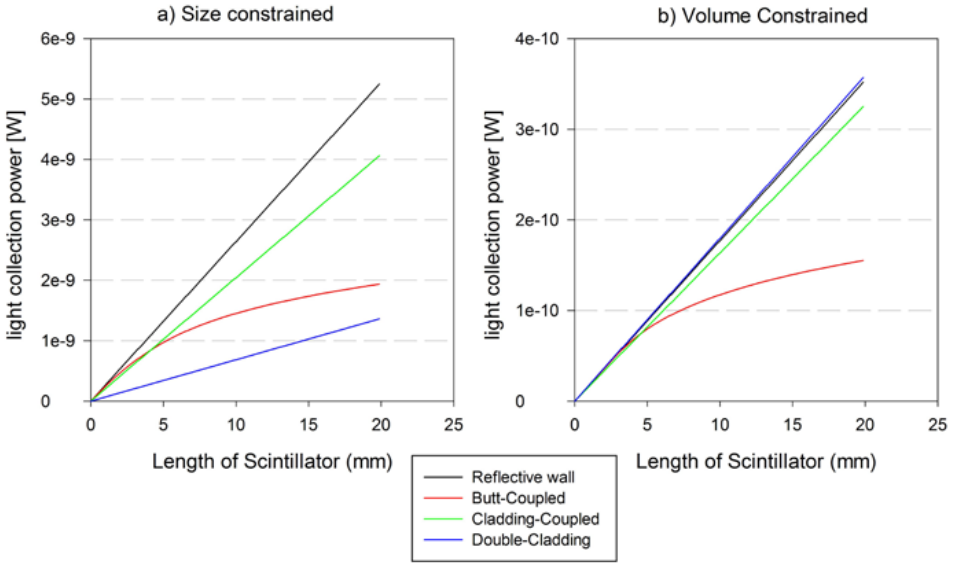

Fig. 11. The total light collection of all four probe designs when constraining: a) the overall size of the probes and b) the volume of the scintillating material.

Figure 11(b) shows the total light collection of the four investigated probes, when constraining the volume of the scintillator. Results show that the novel probe designs have an increase in light collection over the butt-coupled design. Though when compared to the reflective wall design there is no significant increase in light collection.

4.2 Optically attenuating scintillators

The attenuating properties of BeO ceramics are now applied, with an optical attenuation coefficient, $\mu = 2.69 \times 10^{-3}$ m^{-1} [16]. To validate the model for the addition of the optically attenuating scintillator properties, the modelled results for a butt-coupled BeO ceramic design were compared to that experimentally measured, shown in Fig. 12. The results are in good agreement of each other, with an average relative difference of within 1%. The results show that beyond 1 mm of BeO ceramic, that there is virtually no increase in the light collection by the optical fibre, therefore light collection optimisation is crucial.

#201721 - $15.00 USD Received 21 Nov 2013; revised 22 Jan 2014; accepted 22 Jan 2014; published 20 Feb 2014

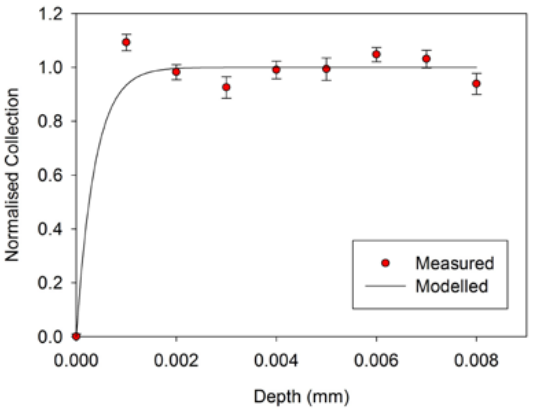

Fig. 12. The comparison between the modelled and experimentally measured light collection for a BeO ceramic butt-coupled design.

Figure 13(a) shows the results for when constraining the overall size of the probe. Results now show that in both the reflective wall and butt-coupled cases, that the total light collection increases linearly with BeO length, until a point, beyond which it increases to an asymptotic limit. Hence the significant increase in the light collection when using a reflective wall over the butt-coupled is lost. This is due to the greater the path length of the ray within the BeO, then the greater the optical attenuation encountered.

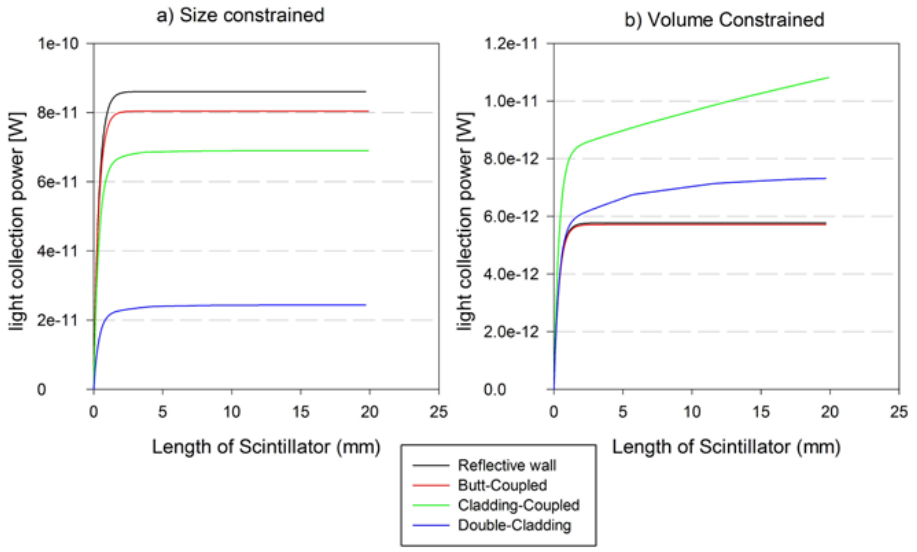

Fig. 13. Modelled total light collection from the four investigated probes when including the optical attenuation of BeO and constraining either: a) the overall size of the probe is constrained and b) the volume of the scintillating material.

Results also indicate that both the butt-coupled and reflective wall collect more light over the novel geometries. As before, this is due to the increase in BeO volume capable with the previous geometries over that of the novel, since the novel geometries size needs to include that of the transparent layer. Even though the rays are more attenuated in the butt-coupled and reflective wall, the overall increase in light emission gives these geometries the most light collection. It can also be seen that the cladding-coupled architecture achieves a higher light collection than the double-cladding. This can be explained by the increase in the thickness of the transparent layer n_1 for the cladding-coupled design.

Again a comparison of the total light collected while the volume of BeO has been kept constant, such that the efficiency of the probes can be investigated is shown in Fig. 13(b). It can be seen that the novel geometries are more efficient in collecting light from the BeO,

#201721 - $15.00 USD Received 21 Nov 2013; revised 22 Jan 2014; accepted 22 Jan 2014; published 20 Feb 2014

which is to be expected since some rays have a less attenuating route to the fibre unlike the butt-coupled and reflective wall. The important factor of the use of n_1 is that light continues to be collected by the fibre beyond the thickness of BeO where the previous probes platoe in their light collections. This is simply due to the fact that the transparent layer, n_1, is shortening the path length of some rays in the BeO, hence lowering the amount by which they are attenuated.

The importance of these two results comes about with the application of the fibre–coupled luminescence dosimeter. For example, where the overall size of the probe is important such as for the application of *in-vivo* dosimetry, then the simple butt-coupled or reflective wall designs are the best option. When the overall size is perhaps not of concern but the sensitive volume of the dosimeter, such as in the dosimetry of small fields and high dose gradient regions, then the novel designs can be employed to significantly increase light collection.

5. Conclusion

A simple model for simulating the light collection from sources located at the tip of a multimode optical fibre has been developed, with the application primarily being fibre-coupled luminescence dosimetry. The model is based on ray optics and includes both meridional and skew rays. It also includes the optical attenuation of the medium, hence enabling the modelling of new scintillator materials, such as beryllium oxide (BeO) ceramics. Using the model, we proposed and evaluated the light collection of four different designs: the butt-coupled, reflective wall, double-cladding and cladding-coupled, for which we considered the combination of transparent and attenuating scintillator (BeO ceramics) materials.

The model was partially verified by the comparison of measured results for the butt-coupled and reflective wall geometries using a transparent plastic scintillator, and also an optically attenuating design using BeO ceramics. The modelled light collection was in good agreement with the measured results. The results for the transparent butt-coupled and reflective wall design also agrees with those previously reported [15]: the reflective wall geometry has a linear increase in light collection with scintillator length, and the coupling power in the butt-coupled geometry increases linearly to a point and then to an asymptotic limit as the scintillator length increases.

It is important to note that this is only a partial validation of the model, as the light collection of the novel investigated designs has not been verified. Similar designs to the novel probe designs are commercially available, such as double cladding scintillating optical fibres. While these have not been developed for light collection from the inner cladding interface, construction on the novel designs discussed here is certainly possible. Construction and experimental light collection measurements would be of interest for a complete verification of the model discussed here.

It was found that the new designs (double-cladding and cladding-coupled) can significantly increase light collection when constraining the volume of the optically attenuating probe. These results are of significance in possible BeO fibre optic dosimetry [17], especially the fact that the increase in light collection from reflective wall architectures over butt-coupled is minimised due to the optical attenuation of BeO. We therefore conclude that when using non-transparent phosphors in fibre-coupled luminescence dosimetry, the most practical approach for probe architecture is the use of the simple butt-coupled design when the goal is minimising the overall size of the probe, such as that for *in-vivo* brachytherapy dosimetry. However, in some situations minimising the size of the sensitive volume is the major concern, as required in the dosimetry of small field sizes where dose averaging needs to be minimised. The use of more transparent material, as in the double-cladding and cladding-coupled designs, can substantially increase the light collection.

Acknowledgments

S. Afshar V. acknowledges the support of T. Monro's Laureate Fellowship.

#201721 - $15.00 USD Received 21 Nov 2013; revised 22 Jan 2014; accepted 22 Jan 2014; published 20 Feb 2014

3.3 Ray Tracing Validation

In addition to the experimental validation of the model presented in the publication [P1], to ensure that the ray tracing was being performed correctly, figures were produced of the individual rays being traced through the probes. Figure 3.2 shows an example of a ray being traced through the probe to the optical fibre for the most complex designs; a double cladding and cladding coupled design. A blue line represents the initial emission from the inner scintillator material. Subsequent refractions and reflections are show with red lines. The reflection and refraction angles were checked on a random set of figures to ensure that the model was working correctly.

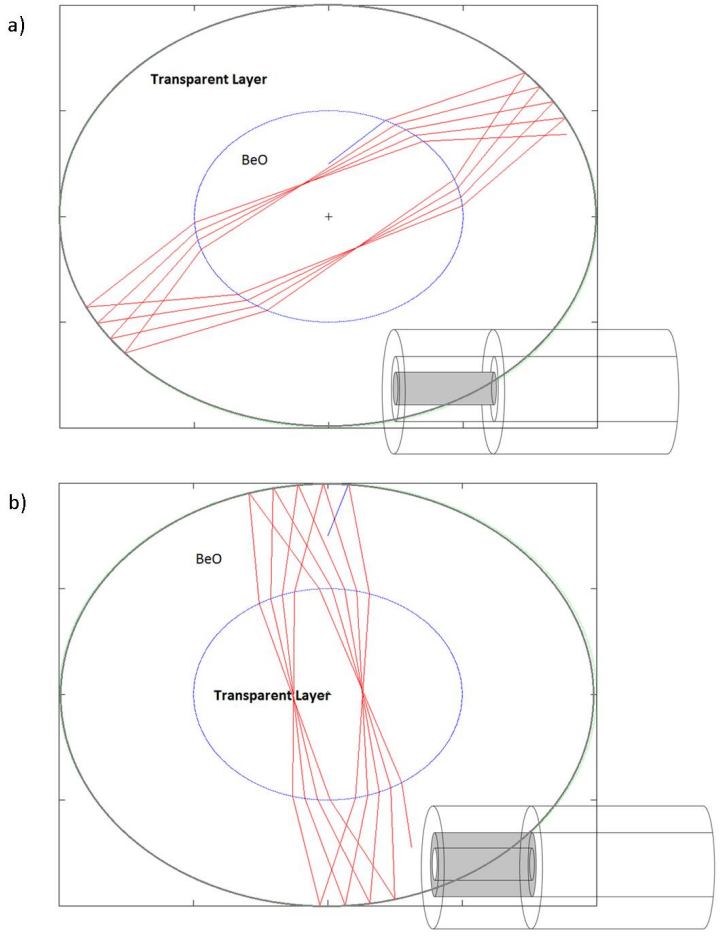

FIGURE 3.2: A example ray being traced through the probe to the optical fibre for an (a) double cladding and (b) cladding coupled probe designs. The blue ray tracing line depicts the rays initial emission, and red ray tracing lines are after any refraction or reflections.

Figure 3.3 depicts an example of all of the rays traced through double cladding design, shown by the red lines. The inner yellow cylinder represents the scintillating material, the middle green cylinder the first cladding, and the outer blue cylinder the second cladding. It can be seen that in figure 3.3 (a) that only very ordered planes of rays were traced through the optical axis. That is because figure 3.3 represents only the meridional rays which were simulated. On the other hand, figure 3.3 (b) shows random rays. This is because 3.3 (b) represents the skew rays which were simulated.

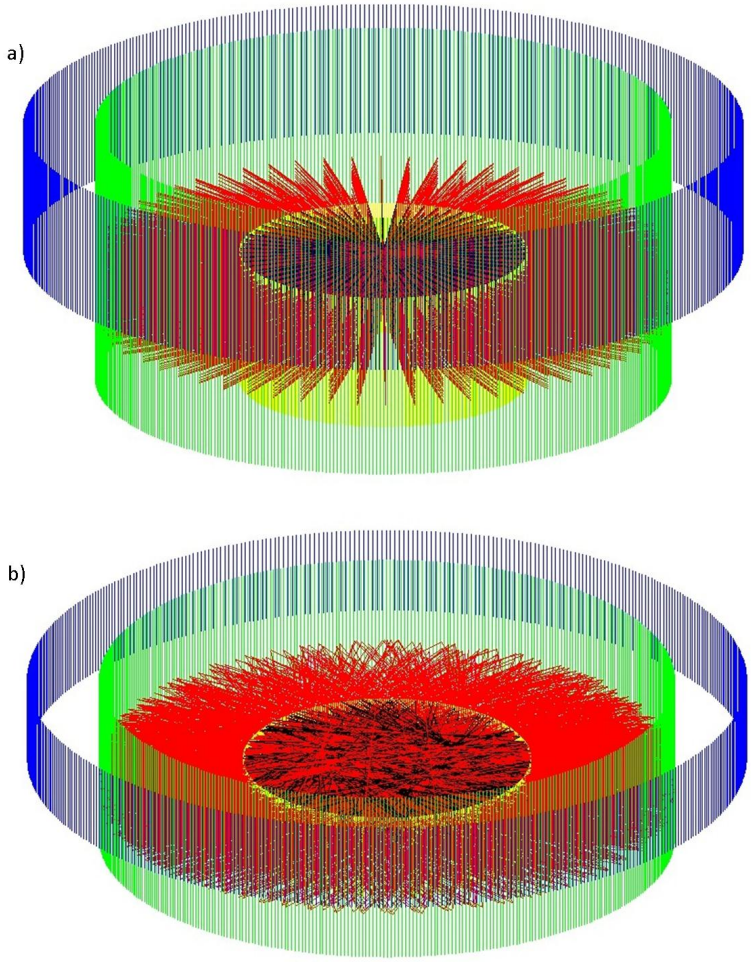

FIGURE 3.3: An example of all the rays traced through a double cladding probe design. Where (a) are only meridional rays and (b) are only skew rays. The inner yellow cylinder represents the scintillating material, the middle green cylinder the first cladding, and the outer blue cylinder the second cladding.

3.4 Discussion and conclusion

A model for the light collected by an optical fibre from a diffuse source at the tip of the fibre was demonstrated. Ray tracing is performed to model both meridional and skew rays, and to account for optical attenuation within the source at the tip of the optical fibre. Validation of the model was performed experimentally with the use of a plastic scintillator, a scintillating fibre and BeO ceramics.

The model was applied to various probe tip designs for a fibre-coupled luminescence dosimetry system. These designs consisted of a bare butt-coupled scintillator, a reflective wall (fibre scintillator), and two designs which utilise a lower refractive index layer named the double-cladding and cladding-coupled designs. The primary objective of the use of a transparent lower refractive index layer was to be applied to highly attenuating scintillators. The added transparent layer may increase the light collection by the optical fibre by providing a less optically attenuating path for the light emitted by the scintillator.

In the case of a transparent scintillator, results indicate that the optimal design was the use of a reflective wall surrounding the scintillator. While for the case of an optically attenuating scintillator, the novel designs utilising a transparent lower refractive index layer could increase the light collection for the same volume of scintillator.

In the case of a BeO ceramic scintillator, the model showed that there is little increase in light collection by adding a reflective wall around the BeO ceramic. Results also indicated that in the case of a 1 mm diameter scintillator, no gain in light collection is observed for lengths of BeO ceramic beyond 1 mm. Hence for the development of a BeO ceramic coupled fibre-coupled dosimetry system a 1 mm diameter, 1 mm long BeO ceramic cylinder was used.

Chapter 4

Beryllium oxide (BeO) ceramic RL dosimetry system

The publication [P2] forms the basis of this chapter.

Alexandre M. Caraça Santos, Mohammad Mohammadi, Johan Asp, Tanya M. Monro and Shahraam Afshar V., Characterisation of a real-time fibre-coupled beryllium oxide (BeO) luminescence dosimeter in X-ray beams, *Radiation Measurements* 53-54, 2013.

4.1 Development overview and motivation

As previously discussed BeO ceramic has some clear advantages as a radiation detector material, mainly its near water equivalence. Therefore it could be an alternative to Al_2O_3:C and a potential to produce an energy independent RL and OSL fibre-coupled luminescence dosimetry system. However, little has been reported about the RL from BeO ceramics. Marcazzó et al. (2007) reported that the RL yield from BeO ceramics was slightly higher than that from Al_2O_3:C. Erfurt and R. Krbetschek (2002) showed that the RL spectrum is similar to the TL spectrum. In this chapter the development and characterisation of an RL BeO ceramic fibre-coupled dosimeter, named RL BeO FOD, is discussed.

4.2 Beryllium safety and handling

One of the major concerns associated with the use of BeO ceramics has been its toxicity. The inhalation of beryllium has been known to cause a serious, chronic lung disease called Chronic Beryllium Disease (CBD). CBD is a hypersensitivity or allergic condition in which tissues of the lungs become inflamed, which when accompanied with fibrosis (scarring), may restrict the exchange of oxygen between the lungs and bloodstream (Committee on Beryllium Alloy Exposures, 2008).

BeO in solid form does not present a health risk, since the inhaled particles must be small enough to reach the air sacs deep in the lungs (Walsh and Vidal, 2009). In the case of powder, where inhalation is possible, proper handling needs to be considered.

4.3 Statement of Contribution

4.3.1 Conception

The idea to investigate the use of BeO ceramics, and to develop the first fibre-coupled radioluminescence dosimeter with a BeO ceramic probe tip was conceptualised by Alexandre M. Caraça Santos.

4.3.2 Realisation

The development of the probe, system reader and the LabView code was performed by Alexandre M. Caraça Santos. The experiments performed to characterise the dosimetry system were performed by Alexandre M. Caraça Santos and Johan Asp.

4.3.3 Documentation

This paper was primarily written by Alexandre M. Caraça Santos. Editing was performed by all authors.

Statement of Authorship

Title of Paper	Characterisation of a real-time fibre-coupled beryllium oxide (BeO) luminescence dosimeter in X-ray beams
Publication Status	☑ Published ☐ Accepted for Publication ☐ Submitted for Publication ☐ Publication Style
Publication Details	Alexandre M. Caraca Santos, Mohammad Mohammadi, Johan Asp, Tanya M. Monro and Shahraam Afshar V., Characterisation of a real-time fibre-coupled beryllium oxide (BeO) luminescence dosimeter in X-ray beams, Radiation Measurements 53-54, 2013.

Principal Author

Name of Principal Author (Candidate)	Alexandre Santos
Contribution to the Paper	Developed the BeO ceramic probe, RL reader system and the LabView program, performed all of the experimental measurements, and wrote the manuscript and acted as corresponding author.
Overall percentage (%)	
Signature	Date 12/1/2016

Co-Author Contributions

By signing the Statement of Authorship, each author certifies that:

i. the candidate's stated contribution to the publication is accurate (as detailed above);

ii. permission is granted for the candidate in include the publication in the thesis; and

iii. the sum of all co-author contributions is equal to 100% less the candidate's stated contribution.

Name of Co-Author	Mohammad Mohammadi
Contribution to the Paper	Supervised development of work and manuscript evaluation.
Signature	Date 12/01/2016

Name of Co-Author	Johan Asp
Contribution to the Paper	Supervised development of work, helped in experimental measurements and data interpretation and manuscript evaluation.
Signature	Date 12/1/2016

Name of Co-Author	Tanya M. Monro

Contribution to the Paper	Provided valuable manuscript evaluation.
Signature	Date: 6 January 2016

Name of Co-Author	Shahraam Afshar V
Contribution to the Paper	Supervised development of work and manuscript evaluation.
Signature	Date: 6/01/2016

Radiation Measurements 53-54 (2013) 1–7

Contents lists available at SciVerse ScienceDirect

Radiation Measurements

journal homepage: www.elsevier.com/locate/radmeas

Characterisation of a real-time fibre-coupled beryllium oxide (BeO) luminescence dosimeter in X-ray beams

Alexandre M. Caraça Santos [a,b,*], Mohammad Mohammadi [a,b], Johan Asp [b], Tanya M. Monro [a], Shahraam Afshar V. [a]

[a] Institute for Photonics & Advanced Sensing, School of Chemistry & Physics, University of Adelaide, Adelaide, South Australia 5000, Australia
[b] Department of Medical Physics, Royal Adelaide Hospital, Adelaide, South Australia 5000, Australia

HIGHLIGHTS

- We construct a fibre-coupled beryllium oxide ceramic radioluminescence (RL) dosimeter.
- RL found to be linear with dose-rate from 100 to 600 cGy/min.
- Integrated RL found to be linear with dose from 1 to 500 cGy.
- 6 MV PDD found to be within 2% agreement with Ion chamber measurements.
- 150 kVp and 120 kVp PDDs found to be within 2.5% and 4%, respectively

ARTICLE INFO

Article history:
Received 12 July 2012
Received in revised form
11 February 2013
Accepted 11 March 2013

Keywords:
Radioluminescence
BeO
Fibre optic dosimetry

ABSTRACT

For the first time the feasibility of using beryllium oxide (BeO) ceramics as a fibre-coupled radioluminescent dosimeter is investigated. BeO ceramic exhibits both radioluminescence (RL) and optically stimulated luminescence (OSL), and has the potential to be a near tissue equivalent alternative to Al_2O_3:C. A BeO fibre-coupled radioluminescence dosimeter is demonstrated and characterised for 6 MV X-rays and superficial X-ray energies, 150 kVp and 120 kVp. Based on the results, we demonstrate the capability of the RL BeO FOD for accurate and reproducible dose measurements with a linear dose rate and dose response. It has also been found that the percentage depth dose curves for 6 MV agreed with ion chamber measurements to within 2%, except in the build up region. For the 150 kVp and 120 kVp photon beams, the depth dose measurements agreed with ion chamber measurements to within 2.5% and 4%, respectively.

1. Introduction

Optical fibre-coupled scintillation dosimetry has been shown to have the potential to meet the needs of current radiotherapy, with characteristics including real-time, small volume, highly sensitive and reproducible dosimetry. Hence allowing fibre-coupled scintillation dosimetry to be applied to such fields as small field dosimetry (Archambault et al., 2007; Beddar et al., 2001; Klein et al., 2010; Lambert et al., 2010; Letourneau et al., 1999), *in-vivo* brachytherapy (Andersen et al., 2009a, 2009b; Lambert et al., 2006) and mammography (Aznar et al., 2005). This approach uses a scintillating material placed at a point of interest. Upon exposure to ionising radiation, part of the energy absorbed by the scintillating material is emitted as light, known as radioluminescence (RL) or scintillation. An optical fibre is coupled to the scintillator such that a portion of the emission is collected and guided to a detector system, allowing the measurement of the RL signal which is generally proportional to the dose-rate (Beddar et al., 1992a).

Plastic scintillators have certainly been the most commonly investigated scintillating material and had a large influence on the success of this approach. This is due to the attractive attributes of plastic scintillators compared with other investigated scintillators; easy commercial accessibility, small volume, and near water equivalence. Plastic scintillators have been shown to be energy independent in the megavoltage X-ray energy range, and have a response linear with dose rate and dose (Beddar et al., 1992a,b). One disadvantage of the use of plastic scintillators, however, is that they exhibit a significant decrease in response to low energy x-rays relative to megavoltage X-rays (Williamson et al., 1999).

* Corresponding author. Department of Medical Physics, Royal Adelaide Hospital, Adelaide, South Australia 5000, Australia. Tel.: +61 8 8222 2701.
E-mail address: alexandre.santos@adelaide.edu.au (A.M.C. Santos).

1350-4487/$ – see front matter © 2013 Elsevier Ltd. All rights reserved.
http://dx.doi.org/10.1016/j.radmeas.2013.03.003

A major drawback of fibre-coupled scintillation dosimetry has been the existence of the stem effect, which is light produced by the optical fibre itself when exposed to ionising radiation. In the megavoltage case, the main contribution is from Cerenkov radiation (Beddar et al., 1992b). Several techniques have been investigated to either remove or correct for the stem effect; including the use of a second background fibre (Beddar et al., 1992a), a spectral discrimination method (Fontbonne et al., 2002) and a temporal method for pulsed radiation (Clift et al., 2002). Possibly the most promising method is the air-core fibre method (Lambert et al., 2008, 2010; Liu et al., 2011). Unlike most of the other techniques which work based on correcting for the stem effect, the use of an air-core fibre will not produce Cerenkov and hence eliminates the stem effect.

Another approach uses phosphors which exhibit optically stimulated luminescence (OSL) (Polf et al., 2002, 2004). When exposed to ionising radiation some phosphors are able to store some charge in defects within their structure. The stored or trapped charge can be stimulated by light to emit luminescence, known as optically stimulated luminescence (OSL). Using a different stimulation wavelength to that emitted, the OSL signal can be measured after irradiation. The OSL signal is proportional to the accumulated dose of the phosphor and is unaffected by the stem effect since the optical fibre is no longer being exposed to ionising radiation. With phosphors that exhibit both RL and OSL, it is possible to have two independent dose measurements for one source of irradiation. Carbon-doped aluminium oxide (Al_2O_3:C) crystals have been the most investigated material for this RL/OSL technique. However, Al_2O_3:C crystals are not tissue equivalent (Z_{eff} ~ 11.3) and have been shown to over respond to lower energy x-rays by a factor up to ~3 (Bos, 2001). Perhaps the most significant drawback of Al_2O_3:C is that its RL signal increases with the accumulated dose and hence necessary corrections are required to be applied (Andersen et al., 2006).

Beryllium oxide (BeO) ceramic is a commercially available material known to be capable of both OSL and thermoluminescence. BeO ceramic was initially investigated as a potential thermoluminescent dosimeter material (Albrecht and Mandeville, 1956; Rhyner and Miller, 1970; Scarpa, 1970; Tochilin et al., 1969). Only recently have in depth investigations into the luminescence properties of BeO been undertaken (Bulur and Göksu, 1998; Sommer et al., 2007, 2008). It has been found that the OSL emission spectrum shows two emission bands at ~310 nm and ~370 nm, the OSL intensity increases with decreasing stimulation wavelengths, and an RL emission band exists at ~280 nm (Yukihara, 2011).

Unlike Al_2O_3:C crystals, BeO ceramics are near water equivalent (Z_{eff} ~7.2), and hence have the potential to be a near water equivalent alternative to Al_2O_3:C, although its potential use as a BeO-coupled fibre optic dosimeter (FOD) has not yet been investigated. BeO may prove to be a more versatile FOD, which can bridge the gap between the near tissue equivalent plastic scintillators and OSL based Al_2O_3:C crystals.

A common concern with the use of BeO ceramics has been the toxicity. Inhalation of Beryllium has been known to cause a chronic disease called Chronic Beryllium Disease (CBD) (Exposures et al., 2008). BeO in solid form has not been shown to present any health risk, only in its powder form where inhalation is possible does proper handling need to be considered (Walsh and Vidal, 2009).

In this work the first investigation into the use of BeO ceramics as the scintillating probe for a fibre-coupled luminescence dosimeter is presented, and its feasibility for potential use in radiotherapy dosimetry is demonstrated. A radioluminescence BeO fibre-coupled dosimeter (RL BeO FOD) is constructed and its response is evaluated for 6 MV and superficial x-rays of 150 kVp and 120 kVp.

2. Materials and methods

2.1. Dosimeter design

The BeO ceramic samples used in this study are 1.0 mm diameter cylinders of 1.0 mm length (Thermalox 995, Materion), butt-coupled to a polymethyl methacrylate (PMMA) optical fibre, ESKA Ck-20 with ~0.5 mm core diameter and ~1.0 mm outer jacket diameter (Mitsubishi Rayon Co., LTD, Tokyo, Japan). A PMMA optical fibre was chosen because of its availability and low cost, and to minimise the influence of the stem effect, since PMMA optical fibres have been shown to produce the least stem effect in the megavoltage range (Nowotny, 2007).

In our setup, the BeO ceramic is in solid form, and hence does not present any health risks. To minimise any possible contamination, a light tight heat shrink was used to encapsulate the BeO ceramic and the optical fibre. This encapsulation also prevents any external light entry. While the use of heat shrink will not be capable for clinical use, it is sufficient for the evaluation of the BeO ceramic.

The optical fibre was 20 m in length sufficient to guide the collected light to a reader located outside of the treatment bunker, to ensure that the reader was not affected by any scattered radiation. The reader consists of a bialkali photomultiplier tube (PMT), Burle 8575 (Burle Technologies, Inc., USA), a photon counter unit which outputs transistor–transistor logic (TTL) signals, Hamamatsu C9744 (Hamamatsu, Japan), and a data acquisition card (DAQ), National Instruments USB-6341 (National Instruments Inc., USA), which has four 32 bit counters with a time base of up to 100 MHz. A customised LabVIEW™ (National Instruments Inc., USA) program reads the counters of the USB-DAQ, displaying the count rate directly, as shown in Fig. 1. Unless stated, a sampling rate of 1 Hz was used when reading the counters, corresponding to 1 s integrations. The counts per sample were then converted to counts per second.

The stem effect produced in the optical fibre was accounted for by using a second optical fibre that does not have a BeO ceramic tip, placed alongside the RL BeO FOD such that it measures the background light. The background fibre was first connected to the reader to measure the stem effect, and then replaced by the RL BeO FOD. The light measured by the background fibre was then subtracted from that measured by the RL BeO FOD. The stem effect measured without the BeO ceramic was compared to that from the background fibre to determine if any corrections were needed. Since the stem effect is not being investigated in the current study, at all times the RL BeO FOD was oriented perpendicular to the beam and in the central axis of the beam, such that any angular dependence from the stem effect can be controlled. While this method may not be adequate in a clinical situation, it was considered

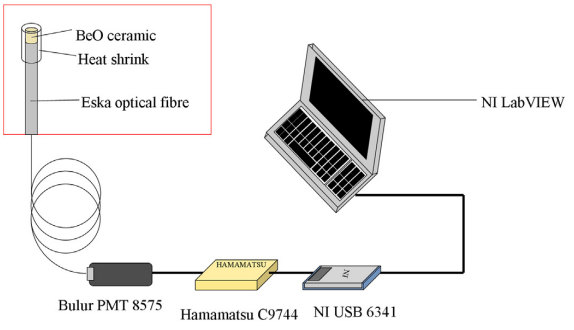

Fig. 1. The detector setup for RL measurements of the RL BeO FOD.

sufficient for the purpose of evaluating the BeO ceramic. All measurements were performed in a solid water phantom (Gammex RMI, Middleton, U.S.A).

2.2. 6 MV X-ray beam

A 6 MV X-ray beam from a linear accelerator (linac), clinac 600C/D (Varian Medical Systems, Inc., Palo Alto, CA, USA) was utilized to investigate the response of the RL BeO FOD. The setup within the solid water phantom was in reference conditions at all times, corresponding to a field size of 10 × 10 cm^2 and a Source to Surface Distance (SSD) of 100 cm, allowing for the properties of the RL BeO FOD to be evaluated for representative therapeutic beam properties. This setup is depicted in Fig. 2.

The temporal resolution of the RL was investigated at a higher sampling rate of 3 kHz. An Al_2O_3:C probe was constructed similar to the RL BeO FOD, using 1 mm × 1 mm × 1 mm cubes cut from 5 mm diameter × 1 mm thick chips (Landauer, Stillwater, Oklahoma, U.SA), and used as a comparison. The mean stem effect signal was measured at 3 kHz and subtracted from the measured signals. The linac pulse repetition rate for varying dose-rates was investigated using the 3 kHz sampling rate.

2.2.1. Reproducibility

The reproducibility of the RL BeO FOD after repeated use was investigated, its RL intensity was recorded for seven consecutive 1 Gy irradiations, with a dose rate of 300 cGy/min at a depth of 1.3 cm within the solid water phantom corresponding to d_{max} (depth of maximum dose) of the 6 MV X-ray beam. For each irradiation the mean value of the RL intensity was computed, these values were then normalised to the mean of the seven measurements.

For all other measurements, three readings were taken and their mean values given. The uncertainties given correspond to two standard deviations of the readings from the mean values.

2.2.2. Dose and dose rate response

Since the RL intensity of the RL BeO FOD should be proportional to the dose-rate, it is important to observe a linear RL response with varying dose-rate. The RL BeO FOD was therefore exposed to dose-rates from 100 cGy/min to 600 cGy/min. This was performed at a depth of 1.3 cm within the solid water phantom. The dose response was also investigated for doses from 1 cGy to 500 cGy, by integrating the RL signal over the total exposure time.

2.2.3. Percentage depth dose

The response of the RL BeO FOD to dose-rate and dose is important when investigating its feasibility for routine radiotherapy dosimetry. However, a percentage depth dose (PDD) curve is perhaps the most relevant measurement since it indicates whether the detector shows a water-equivalent response. A PDD was measured in the solid water for depths from 0.7 cm to 30 cm, and compared to that collected by an IC15 ion chamber (Wellhofer Dosimetrie, Germany), during the beam data acquisition.

2.3. Superficial X-rays

The response to low energy X-rays of 150 kVp and 120 kVp, was also investigated using a superficial X-ray (SXR) unit, Gulmay D3150 (Gulmay Medical LTD., UK). The temporal resolution of the RL was again investigated and compared to that acquired using an Al_2O_3:C probe.

2.3.1. Percentage depth dose

The RL BeO FOD was placed within the solid water phantom and measurements conducted with a 5 cm diameter cone and an focus-skin distance (FSD) of 15 cm depicted in Fig. 3. PDD curves were measured for depths of 0 mm–40 mm, and compared to a thin window ion chamber (23342 PTW-Freiburg, Germany) routinely used for data collection.

3. Results

The stem effect signal from the optical fibre was found to be of the order of 42% of the RL signal from the RL BeO FOD. Any difference between the stem effect from the background fibre and the RL BeO FOD was found to be negligible, and did not affect results.

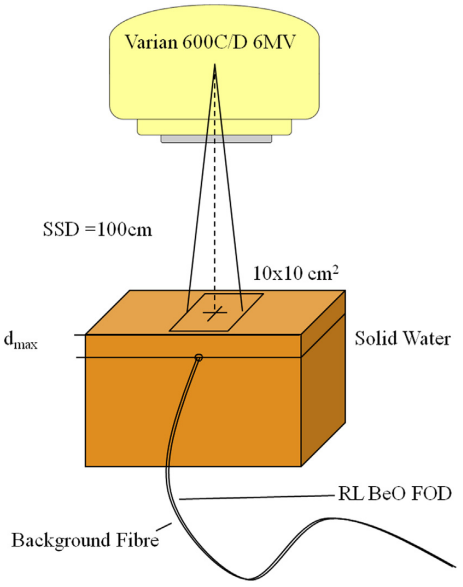

Fig. 2. Setup of the solid water phantom with the background fibre and RL BeO FOD placed perpendicular to the beam and in the central axis of the 10 × 10 cm^2 field for 6 MV X-ray measurements.

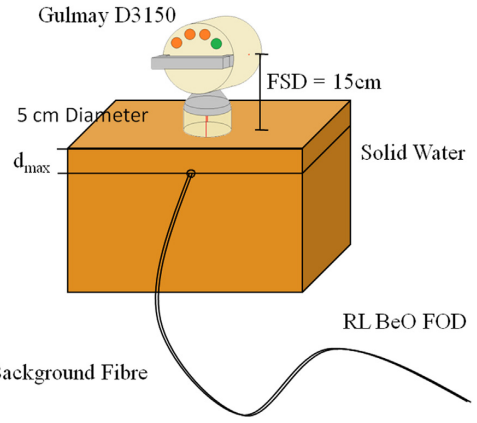

Fig. 3. Setup of the solid water phantom with the background fibre and RL BeO FOD placed perpendicular to the beam and in the central axis of the 5 cm diameter cone for superficial measurements.

3.1. 6 MV X-ray beam

The RL at the sampling rate of 3 kHz when using the RL BeO FOD is shown in Fig. 4a & b), and with the Al_2O_3:C FOD shown in Fig. 4c & d). The measurement with 1 Hz sampling rate is also plotted to show the signal stability. Unlike the Al_2O_3:C, RL from the BeO ceramic has little phosphorescence, allow for the individual radiation pulses produced by the linac to be easily resolved.

The pulse repetition rate for varying dose-rates results are shown in Fig. 5. As expected a linear response was found between the pulse repetition rate and the dose-rate, with an R^2 of 1.000.

3.1.1. Reproducibility

The normalised RL response over seven measurements is shown in Fig. 6. The reproducibility of the RL was found to vary by only 0.5%, corresponding to two standard deviations of the seven mean RL intensities.

3.1.2. Dose and dose rate response

The response of the RL BeO FOD to varying dose rates is shown in Fig. 7a). This demonstrates that the response of the BeO FOD is linear to therapeutic dose-rates, with an R^2 of 0.9998. Hence it can

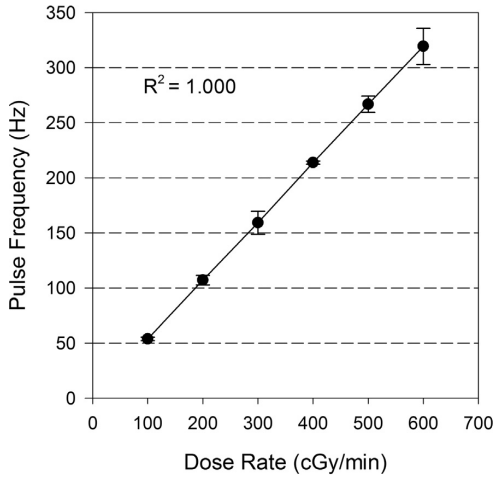

Fig. 5. The pulse repetition rate to dose-rate measured in a solid water phantom with a field-size of 10 × 10 cm^2, an SDD of 100 cm and at a depth of 1.3 cm.

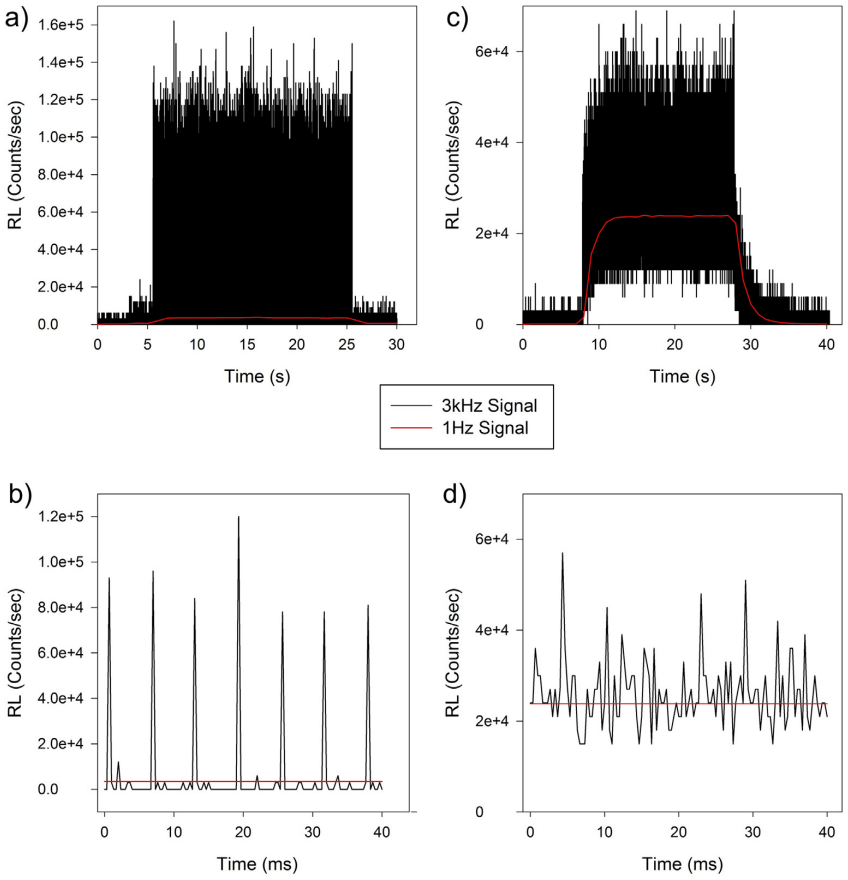

Fig. 4. The radioluminescence signal when sampling at 3 kHz for BeO; a) the total RL during irradiation and b) with a narrower temporal window, and for Al_2O_3:C; c) the total RL during irradiation and d) with a narrower temporal window. A sampling rate of 1 Hz is also shown in red. (For interpretation of the references to colour in this figure legend, the reader is referred to the web version of this article.)

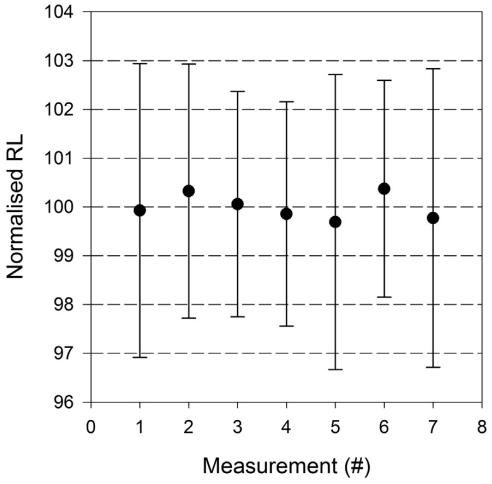

Fig. 6. Repeatability of the radioluminescence measurements normalised by the mean value of the seven measurements, performed at d_{max} of 6 MV X-ray beam with dose rate 300 cGy/min.

be said the RL BeO FOD is dose-rate independent and could be utilised in cases where the dose-rate is varying.

Fig. 7b) demonstrates the linear response of the RL BeO FOD to therapeutic doses from 1 cGy to 500 cGy, with an R^2 of 1.000. The resulting linear response is similarly important since it is necessary that dose measurements be accurate within a therapeutically relevant range of doses.

3.1.3. Percentage depth dose

Fig. 8 shows the PDD measured in the solid water for depths from 0.7 cm to 30 cm. The difference between the RL BeO FOD and IC15 ion chamber PDD shows that for depths below d_{max} the largest discrepancy of up to 3% at the surface. This difference is most likely due to the positioning uncertainty of the RL BeO FOD, since this is a high dose gradient region a small change in the depth of the RL BeO FOD has a large impact of the dose. Discarding the build up region, the discrepancies are no greater than 2%, with the two becoming closely matched at depths beyond d_{max}. The importance of the achieved results is to show that for the 6 MV x-ray beam that the RL BeO FOD has a response similar to that of water.

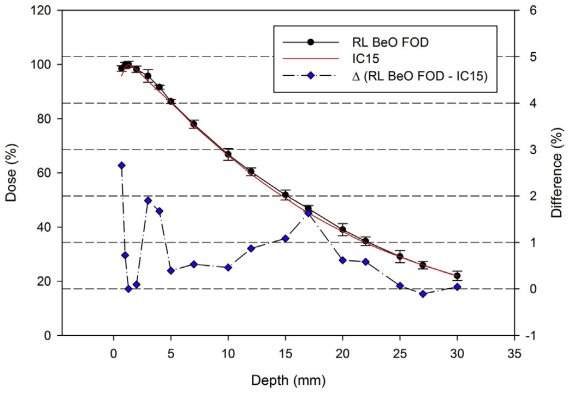

Fig. 8. The PDD curve obtained with the RL BeO FOD and an IC15 ion chamber in a solid water phantom with an SSD of 100 cm and a field size 10 × 10 cm^2. The discrepancy between the RL BeO FOD and the IC15 ion chamber is also shown in secondary axis.

3.2. Superficial X-rays

Fig. 9a) shows the RL signal intensity of the RL BeO FOD during exposure to the superficial x-rays (SXR), with that from the Al_2O_3:C shown in Fig. 9b). Again the BeO ceramic is shown to have much less phosphorescence than the Al_2O_3:C probe. Analysis of the RL of the BeO ceramic using the SXR shows the initial ramp up of the SXR, which is of approximately 5 s duration for the SXR used, and is due to the increasing dose-rate while the current and voltage of the SXR are increasing. Once stabilised a steady state dose-rate is established, and hence the constant RL intensity. Finally, the rapid drop in dose-rate is shown with the RL BeO FOD, again a sign of the little phosphorescence.

3.2.1. Percentage depth dose

Fig. 10a) shows the PDD measured with the RL BeO FOD for superficial X-rays of 150 kVp with a 0.5 mm Cu half value layer (HVL), and also that measured using a thin window ion chamber. The RL BeO FOD measurements were found to be within 2.5% of those measured from the thin window chamber. Fig. 10b) shows the PDD measured for superficial x-rays of 120 kVp with 5 mm Al HVL. A close

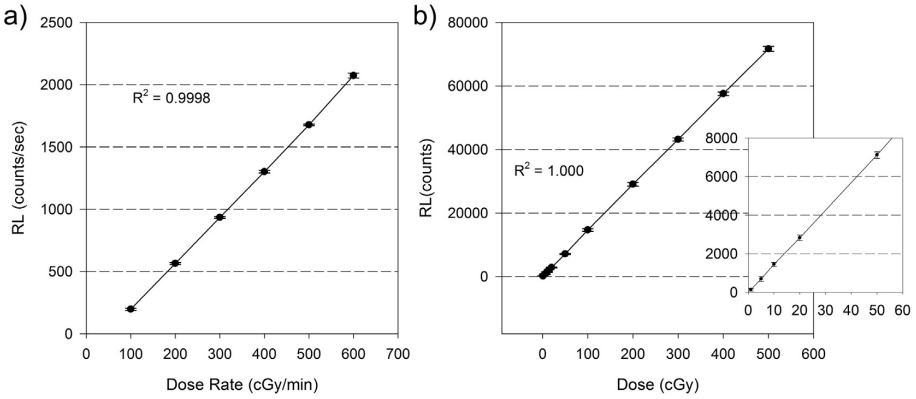

Fig. 7. The response of the RL BeO FOD to therapeutic a) dose-rates and b) doses, with the lower dose values magnified.

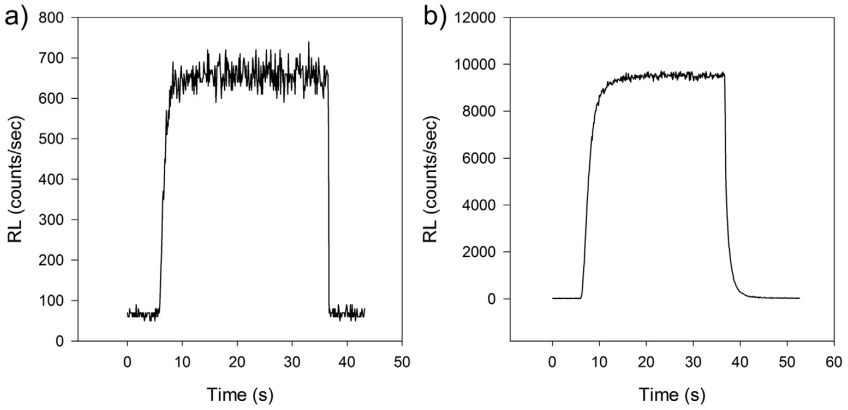

Fig. 9. The RL signal during the exposure of superficial X-rays for a) the RL BeO FOD and b) Al_2O_3:C.

agreement was found between the RL BeO FOD measurements and the thin window chamber, with no differences greater than 4%. These are acceptable discrepancies considering the difficulty of accurate measurements of superficial X-rays.

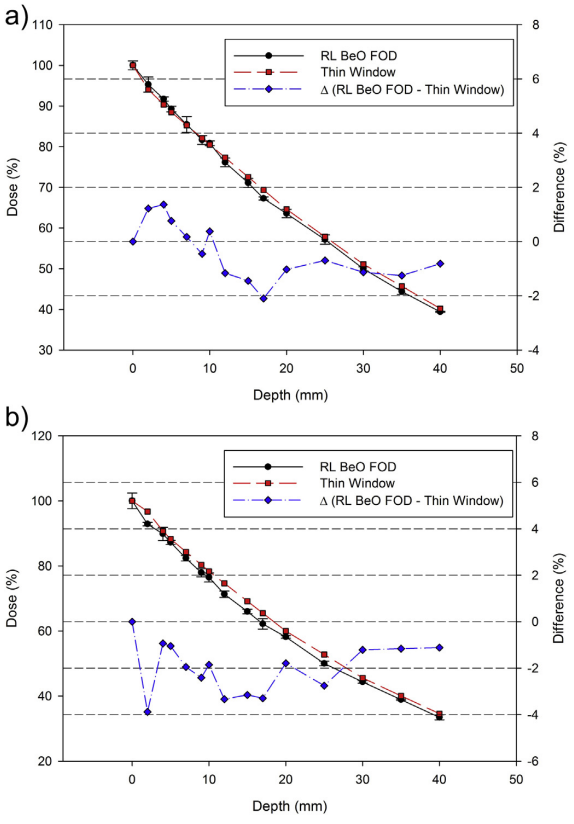

Fig. 10. The PDD curve for the RL BeO FOD and thin window ion chamber obtained using superficial X-rays of a) 150 kVp with HVL 0.5 mm Cu and b) 120 kVp with HVL 5 mm Al. The discrepancy between the RL BeO FOD and the thin window ion chamber is also shown in secondary axis.

4. Discussion

Using the high temporal resolution of the RL BeO FOD shown in Fig. 4, it is able to give a further understanding of the radiation produced by the linac, allowing for measurements such as dose per pulse and pulse repetition rate measurements recently investigated using plastic scintillators (Beierholm et al., 2011). Fig. 5 shows that the linac utilises the pulse repetition rate to control the delivered dose-rate. This property of BeO ceramic could be used for further investigation into the understanding of the radiation from linac systems.

It is important to note that the higher RL intensity shown in the 3 kHz measurements compared to the 1 Hz measurements is due to the duty-cycle of the linac radiation beam. In the case of the 1 Hz measurements the majority of each sample is between the radiation pulses, and hence a lower count rate. The use of the 3 kHz measurements for dosimetric purposes would require a more accurate stem effect removal technique. In the current study, the mean stem effect was subtracted from the entire RL measurement. However, a more appropriate method is required to measure the stem effect concurrently with the RL measurements and then subtract it from the signal. Considering the limitations of our setup, this will be considered in future studies.

The short radioluminescence lifetime, i.e. little phosphorescence measured from the BeO ceramic indicates that a temporal Cerenkov removal technique would not be plausible, but the linac radiation pulse information attainable is useful for a greater understanding of the radiation produced by linacs. With the RL emission band from BeO ceramic being ~280 nm, this would also make a Cerenkov spectral removal technique not feasible, due to the Cerenkov intensity being inversely proportional to wavelength. The best technique for optical fibre stem effect removal for the use of a BeO ceramic may be the use of an air-core optical fibre.

One disadvantage of the use of BeO ceramic is the lower RL intensity, which is shown in the comparison against Al_2O_3:C in Fig. 9. This is most likely due to a combination of lower RL efficiency for BeO ceramic, and the optical attenuation within the BeO ceramic (Lembo et al., 1990). PMMA optical fibres are also highly attenuating at the BeO ceramic emission wavelengths, other fibres such as silica fibres are less attenuating and could increase the sensitivity. The decrease in signal strength ultimately has an effect on the sensitivity of the dosimeter, which has not been found to be a problem in this study.

5. Conclusion

A BeO ceramic fibre optic dosimeter of small sensitive volume has been constructed. It has been found that the RL from a BeO ceramic has the potential for use as a reliable dosimeter in radiotherapy. The RL response from the BeO FOD has been shown to be linear for a range of therapeutic dose rates and doses. The percentage depth dose curves measured have shown that the BeO FOD shows no energy dependency in the megavoltage and superficial energy range, and hence shows promise for radiotherapy dosimetry. Further studies are necessary to investigate true energy independence of BeO ceramics response.

Summarizing, these results provide confidence of the application of BeO RL for dosimetry and to advance with investigations and construction of an RL/OSL BeO dosimeter, such that the OSL signal from a BeO detector can be characterised for accumulated dose measurements. BeO ceramics show promise to be a near tissue equivalent alternative to Al_2O_3:C crystals for fibre optic dosimetry, making it a more versatile dosimeter. Future applications of the BeO FOD will be use in *in-vivo* brachytherapy dosimetry and the dosimetry of superficial kV X-rays, where its near tissue equivalence will play a useful role.

Acknowledgements

The authors would like to thank Prof. Nigel Spooner of DSTO for the useful input to the project. The authors also thank Materion and Landauer for providing the BeO ceramic and Al_2O_3:C samples.

References

Albrecht, H.O., Mandeville, C.E., 1956. Storage of energy in beryllium oxide. Phys. Rev. 101, 1250.

Andersen, C.E., Marckmann, C.J., Aznar, M.C., Botter-Jensen, L., Kjaer-Kristoffersen, F., Medin, J., 2006. An algorithm for real-time dosimetry in intensity-modulated radiation therapy using the radioluminescence signal from Al_2O_3:C. Radiat. Prot. Dosim. 120, 7–13.

Andersen, C.E., Nielsen, S.K., Greilich, S., Helt-Hansen, J., Lindegaard, J.C., Tanderup, K., 2009a. Characterization of a fiber-coupled Al_2O_3:C luminescence dosimetry system for online in vivo dose verification during ^{192}Ir brachytherapy. Med. Phys. 36, 708–718.

Andersen, C.E., Nielsen, S.K., Lindegaard, J.C., Tanderup, K., 2009b. Time-resolved in vivo luminescence dosimetry for online error detection in pulsed dose-rate brachytherapy. Med. Phys. 36, 5033–5043.

Archambault, L., Beddar, A.S., Gingras, L., Lacroix, F., Roy, R., Beaulieu, L., 2007. Water-equivalent dosimeter array for small-field external beam radiotherapy. Med. Phys. 34, 1583–1592.

Aznar, M.C., Hemdal, B., Medin, J., Marckmann, C.J., Andersen, C.E., Botter-Jensen, L., Andersson, I., Mattsson, S., 2005. In vivo absorbed dose measurements in mammography using a new real-time luminescence technique. Br. J. Radiol. 78, 328–334.

Beddar, A.S., Kinsella, K.J., Ikhlef, A., Sibata, C.H., 2001. A miniature "scintillator-fiberoptic-PMT" detector system for the dosimetry of small fields in stereotactic radiosurgery. Nucl. Sci., IEEE Trans. 48, 924–928.

Beddar, A.S., Mackie, T.R., Attix, F.H., 1992a. Water-equivalent plastic scintillation detectors for high-energy beam dosimetry: I. Physical characteristics and theoretical consideration. Phys. Med. Biol. 37, 1883–1900.

Beddar, A.S., Mackie, T.R., Attix, F.H., 1992b. Water-equivalent plastic scintillation detectors for high-energy beam dosimetry: II. Properties and measurements. Phys. Med. Biol. 37, 1901.

Beierholm, A.R., Ottosson, R.O., Lindvold, L.R., Behrens, C.F., Andersen, C.E., 2011. Characterizing a pulse-resolved dosimetry system for complex radiotherapy beams using organic scintillators. Phys. Med. Biol. 56, 3033.

Bos, A.J.J., 2001. High sensitivity thermoluminescence dosimetry. Nucl. Instrum. Meth. Phys. Res. Section B: Beam Interact. Mat. Atoms 184, 3–28.

Bulur, E., Göksu, H.Y., 1998. OSL from BeO ceramics: new observations from an old material. Radiat. Meas. 29, 639–650.

Clift, M.A., Johnston, P.N., Webb, D.V., 2002. A temporal method of avoiding the Cerenkov radiation generated in organic scintillator dosimeters by pulsed mega-voltage electron and photon beams. Phys. Med. Biol. 47, 1421–1433.

Exposures, N.R.C.U.S.C.o.B.A., Toxicology, N.R.C.U.S.C.o., Toxicology, N.R.C.U.S.-B.o.E.S.a., (U.S.), N.A.P., NetLibrary, I., 2008. Managing Health Effects of Beryllium Exposure National Academies Press, p. 50.

Fontbonne, J.M., Iltis, G., Ban, G., Battala, A., Vernhes, J.C., Tillier, J., Bellaize, N., Brun, C.L., Tamain, B., Mercier, K., Motin, J.C., 2002. Scintillating fiber dosimeter for radiation therapy accelerator. IEEE Trans. Nucl. Sci. 49.

Klein, D.M., Tailor, R.C., Archambault, L., Wang, L., Therriault-Proulx, F., Beddar, A.S., 2010. Measuring output factors of small fields formed by collimator jaws and multileaf collimator using plastic scintillation detectors. Med. Phys. 37, 5541–5549.

Lambert, J., McKenzie, D.R., Law, S., Elsey, J., Suchowerska, N., 2006. A plastic scintillation dosimeter for high dose rate brachytherapy. Phys. Med. Biol. 51, 5505–5516.

Lambert, J., Yin, Y., McKenzie, D.R., Law, S., Suchowerska, N., 2008. Cerenkov-free scintillation dosimetry in external beam radiotherapy with an air core light guide. Phys. Med. Biol. 53, 3071–3080.

Lambert, J., Yin, Y., McKenzie, D.R., Law, S.H., Ralston, A., Suchowerska, N., 2010. A prototype scintillation dosimeter customized for small and dynamic megavoltage radiation fields. Phys. Med. Biol. 55, 1115–1126.

Lembo, L., Pimpinella, M., Mukherjee, B., 1990. Self optical attenuation coefficient of TL glow in BeO detectors. Radiat. Prot. Dosim. 33, 43–45.

Letourneau, D., Pouliot, J., Roy, R., 1999. Miniature scintillating detector for small field radiation therapy. Med. Phys. 26, 2555–2561.

Liu, P.Z.Y., Suchowerska, N., Lambert, J., Abolfathi, P., McKenzie, D.R., 2011. Plastic scintillation dosimetry: comparison of three solutions for the Cerenkov challenge. Phys. Med. Biol. 56, 5805.

Nowotny, R., 2007. Radioluminescence of some optical fibres. Phys. Med. Biol. 52, N67–N73.

Polf, J.C., McKeever, S.W., Akselrod, M.S., Holmstrom, S., 2002. A real-time, fibre optic dosimetry system using Al_2O_3 fibres. Radiat. Prot. Dosim. 100, 301–304.

Polf, J.C., Yukihara, E.G., Akselrod, M.S., McKeever, S.W., 2004. Real-time luminescence from Al_2O_3:C fiber dosimeters. Radiat. Meas. 38, 227–240.

Rhyner, C.R., Miller, W.G., 1970. Radiation dosimetry by optically-stimulated luminescence of BeO. Health Phys. 18, 681–684.

Scarpa, G., 1970. The dosimetric use of beryllium oxide as a thermoluminescent material: a preliminary study. Phys. Med. Biol. 15, 667.

Sommer, M., Freudenberg, R., Henniger, J., 2007. New aspects of a BeO-based optically stimulated luminescence dosimeter. Radiat. Meas. 42, 617–620.

Sommer, M., Jahn, A., Henniger, J., 2008. Beryllium oxide as optically stimulated luminescence dosimeter. Radiat. Meas. 43, 353–356.

Tochilin, E., Goldstein, N., Miller, W.G., 1969. Beryllium oxide As a thermoluminescent dosimeter. Health Phys. 16, 1–7.

Walsh, K.A., Vidal, E.E., 2009. Beryllium Chemistry and Processing. ASM International, p. 508.

Williamson, J.F., Dempsey, J.F., Kirov, A.S., Monroe, J.I., Binns, W.R., Hedtjarn, H., 1999. Plastic scintillator response to low-energy photons. Phys. Med. Biol. 44, 857–871.

Yukihara, E.G., 2011. Luminescence properties of BeO optically stimulated luminescence (OSL) detectors. Radiat. Meas. 46, 580–587.

4.4 RL BeO FOD labview

The developed LabView software had a number of different versions through this project. Initially, the method of controlling the sampling rate was by utilising an 'Elapsed Time' wait block. Unfortunately this was not an accurate method of doing this since the required wait time was very short. Figure 4.1 shows the final LabView block diagram used. A second counter is used as a clock for the sampling rate control. This is faster and hence more accurate than using the internal clock with the 'Elapsed Time' block.

In the case of the radiation pulse measurements discussed in the publication [P2], in order to speed up the recording system to achieve the high sampling rates necessary, the graphing function was removed from the LabView software. Therefore the data was not displayed in real-time and could only be analysed post exposure.

4.5 Discussion and conclusion

A small fibre-coupled BeO ceramic dosimetry system was developed capable of real-time RL measurements, named RL BeO FOD. Figure 4.2 shows the small BeO ceramic sensitive volume and optical fibre, side by side with a CC01 ionisation chamber (Wellhofer Dosimetrie, Germany). A portable RL reader system was developed that could be easily moved to a treatment suite for measurements, shown in figure 4.2. The RL BeO FOD was characterised with the use of a high energy 6 MV x-ray beam, and a 150 kVp and 120 kVp superficial x-ray beams.

Results showed that the response from the RL BeO FOD was reproducible and linear for a range of dose rates and doses. The percentage depth doses were within 3% agreement for the 6 MV beam and within 4% agreement for the superficial x-ray beams, indicating little energy dependence. These promising results provide confidence to proceed with developing and investigating an RL and OSL BeO ceramic dosimetry system.

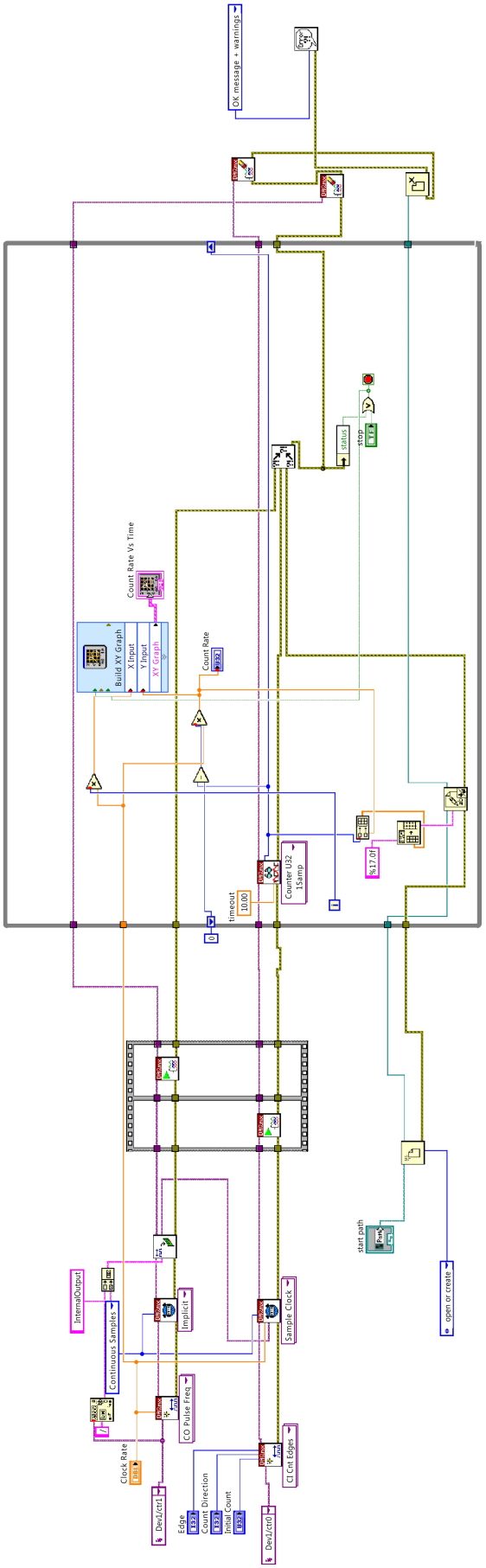

FIGURE 4.1: The block diagram of the final LabView software for the RL dosimetry system.

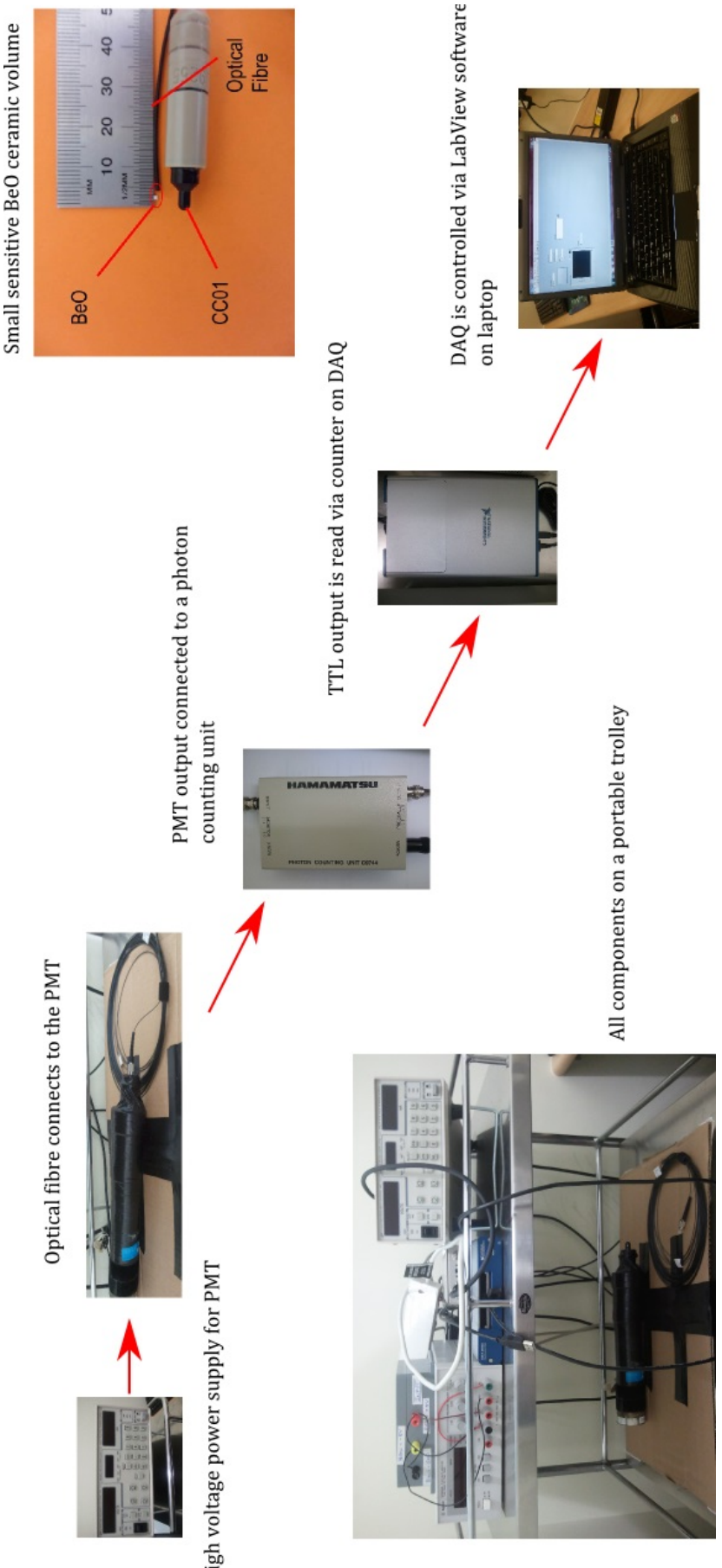

FIGURE 4.2: The RL reader system consisting of a 1 mm diameter, 1 mm long BeO ceramic sample butt-coupled to a polymethyl methacrylate (PMMA) optical fibre. The PMMA fibre is connected to a photomultiplier tube, which is connected to a photon counting unit. A data acquisition card (DAQ) is then used to count the TTL output from the photon counting unit.

Chapter 5

Beryllium oxide (BeO) ceramic RL & OSL dosimetry system

The publication [P3] forms the basis of this chapter.

Alexandre M. Caraça Santos, Mohammad Mohammadi and Shahraam Afshar V., Investigation of a fibre-coupled beryllium oxide (BeO) ceramic luminescence dosimetry system, *Radiation Measurements* 52-58, 2014.

5.1 Development overview and motivation

Continuing from the promise shown by the RL BeO FOD measurements, developing a dosimetry system which was capable of both RL and OSL was the following objective. As previously discussed, the OSL from BeO ceramics has been extensively investigated, however its potential use as an RL and OSL fibre-coupled dosimeter had not. In this chapter, the design, development and characterisation of the first RL and OSL BeO ceramic fibre-coupled dosimetry system, named RL/OSL BeO FOD, will be discussed.

5.2 Statement of Contribution

5.2.1 Conception

The idea to continue with the BeO ceramic probe and develop a radioluminescence and optically stimulated luminescence reader was conceptualised by Alexandre M. Caraça Santos.

5.2.2 Realisation

The development of the probe, system reader and the LabView code was performed by Alexandre M. Caraça Santos. The experiments performed to characterise the dosimetry system were also performed by Alexandre M. Caraça Santos.

5.2.3 Documentation

This paper was primarily written by Alexandre M. Caraça Santos. Editing was performed by all authors.

Statement of Authorship

Title of Paper	Investigation of a fibre-coupled beryllium oxide (BeO) ceramic luminescence dosimetry system
Publication Status	☑ Published ☐ Accepted for Publication ☐ Submitted for Publication ☐ Publication Style
Publication Details	Alexandre M. Caraca Santos, Mohammad Mohammadi and Shahraam Afshar V., Investigation of a fibre-coupled beryllium oxide (BeO) ceramic luminescence dosimetry system, Radiation Measurements 52-58, 2014.

Principal Author

Name of Principal Author (Candidate)	Alexandre Santos
Contribution to the Paper	Developed the OSL/RL reader system and the LabView program, performed all of the experimental measurements, and wrote the manuscript and acted as corresponding author.
Overall percentage (%)	
Signature	Date 12/1/2016

Co-Author Contributions

By signing the Statement of Authorship, each author certifies that:

i. the candidate's stated contribution to the publication is accurate (as detailed above);

ii. permission is granted for the candidate in include the publication in the thesis; and

iii. the sum of all co-author contributions is equal to 100% less the candidate's stated contribution.

Name of Co-Author	Mohammad Mohammadi
Contribution to the Paper	Supervised development of work and manuscript evaluation.
Signature	Date 12,01,2016

Name of Co-Author	Shahraam Afshar V.
Contribution to the Paper	Supervised development of work and manuscript evaluation.
Signature	Date 6/01/2016.

Radiation Measurements 70 (2014) 52–58

Contents lists available at ScienceDirect

Radiation Measurements

journal homepage: www.elsevier.com/locate/radmeas

Investigation of a fibre-coupled beryllium oxide (BeO) ceramic luminescence dosimetry system

Alexandre M. Caraça Santos [a, b, *], Mohammad Mohammadi [a, c], Shahraam Afshar V. [b]

[a] Department of Medical Physics, Royal Adelaide Hospital, Adelaide, South Australia, Australia
[b] Institute for Photonics & Advanced Sensing and School of Chemistry & Physics, University of Adelaide, Adelaide, South Australia, Australia
[c] Department of Medical Physics, Faculty of Medicine, Hamadan University of Medical Sciences, Hamadan, Iran

HIGHLIGHTS

- A fibre-coupled Beryllium oxide (BeO) ceramic dosimeter was developed, named RL/OSL BeO FOD.
- The RL/OSL BeO FOD is capable of real-time RL measurements and post exposure OSL measurements.
- 6 MV PDD found to be within 5% agreement with Ion chamber measurements.
- The RL is shown to be insensitive to the accumulated dose.

ARTICLE INFO

Article history:
Received 21 May 2014
Received in revised form
24 July 2014
Accepted 14 September 2014
Available online 22 September 2014

Keywords:
Fibre-coupled luminescence dosimetry
Beryllium oxide (BeO) ceramic
Radioluminescence
Scintillation
Optically stimulated luminescence

ABSTRACT

The purpose of this study is to investigate the potential use of a beryllium oxide (BeO) ceramic as a radioluminescence (RL) and optically stimulated luminescence (OSL) probe material for fibre-coupled luminescence dosimetry. A portable dosimetry system, named RL/OSL BeO FOD was developed, consisting of a 1 mm diameter, 1 mm long BeO ceramic cylinder coupled to a silica/silica optical fibre. The reader measures the RL signal and also uses a 450 nm laser diode to stimulate the BeO ceramic. A second background optical fibre is used to remove the stem effect. The RL/OSL BeO FOD was characterised in a solid water phantom, using a 6 MV x-ray beam. The RL was found to be reproducible and have a linear response to doses ranging from 30 cGy–15 Gy and dose rates from 100 cGy/min – 600 cGy/min. The OSL response was linear to doses of 10 Gy, becoming supralinear at higher doses. Measured percentage depth curves using the RL/OSL BeO FOD agreed with those measured using an IC15 ion chamber to within 5%, beyond the build up region. It was also found that the RL from BeO ceramic is unaffected by the delivered dose to the probe and hence, it remains constant for a given dose-rate. The insensitivity of the RL to accumulated dose makes BeO ceramic potentially capable of accurate dose-rate measurements without any corrections for the accumulated dose. This study demonstrates the feasibility of BeO ceramic as a versatile fibre-coupled luminescence dosimeter probe.

1. Introduction

Fibre-coupled luminescence dosimeters have been extensively investigated due to their desirable characteristics such as: small detector size, high sensitivity, low cost and all optical setup. These dosimeters are based on the use of a light emitting phosphor probe attached to an optical fibre. Various probes have been investigated, with the most interest being on the use of plastic scintillators (Beddar et al., 1992a,b) and Al_2O_3:C crystals (Polf et al., 2002).

Plastic scintillators are near water equivalent materials which emit light when exposed to ionising radiation, known as radioluminescence (RL) or scintillation. Their RL response has been reported to be proportional to the radiation dose-rate and independent of energy (Beddar et al., 1992a,b). When attached to an optical fibre and guided to an optical reader, plastic scintillators make for an ideal real-time dosimeter. These scintillation dosimeters have been applied to such areas as; small field dosimetry (Archambault et al., 2007; Beddar et al., 2001; Klein et al., 2010; Lambert et al., 2010; Letourneau et al., 1999) and brachytherapy dosimetry (Cartwright et al., 2010; Lambert et al., 2006a; Suchowerska et al., 2011).

* Corresponding author. Department of Medical Physics, Royal Adelaide Hospital, Adelaide, South Australia 5000, Australia. Tel.: +61 8 8222 5658.
E-mail address: alexandre.santos@adelaide.edu.au (A.M.C. Santos).

http://dx.doi.org/10.1016/j.radmeas.2014.09.007
1350-4487/

The major issue with scintillation fibre coupled dosimeters has been their susceptibility to the "stem effect", which is light produced in the optical fibre during its exposure to ionising radiation, either due to Cerenkov radiation or luminescence of the optical fibre (Beddar et al., 1992b; Nowotny, 2007; Therriault-Proulx et al., 2013). This is unwanted light collected by the system and needs to be removed or corrected for. The most recent techniques used to remove this stem effect have been the use of hyperspectral signal processing (Archambault et al., 2012), and the addition of an air-core optical fibre, which itself will not produce Cerenkov radiation (Lambert et al., 2009, 2010; Liu et al., 2011).

Plastic scintillators are expected to have a reduced response to low energy x-rays, where interaction processes are dominated by the photoelectric effect, due to a lower effective atomic number (Z_{eff}~5.7 and ρ~1.032–1.060 gcm^{-3}, for both polystyrene (PS) and polyvinyltoluene (PVT)), than water (Z_{eff}~7.4 and ρ~1.000 gcm^{-3}). Previous investigations have loaded plastic scintillators with higher atomic number elements to match the effective atomic number of water (Williamson et al., 1999). Along with the lower effective atomic number, plastic scintillators also have a non-linear response to low energy x-rays, known as ionisation quenching. Ionisation quenching has been reported to occur for electron energies below ~125 keV, making them not ideal for low energy x-rays (Williamson et al., 1999).

Al_2O_3:C crystals are inorganic materials which also exhibit RL, but unlike plastic scintillators, also store some charge when exposed to ionising radiation. These "trapped charges" can later be stimulated either by light or heat, such that they release their energy in the form of luminescence, known as optically stimulated luminescence (OSL) and thermoluminescence (TL), respectively. Al_2O_3:C crystal dosimeters are not only capable of the RL real-time dose-rate measurements, similar to plastic scintillators, but they are also able to have an OSL accumulated dose measurement after exposure (Polf et al., 2002, 2004). Hence the OSL brings another dimension to the dosimeter, making it capable of two readings from one exposure. This is a major advantage not only to improve the confidence in the dose measurement, but also to avoid the unwanted Cerenkov radiation, which plays no part in the OSL signal.

The major disadvantages of the use of Al_2O_3:C crystals are the high effective atomic number (Z_{eff}~11.1 and ρ~3.97 gcm^{-3}), and over response to low energy x-rays by a factor up to 3 relative to 1.25 MeV photons (Bos, 2001). The RL from Al_2O_3:C crystals has been reported to increase with increasing accumulated dose to the crystal. This is an issue since the RL is not constant for a constant dose-rate exposure, making it difficult to measure the dose-rate in a varying dose-rate field if the RL is not proportional to dose-rate (Andersen et al., 2006; Damkjaer et al., 2008). Though if operating in a saturated protocol, the RL is insensitive to dose but the Al_2O_3:C crystals can no longer be used for OSL readings (Andersen et al., 2011).

Beryllium oxide (BeO) ceramics also exhibit both RL and OSL, but in contrast to Al_2O_3:C crystals, have an effective atomic number comparable to water (Z_{eff}~7.1 and ρ~3.01 gcm^{-3}). BeO ceramic was initially investigated as a potential thermoluminescent dosimeter (TLD) material (Albrecht and Mandeville, 1956; Rhyner and Miller, 1970; Scarpa, 1970; Tochilin et al., 1969). Inhalation of beryllium has been known to cause a disease called Chronic Beryllium Disease (CBD) (Exposures et al., 2008). Therefore the use of BeO ceramic as a powder TLD is impractical and hence research activities stopped. However, BeO ceramic in solid form has not been shown to present any health risk, since if handled properly inhalation is unlikely (Walsh and Vidal, 2009).

Recent investigations into the luminescence properties of BeO have been undertaken (Bulur and Göksu, 1998; Sommer et al., 2007, 2008). Findings show that the OSL emission spectrum has two emission bands at ~310 nm and ~370 nm, and that the OSL intensity increases with decreasing stimulation wavelengths. The RL emission does not correspond to that of the OSL and has a peak at ~280 nm (Yukihara, 2011). The OSL dose response has been reported to be reproducible and linear up to a dose of 10 Gy and supralinear at higher doses. No energy dependency has been investigated for the RL, though the OSL has been shown to underrespond to low energy x-rays (Jahn et al., 2013). Due to the closely matched effective atomic number of BeO ceramics to water, they may prove to be a versatile probe.

In this study, we develop a fibre-coupled luminescence dosimeter that utilises a BeO probe for RL and OSL measurements. This is an extension of our previous investigation (Santos et al., 2013), in which we only considered the use of the RL from BeO ceramic, independent from OSL. Here, a portable RL and OSL BeO ceramic fibre optic dosimeter (FOD) is built, named RL/OSL BeO FOD, which uses the RL from a BeO ceramic probe for real-time dose-rate measurements and also stimulates the BeO ceramic to perform OSL readings for accumulated dose measurements. We report on the characterisation of the RL/OSL BeO FOD for 6 MV x-rays. In particular, we show that the RL/OSL BeO FOD does not have the issue of the RL response increasing with accumulated dose for a constant dose-rate, which has been the case for Al_2O_3:C crystals.

2. Materials and methods

2.1. Dosimeter design

Fig. 1 depicts the dosimetry system. A single probe was constructed, consisting of a 1.0 mm diameter cylinder of 1.0 mm length BeO ceramic probe (Thermalox 995, Materion, USA). The BeO ceramic probe is butt-coupled to a 15 m long silica/silica optical fibre, with a core diameter of 0.4 mm (PolymicroTechnologies™, Molex, U.S.A.). The BeO ceramic is in solid form, and hence does not present any health risks. BeO ceramics are self optically attenuating, hence attenuating its own light (Lembo et al., 1990). Our previous investigation into this property showed that for a butt-coupled design there is no increase in light collection beyond a 1 mm length probe (Santos et al., 2014). The silica/silica optical fibre was chosen because of its low attenuation for the BeO ceramic emission spectrum, with a typical attenuation of 0.1 dB/m at a wavelength of 350 nm. A light tight heat shrink was used to encapsulate the BeO ceramic and the optical fibre, and to prevent any external light entry. The optical fibre is then connected to an in-house built portable reader located outside of the treatment bunker.

The reader consists of a Z-laser ZM18, 40 mW blue (450 nm) laser diode (Z-laser, Germany), to stimulate the BeO ceramic, which is coupled to the optical fibre using a fibre collimator. The OSL is read in continuous-wave mode, where the BeO ceramic is continuously illuminated by the laser. A blue light stimulation source was chosen because it has the best probability of OSL stimulation (Yukihara, 2011). The stimulated OSL signal is guided back to the reader by the same optical fibre, and reflected towards a Hamamatsu H7360-01 photon counting head (Hamamatsu, Japan) using a UV-blue dichroic beamsplitter. To separate any stimulation light still reflected by the beamsplitter from the BeO ceramic emission six 2.5 mm thick Hoya U-340 optical filters (UQG Ltd., England) were placed in front of the photon counter head. All components are enclosed within a light tight, metallic enclosure.

A data acquisition card (DAQ), USB-6341 (National Instruments Inc., USA), which has four 32 bit counters with a time base of up to 100 MHz, was used to control the laser and read the photon counter head. A customised LabVIEW™ (National Instruments Inc., USA) program was developed to interface with the USB-DAQ. Unless stated, a sampling rate of 10 Hz was used when reading the counters.

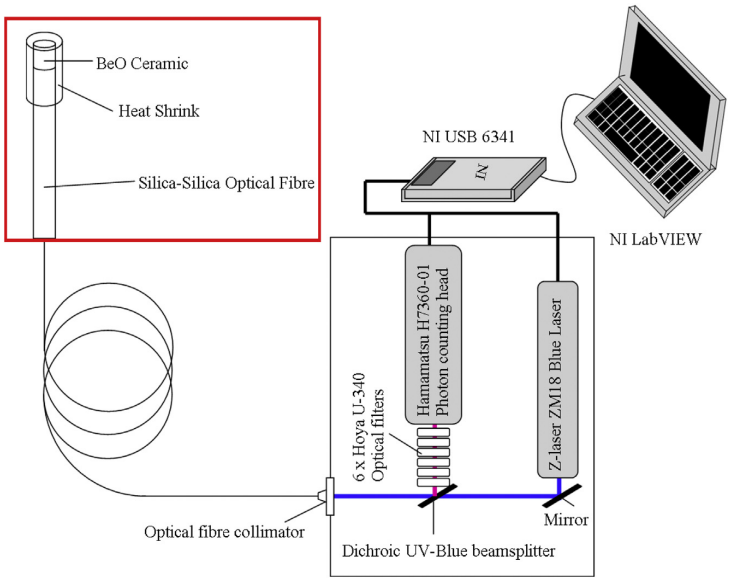

Fig. 1. The portable RL/OSL BeO FOD setup, capable of real time RL measurements and CW-OSL measurements. A second background optical fibre is used to remove the stem effect.

During exposure to ionising radiation, the RL is guided by the optical fibre to the reader. At the reader, the RL is reflected by the beamsplitter toward the photon counting head. After exposure, the OSL can be stimulated and measured as discussed above. The measurement procedure is depicted in Fig. 2. During the OSL measurement the BeO ceramic is optically bleached. This is where the laser is turned on for a time period long enough to release any trapped charge in the BeO ceramic, preparing it for its next irradiation. For all measurements the optical stimulation following exposure was for 180s. A background subtraction was made using the mean value from the last 20 s of the OSL decay curve. This background estimate accounts for residual laser light due to imperfect filtration.

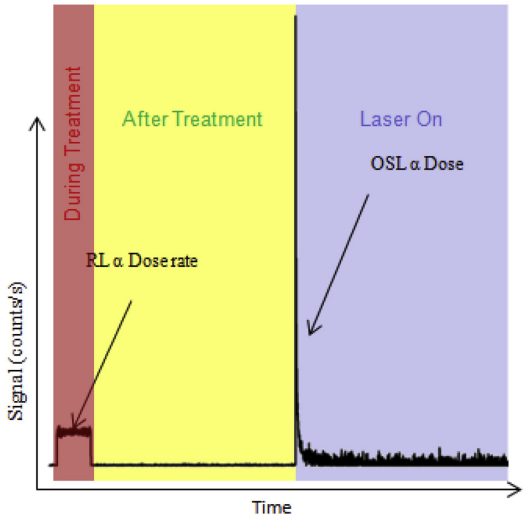

Fig. 2. The measurement procedure used to determine the dose-rate in real-time from the RL signal and the accumulated dose from the integrated OSL signal.

During the RL measurements, the stem effect produced in the optical fibre was accounted for by using a second optical fibre that does not have a BeO ceramic tip. This background fibre was placed alongside the RL/OSL BeO FOD such that it measures the background light. For each measurement of the RL/OSL BeO FOD, a repeat was performed and a reading from the background fibre taken. The light measured by the background fibre was then subtracted from that measured by the RL/OSL BeO FOD. At all times the RL/OSL BeO FOD was oriented perpendicular to the beam and in the central axis of the beam, such that any angular dependence from the stem effect can be controlled. Clinically this method would not be adequate, but it was considered sufficient for the purpose of evaluating the BeO ceramic probe.

A 6 MV x-ray beam from a linear accelerator (linac), Clinac 600C/D (Varian Medical Systems, Inc., Palo Alto, CA, USA) was utilized to investigate the response of the RL/OSL BeO FOD. All measurements were performed in a solid water phantom (Gammex RMI, Middleton, U.S.A). The setup within the solid water phantom was in reference conditions at all times, corresponding to a field size of 10×10 cm^2, and a source to surface distance (SSD) of 100 cm, allowing for the properties of the RL/OSL BeO FOD to be evaluated for representative therapeutic beam properties. The RL/OSL BeO FOD was placed at a depth of 1.5 cm, sandwiched between 2 mm thick slabs of solid water, which did not allow for large air gaps.

Unless stated all presented data corresponds to the mean of five measurements, and all uncertainties presented correspond to two standard deviations on the mean measurements.

2.2. Radioluminescence response with accumulated dose

The RL response of BeO ceramic as the accumulated dose increases was investigated. This was performed by initially bleaching the BeO ceramic with the laser light, followed by delivering a dose of 20 Gy to the RL/OSL BeO FOD. We then observed the RL as the accumulated dose to the BeO ceramic increased.

2.3. Fading

Fading of the OSL signal may occur as the time between exposure and reading of the OSL is increased. Ideally, in a clinical situation the OSL would be read directly after the exposure has taken place. Therefore a 30 s to 10 min delay period was chosen to investigate the short-term fading. This was done by delivering a clinically appropriate dose of 1 Gy, and comparing the measured OSL for different delay periods between the exposure and the laser being turned on. For all other experiments a delay time of 1 min was applied.

2.4. Reproducibility

The reproducibility of the RL/OSL BeO FOD after repeated use was investigated by exposing the RL/OSL BeO FOD to a dose of 1 Gy. This was performed ten times to investigate how both the RL and OSL vary with repeated measurements. During this measurement all of the experimental parameters were kept constant.

2.5. Dose and dose-rate response

The linearity of both the RL and OSL was investigated for both dose rate and dose. The dose-rate response was investigated by varying the repetition rate of the linac for dose rates from 100 cGy/min to 600 cGy/min, with 1 Gy delivered. The dose response was investigated for a range from 30 cGy–15 Gy. This dose range was chosen because of its clinical use.

2.6. Percentage depth dose

Percentage depth dose (PDD) curves were measured in solid water for depths from 0.7 cm to 30 cm, for both the RL and OSL. The measured PDDs were then compared to PDDs collected by a Wellhofer IC15 ion chamber (0.13 cm^3 volume, 0.6 cm internal diameter), oriented perpendicularly to the beam during the beam data acquisition in a water tank.

3. Results and discussion

For the RL measurements the stem effect signal from the optical fibre for our setup was found to be of the order of 50% of the RL signal, and hence very significant. For the OSL measurements, the decay lifetime was very fast, with a decay constant for a 1 Gy delivered dose of approximately 0.5 s. Therefore for all measurements the OSL was defined as the integration of the first 10 s of the OSL decay. There was a residual OSL stimulation laser light of ~7500 counts/s, which is corrected from each OSL measurement. The background estimate used in the OSL readings was not observed to systematically increase from one OSL reading to the next. Therefore it was assumed that there was no residual OSL signal in the background estimate, and that each OSL reading was assumed to be fully bleaching the BeO ceramic. Also, no OSL was measured from the background optical fibre with no BeO ceramic attached.

3.1. Radioluminescence response to accumulated dose

Fig. 3 shows the RL response with accumulated dose after bleaching, for a 20 Gy dose at 300 cGy/min. The mean value for the RL response of 2.42×10^3 counts/s is also plotted, with the RL response having a standard deviation of 1.8% over the exposure. Therefore it can be seen that there is little variation on the measured RL with accumulated dose, and hence can be treated as constant for a constant dose-rate. This is an important result as it implies that the RL/OSL BeO FOD is capable of measuring dose-rate and the change in dose-rate without any corrections for the accumulated dose to the sensitive material, which is not the case in Al_2O_3:C crystals unless operating in a saturated protocol (Andersen et al., 2011).

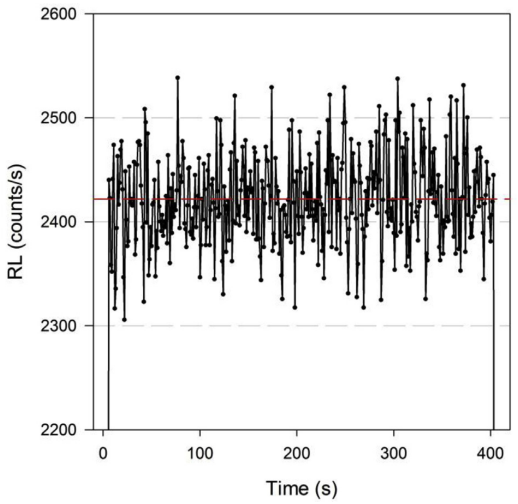

Fig. 3. The radioluminescence response for a 20 Gy irradiation, with the mean RL plotted in red. (For interpretation of the references to colour in this figure legend, the reader is referred to the web version of this article.)

The accumulated dose insensitivity observed, may be due to the BeO ceramic being in a stable state. This may be caused by the optical bleaching not entirely emptying the traps in BeO ceramic.

3.2. Fading

Fig. 4 shows the short term fading of the OSL response, normalised to the mean of all delay periods. As can be seen, no change in the response is observed. Hence the fading of the OSL for the BeO ceramic within the first 10 min after exposure is negligible. The shortest delay measurement at 30 s is also less reproducible than the others. This may be due to the presence of unstable shallow traps.

While we have not observed any noticeable fading of OSL signal at 1 Gy in our study, there is a report of a few percent fading in the

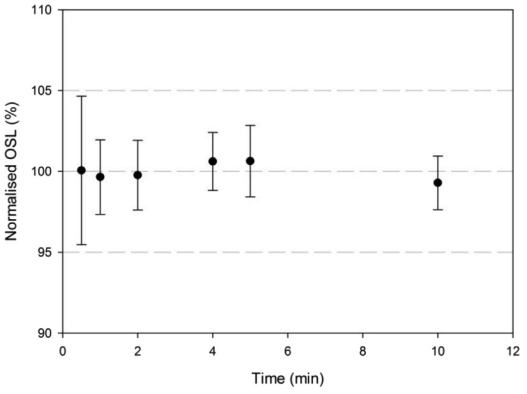

Fig. 4. The normalised OSL response for different delay periods between the exposure and the laser stimulation.

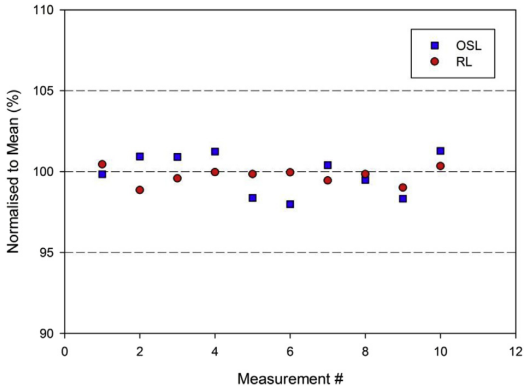

Fig. 5. The normalised RL and OSL response for 10 consecutive 1 Gy exposures.

OSL of BeO ceramic at low doses of 1 mGy (Jahn et al., 2013). This discrepancy may be because of the different dose ranges for which the fading was investigated. It should be noted that the aim of this study is to develop a fibre-based dosimeter for clinical applications in which the radiation dose are typically > 1Gy. Hence, it is expected that fading does not introduce any noticeable effect in clinical applications.

3.3. Reproducibility

Fig. 5 shows the mean RL and the corresponding OSL for 10 consecutive measurements. They are displayed as a percentage of the calculated mean of all 10 measurements. It can be seen that the mean RL and OSL are reproducible to within 2.5%, with a two standard deviation uncertainty of 2.6% for the OSL and 1.03% for the RL.

3.4. Dose and dose-rate response

Fig. 6 shows the dose response for the integrated OSL and RL signals for a dose range of 30 cGy–15 Gy. The RL dose response shown in Fig. 6a) is linear in the investigated dose range. The percentage deviation from a linear curve is also shown in Fig. 6a), with a 2.5% maximum deviation from a linear fit.

The OSL dose response is linear up ~10 Gy, becoming supralinear at higher doses. A supralinearity factor of 9.4% at 15 Gy was measured for the OSL response. Therefore a quadratic polynomial curve was fit to the OSL response and the percentage deviation from this curve is given in Fig. 6b). It can be seen that the curve is best fit at higher doses. Using the dose response curves from Fig. 6, the reproducibility of the RL/OSL BeO FOD from Fig. 5 can now be presented in terms of dose. We have measured 1.00 ± 0.03 Gy and 1.00 ± 0.01 Gy, for the OSL and RL respectively.

Fig. 7 shows the dose-rate response of the RL and OSL measurements by varying the repetition rate on the linac for a range from 100 cGy/min – 600 cGy/min. It can be seen that the RL has a linear response with dose-rate. The percentage deviation from a linear curve is given in Fig. 7a), with a 1% maximum deviation. The OSL response can be seen to be independent to dose-rate.

3.5. Percentage depth dose

Fig. 8 shows the measured 6 MV PDDs for both the OSL and RL signals, normalised to the depth of maximum dose measured by the IC15 ion chamber. It can be seen that beyond the build-up region the mean value for both the RL and the corresponding OSL measurements agree with the IC15 ion chamber measurements within 5%, and within statistical uncertainty. This indicates that the RL/OSL BeO FOD response is similar to water in the megavoltage x-ray energy range.

Within the build-up region there is a discrepancy between the RL/OSL BeO FOD and IC15 ion chamber measurements of above 5%. Further investigation is needed to identify the reason for this discrepancy. It can also be seen that at depth, the RL measured PDD is in better agreement with the IC15 ion chamber than the OSL measured PDD. This is due to the greater dynamic range and reproducibility of the RL signal from the RL/OSL BeO FOD.

4. Conclusion

In summary, a RL/OSL BeO FOD has been developed and tested. This dosimeter utilises the RL signal from a BeO ceramic probe for real-time dose rate measurements, and the OSL signal for an accumulated dose measurement. A second background optical fibre is used to remove the stem effect. We have shown both the RL and OSL signals to be reproducible. No OSL fading within the first 10 min after exposure is seen, and the OSL response is shown to be

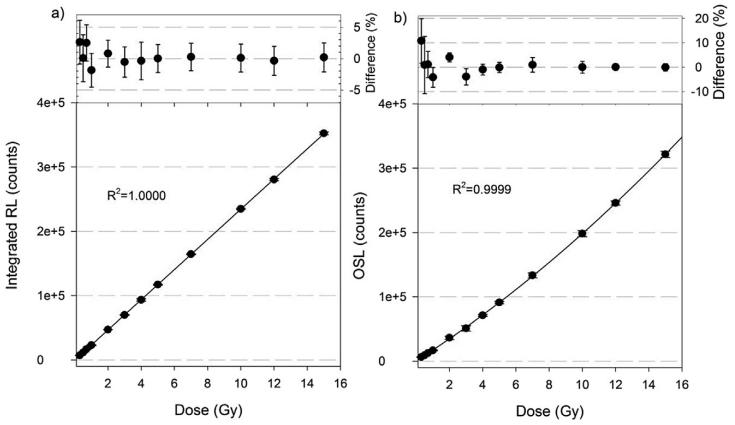

Fig. 6. The dose response for a) the integrated RL measurements and b) the OSL measurements, with the percentage deviation from their curves of best fit graphed above each.

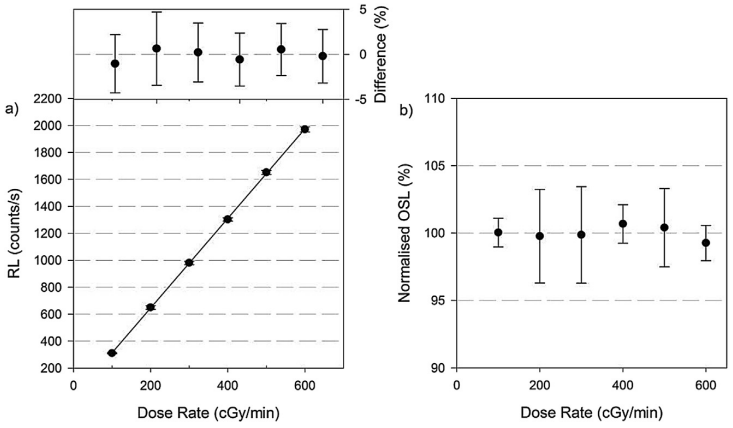

Fig. 7. The dose-rate response by varying the nominal repetition rate for a) the RL intensity and b) the OSL measurements, with the percentage deviation from their curves of best fit graphed above each.

supralinear to doses greater than 10 Gy, and independent to dose-rate. The RL is shown to be linear to dose-rates from 100 cGy/min – 600 cGy/min, and that the integral of the RL responded linearly to doses from 30 cGy–15 Gy. PDD curves measured are within 5% agreement to ion chamber measurements, further confirming the feasibility of BeO ceramic as an MV dosimeter.

The use of both plastic scintillators and Al_2O_3:C crystals has disadvantages. While plastic scintillators are near water equivalent, they have a decreased response at lower energy x-rays due to ionisation quenching (Williamson et al., 1999). This general problem still remains to be investigated for BeO ceramic. Al_2O_3:C crystals exhibit OSL, but have a high effective atomic number and have an RL response which increases with increasing dose to the probe (Damkjaer et al., 2008). We find that the RL from BeO ceramic does not increase with increasing dose to the probe, which has been possibly the biggest disadvantage of Al_2O_3:C crystals.

Optimisation of the optics in the reader, such as the optical filters, would be of interest to increase the dynamic range of the detector. In measuring the RL, stem effect from the optical fibre has been shown to be of significance, ~50% of the RL signal measured. While we use a background fibre to correct for the stem effect, future investigations into novel stem effect removal techniques, as discussed in the introduction, will be helpful to increase the signal-to-noise of the RL. Previous work has shown that a time-resolved removal of the stem effect for pulsed radiation is unlikely to be possible for BeO ceramic due to a short lifetime for the RL (Santos et al., 2013).

The OSL and RL from BeO ceramics are less sensitive than those from Al_2O_3:C crystals (Santos et al., 2013; Yukihara, 2011). Future work comparing plastic scintillators, BeO ceramics and Al_2O_3:C crystals would be of interest. Both plastic scintillators and Al_2O_3:C crystals have been applied to high dose rate (HDR) brachytherapy (Andersen et al., 2009a,b; Cartwright et al., 2010; Kertzscher et al., 2011; Lambert et al., 2006b; Suchowerska et al., 2011). The closely matched effective atomic number of BeO ceramics and water may be of interest for clinical treatments where lower energy photons are used, such as HDR brachytherapy. Further investigations into energy and angular dependency are required to evaluate the applicability of the system to HDR brachytherapy.

In this study only a single probe was developed and characterised. In future investigations it would be of interest to compare a number of RL/OSL BeO FODs in order to characterise inter detector variability.

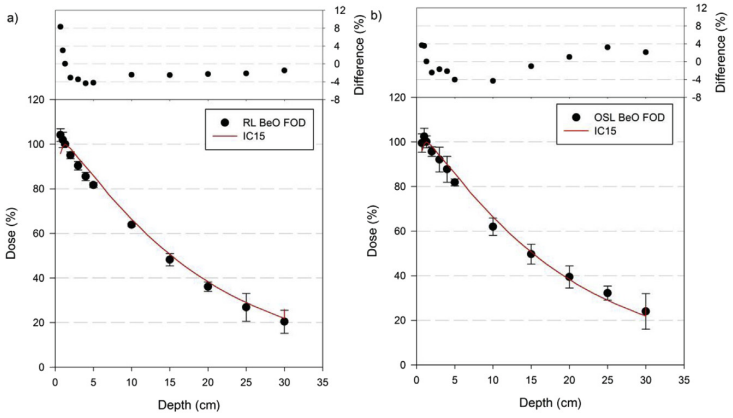

Fig. 8. The measured 6 MV PDDs using a) the RL measurements and b) the OSL measurements, with the percentage difference between the RL/OSL BeO FOD and IC15 ion chamber graphed above each.

Acknowledgements

The authors would like to thank Mr. John Schneider, from the Royal Adelaide Hospital, for his help in the design and construct of the light tight, metallic enclosure for the reader. We also acknowledge the funding support of the School of Chemistry and Physics of the University of Adelaide.

References

Albrecht, H.O., Mandeville, C.E., 1956. Storage of energy in beryllium oxide. Phys. Rev. 101, 1250.
Andersen, C.E., Damkjær, S.M.S., Kertzscher, G., Greilich, S., Aznar, M.C., 2011. Fiber-coupled radioluminescence dosimetry with saturated Al_2O_3:C crystals: characterization in 6 and 18 MV photon beams. Radiat. Meas. 46, 1090–1098.
Andersen, C.E., Marckmann, C.J., Aznar, M.C., Botter-Jensen, L., Kjaer-Kristoffersen, F., Medin, J., 2006. An algorithm for real-time dosimetry in intensity-modulated radiation therapy using the radioluminescence signal from Al_2O_3:C. Radiat. Prot. Dosim. 120, 7–13.
Andersen, C.E., Nielsen, S.K., Greilich, S., Helt-Hansen, J., Lindegaard, J.C., Tanderup, K., 2009a. Characterization of a fiber-coupled Al_2O_3:C luminescence dosimetry system for online in vivo dose verification during I192r brachytherapy. Med. Phys. 36, 708–718.
Andersen, C.E., Nielsen, S.K., Lindegaard, J.C., Tanderup, K., 2009b. Time-resolved in vivo luminescence dosimetry for online error detection in pulsed dose-rate brachytherapy. Med. Phys. 36, 5033–5043.
Archambault, L., Beddar, A.S., Gingras, L., Lacroix, F., Roy, R., Beaulieu, L., 2007. Water-equivalent dosimeter array for small-field external beam radiotherapy. Med. Phys. 34, 1583–1592.
Archambault, L., Therriault-Proulx, F., Beddar, S., Beaulieu, L., 2012. A mathematical formalism for hyperspectral, multipoint plastic scintillation detectors. Phys. Med. Biol. 57, 7133.
Beddar, A.S., Kinsella, K.J., Ikhlef, A., Sibata, C.H., 2001. A miniature "scintillator-fiberoptic-PMT" detector system for the dosimetry of small fields in stereotactic radiosurgery. Nucl. Sci. IEEE Trans. 48, 924–928.
Beddar, A.S., Mackie, T.R., Attix, F.H., 1992a. Water-equivalent plastic scintillation detectors for high-energy beam dosimetry: I. physical characteristics and theoretical consideration. Phys. Med. Biol. 37, 1883–1900.
Beddar, A.S., Mackie, T.R., Attix, F.H., 1992b. Water-equivalent plastic scintillation detectors for high-energy beam dosimetry: II. properties and measurements. Phys. Med. Biol. 37, 1901.
Bos, A.J.J., 2001. High sensitivity thermoluminescence dosimetry. Nucl. Instrum. Methods Phys. Res. Sect. B Beam Interact. Mater. Atoms 184, 3–28.
Bulur, E., Göksu, H.Y., 1998. OSL from BeO ceramics: new observations from an old material. Radiat. Meas. 29, 639–650.
Cartwright, L.E., Suchowerska, N., Yin, Y., Lambert, J., Haque, M., McKenzie, D.R., 2010. Dose mapping of the rectal wall during brachytherapy with an array of scintillation dosimeters. Med. Phys. 37, 2247–2255.
Damkjaer, S.M.S., Andersen, C.E., Aznar, M.C., 2008. Improved real-time dosimetry using the radioluminescence signal from Al_2O_3:C. Radiat. Meas. 43, 893–897.
Exposures, N.R.C.U.S.C.o.B.A., Toxicology, N.R.C.U.S.C.o., Toxicology, N.R.C.U.S.-B.o.E.S.a., (U.S.), N.A.P., NetLibrary, I., 2008. Managing Health Effects of Beryllium Exposure. National Academies Press, p. 50.
Jahn, A., Sommer, M., Ullrich, W., Wickert, M., Henniger, J., 2013. The BeOmax system – dosimetry using OSL of BeO for several applications. Radiat. Meas. 56, 324–327.
Kertzscher, G., Andersen, C.E., Siebert, F.-A., Nielsen, S.K., Lindegaard, J.C., Tanderup, K., 2011. Identifying afterloading PDR and HDR brachytherapy errors using real-time fiber-coupled Al_2O_3:C dosimetry and a novel statistical error decision criterion. Radiother. Oncol. J. Eur. Soc. Ther. Radiol. Oncol. 100, 456–462.
Klein, D.M., Tailor, R.C., Archambault, L., Wang, L., Therriault-Proulx, F., Beddar, A.S., 2010. Measuring output factors of small fields formed by collimator jaws and multileaf collimator using plastic scintillation detectors. Med. Phys. 37, 5541–5549.
Lambert, J., McKenzie, D.R., Law, S., Elsey, J., Suchowerska, N., 2006a. A plastic scintillation dosimeter for high dose rate brachytherapy. Phys. Med. Biol. 51, 5505–5516.
Lambert, J., McKenzie, D.R., Law, S., Elsey, J., Suchowerska, N., 2006b. A plastic scintillation dosimeter for high dose rate brachytherapy. Phys. Med. Biol. 51, 5505.
Lambert, J., Yin, Y., McKenzie, D.R., Law, S., Suchowerska, N., 2009. Cerenkov light spectrum in an optical fiber exposed to a photon or electron radiation therapy beam. Appl. Opt. 48, 3362–3367.
Lambert, J., Yin, Y., McKenzie, D.R., Law, S.H., Ralston, A., Suchowerska, N., 2010. A prototype scintillation dosimeter customized for small and dynamic megavoltage radiation fields. Phys. Med. Biol. 55, 1115–1126.
Lembo, L., Pimpinella, M., Mukherjee, B., 1990. Self optical attenuation coefficient of TL glow in BeO detectors. Radiat. Prot. Dosim. 33, 43–45.
Letourneau, D., Pouliot, J., Roy, R., 1999. Miniature scintillating detector for small field radiation therapy. Med. Phys. 26, 2555–2561.
Liu, P.Z.Y., Suchowerska, N., Lambert, J., Abolfathi, P., McKenzie, D.R., 2011. Plastic scintillation dosimetry: comparison of three solutions for the cerenkov challenge. Phys. Med. Biol. 56, 5805.
Nowotny, R., 2007. Radioluminescence of some optical fibres. Phys. Med. Biol. 52, N67–N73.
Polf, J.C., McKeever, S.W., Akselrod, M.S., Holmstrom, S., 2002. A real-time, fibre optic dosimetry system using Al_2O_3 fibres. Radiat. Prot. Dosim. 100, 301–304.
Polf, J.C., Yukihara, E.G., Akselrod, M.S., McKeever, S.W., 2004. Real-time luminescence from Al_2O_3:C fiber dosimeters. Radiat. Meas. 38, 227–240.
Rhyner, C.R., Miller, W.G., 1970. Radiation dosimetry by optically-stimulated luminescence of BeO. Health Phys. 18, 681–684.
Santos, A.M., Mohammadi, M., Afshar, S.V., 2014. Optimal light collection from diffuse sources: application to optical fibre-coupled luminescence dosimetry. Opt. Express 22, 4559–4574.
Santos, A.M.C., Mohammadi, M., Asp, J., Monro, T.M., Afshar, V.S., 2013. Characterisation of a real-time fibre-coupled beryllium oxide (BeO) luminescence dosimeter in X-ray beams. Radiat. Meas. 53–54, 1–7.
Scarpa, G., 1970. The dosimetric use of beryllium oxide as a thermoluminescent material: a preliminary study. Phys. Med. Biol. 15, 667.
Sommer, M., Freudenberg, R., Henniger, J., 2007. New aspects of a BeO-based optically stimulated luminescence dosimeter. Radiat. Meas. 42, 617–620.
Sommer, M., Jahn, A., Henniger, J., 2008. Beryllium oxide as optically stimulated luminescence dosimeter. Radiat. Meas. 43, 353–356.
Suchowerska, N., Jackson, M., Lambert, J., Yin, Y.B., Hruby, G., McKenzie, D.R., 2011. Clinical trials of a urethral dose measurement system in brachytherapy using scintillation detectors. Int. J. Radiat. Oncol. Biol. Phys. 79, 609–615.
Therriault-Proulx, F., Beaulieu, L., Archambault, L., Beddar, S., 2013. On the nature of the light produced within PMMA optical light guides in scintillation fiber-optic dosimetry. Phys. Med. Biol. 58, 2073.
Tochilin, E., Goldstein, N., Miller, W.G., 1969. Beryllium oxide as a thermoluminescent dosimeter. Health Phys. 16, 1–7.
Walsh, K.A., Vidal, E.E., 2009. Beryllium chemistry and processing. ASM Int. 508.
Williamson, J.F., Dempsey, J.F., Kirov, A.S., Monroe, J.I., Binns, W.R., Hedtjarn, H., 1999. Plastic scintillator response to low-energy photons. Phys. Med. Biol. 44, 857–871.
Yukihara, E.G., 2011. Luminescence properties of BeO optically stimulated luminescence (OSL) detectors. Radiat. Meas. 46, 580–587.

5.3 RL/OSL BeO FOD LaBview

Figure 5.1 shows the user interface for the final LabView version. Here the user inputs the RL threshold, laser wait time and laser on time. The system will then control the laser automatically once the RL has fallen below a specified threshold. As shown in figure 5.2 the final block diagram has significantly increased in complexity from the initially used LabView. A Matlab function was included in the final version to automate the RL and OSL analysis for the user.

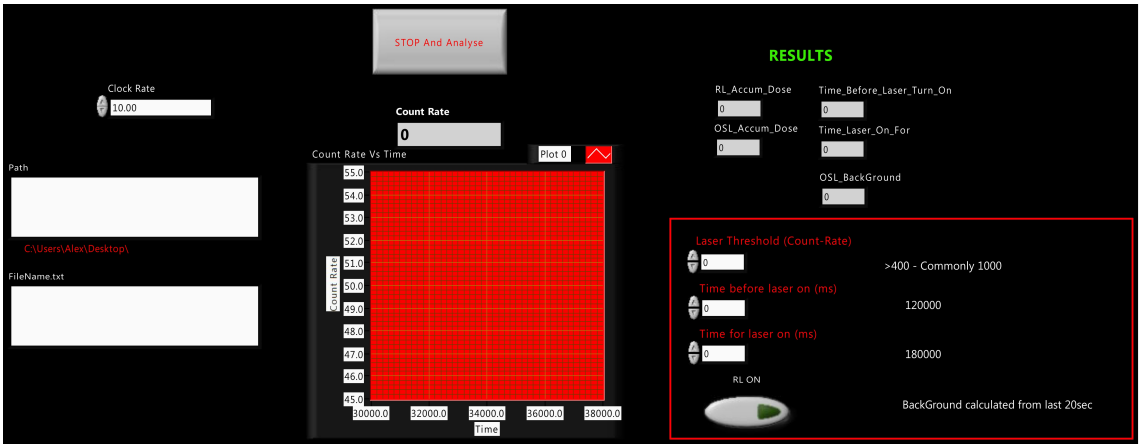

FIGURE 5.1: The final LabView user interface developed to automate the RL and OSL measurements and analysis for the RL/OSL BeO FOD.

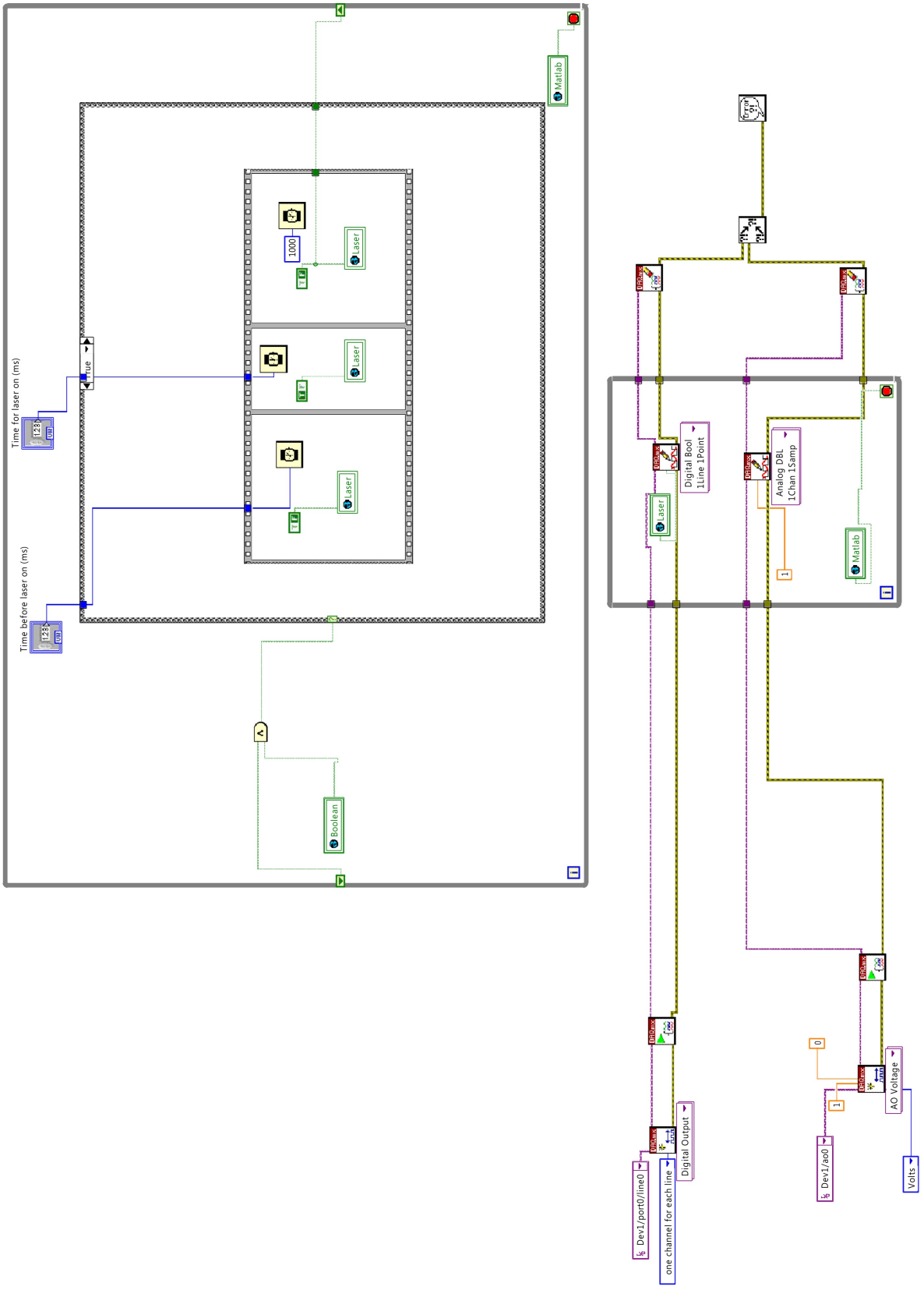
Matlab
1000
Laser
Laser
Laser
True
Time for laser on (ms)
Time before laser on (ms)
Boolean
Digital Bool
1Line 1Point
Analog DBL
1Chan 1Samp
Laser
Matlab
1
0
1
AO Voltage
Volts
Digital Output
one channel for each line
Dev1/port0/line0
Dev1/ao0

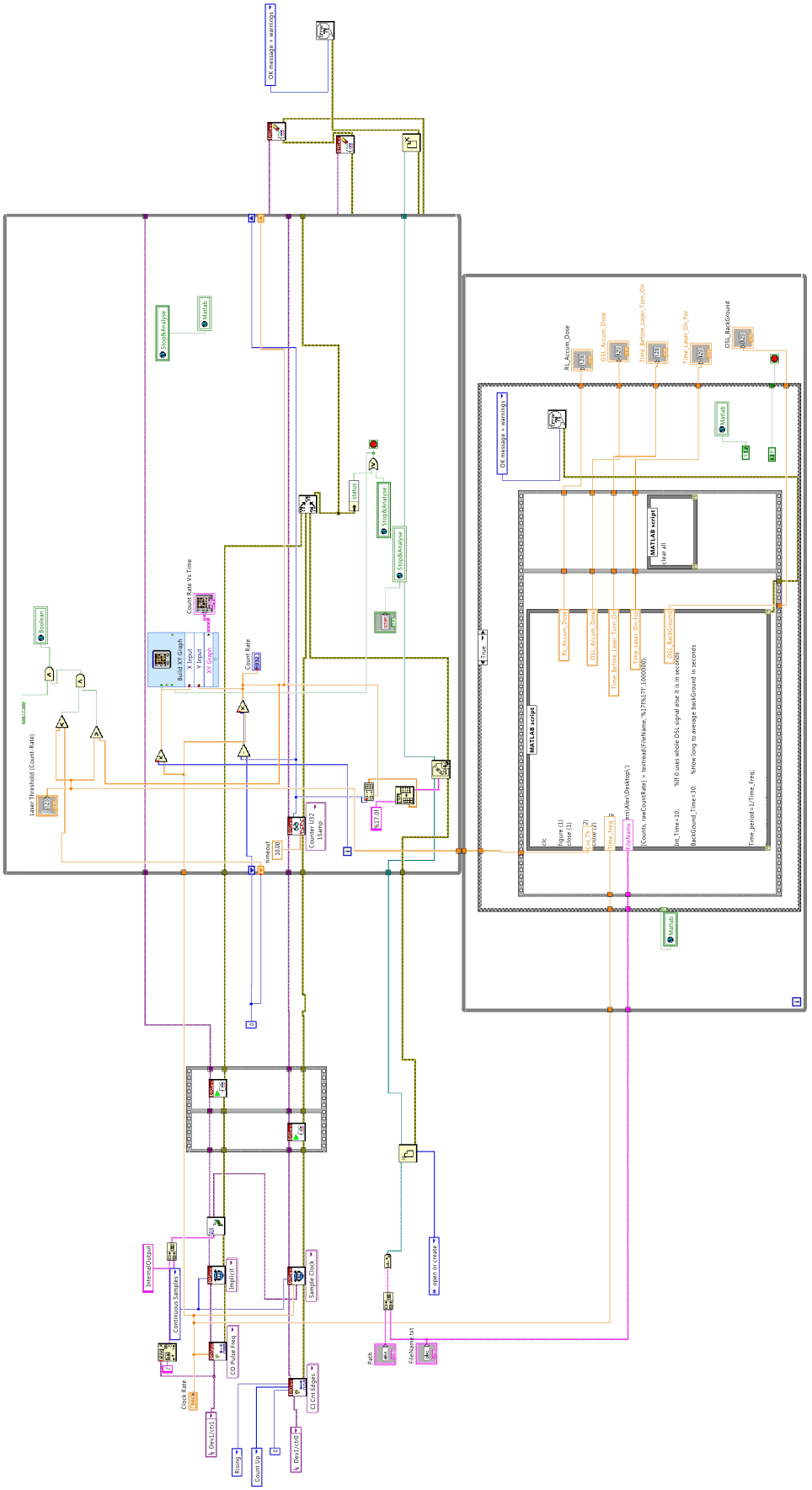

FIGURE 5.2: The block diagram for the final LabView software version use to automate the RL/OSL BeO FOD.

5.4 Discussion and Conclusion

A portable RL and OSL optical fibre reader system has been developed, named RL/OSL BeO FOD. The RL/OSL BeO FOD utilises the RL signal from a BeO ceramic probe for real-time dose rate measurements, and the OSL signal for an accumulated dose measurement. Figure 5.3 (a) shows the light tight metal case for the reader system and figure 5.3 (b) shows all the RL/OSL reader components. The RL/OSL BeO FOD was characterised using a high energy 6 MV x-ray beam.

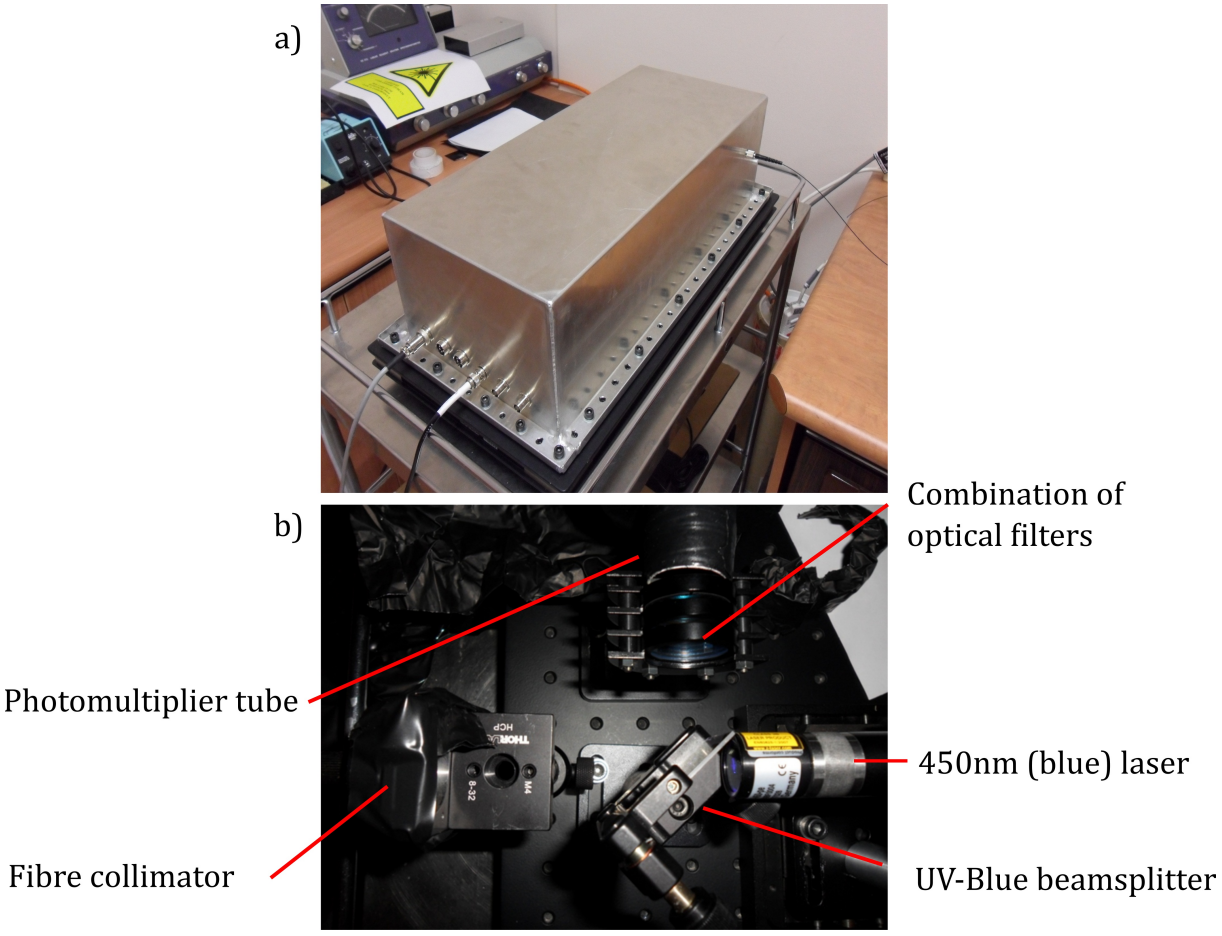

FIGURE 5.3: The portable OSL reader, (a) all enclosed in a light tight metal case, (b) containing the stimulation laser, optics and photomultiplier tube.

Results showed both the RL and OSL signals to be reproducible. For the OSL, no significant fading was observed within the first 10 min after exposure. A supralinear dose response was observed for the OSL signal to doses greater the 10 Gy, and the OSL was

shown to be dose rate independent. The RL response was shown to be linear for dose rates from 100 cGy/min to 600 cGy/min, and that the integral of the RL responded linearly to doses from 30 cGy to 15 Gy. Measured percentage depth dose curves were within 5% agreement to ion chamber measurements, indicating little energy dependence of the RL/OSL BeO FOD in the megavoltage range.

Chapter 6

Energy Dependence

The publication [P4] forms the basis of this chapter.

Alexandre M. Caraça Santos, Mohammad Mohammadi and Shahraam Afshar V., Energy dependency of a water-equivalent fibre-coupled beryllium oxide (BeO) dosimetry system, *Radiation Measurements* 1-6, 2015.

6.1 Development overview and motivation

The major advantage of the use of BeO ceramic as a dosimeter material is the potential little energy dependence. This is due to the effective atomic number of BeO ceramic (Z_{eff}≈7.1) is comparable to that of water (Z_{eff}≈7.4). OSL energy dependence has been shown to be weakly under-responding at lower x-rays energies (Sommer et al., 2007, Sommer and Henniger, 2006, Jahn et al., 2013, 2014). However, there have been no studies investigating the RL energy dependence of BeO ceramic.

In this chapter the energy dependence of the RL/OSL BeO FOD will be discussed. Firstly the theoretical expected absorbed dose energy dependence was estimated with the use of the Burlin Cavity theory. Finally the overall energy dependence of the RL/OSL BeO FOD was experimentally measured with the use of an superficial x-ray unit (Gulmay),

and ^{192}Ir source (Nucletron, Netherlands), and a high energy linear accelerator (Varian Medical Systems, Inc., Palo Alto, USA).

6.2 Statement of Contribution

6.2.1 Conception

The idea to investigate the theoretical and experimental energy dependence of the BeO ceramic dosimetry system was conceptualised by Alexandre M. Caraça Santos.

6.2.2 Realisation

Matlab coding of the theoretical energy dependence of the BeO ceramic dosimetry system and the experiment undertaken were performed by Alexandre M. Caraça Santos. The Matlab code used can be found in App. B.

6.2.3 Documentation

This paper was primarily written by Alexandre M. Caraça Santos. Editing was performed by all authors.

Statement of Authorship

Title of Paper	Energy dependency of a water-equivalent fibre-coupled beryllium oxide (BeO) dosimetry system
Publication Status	☑ Published ☐ Accepted for Publication ☐ Submitted for Publication ☐ Publication Style
Publication Details	Alexandre M. Caraca Santos, Mohammad Mohammadi and Shahraam Afshar V., Energy dependency of a water-equivalent fibre-coupled beryllium oxide (BeO) dosimetry system, Radiation Measurements 1-6, 2015.

Principal Author

Name of Principal Author (Candidate)	Alexandre Santos
Contribution to the Paper	Performed the theoretical absorbed dose energy dependence estimates and all of the experimental measurements, and wrote the manuscript and acted as corresponding author.
Overall percentage (%)	
Signature	Date 12/1/2016.

Co-Author Contributions

By signing the Statement of Authorship, each author certifies that:

i. the candidate's stated contribution to the publication is accurate (as detailed above);

ii. permission is granted for the candidate in include the publication in the thesis; and

iii. the sum of all co-author contributions is equal to 100% less the candidate's stated contribution.

Name of Co-Author	Mohammad Mohammadi
Contribution to the Paper	Supervised development of work and manuscript evaluation.
Signature	Date 12,01,2016

Name of Co-Author	Shahraam Afshar V.
Contribution to the Paper	Supervised development of work and manuscript evaluation.
Signature	Date 6/01/2016.

Radiation Measurements 73 (2015) 1–6

Contents lists available at ScienceDirect

Radiation Measurements

journal homepage: www.elsevier.com/locate/radmeas

Energy dependency of a water-equivalent fibre-coupled beryllium oxide (BeO) dosimetry system

Alexandre M. Caraça Santos [a, b, *], Mohammad Mohammadi [a, c], Shahraam Afshar V. [b]

[a] Department of Medical Physics, Royal Adelaide Hospital, Adelaide, South Australia, Australia
[b] Institute for Photonics & Advanced Sensing and School of Chemistry & Physics, University of Adelaide, Adelaide, South Australia, Australia
[c] Department of Medical Physics, Faculty of Medicine, Hamadan University of Medical Sciences, Hamadan, Iran

HIGHLIGHTS

- The photon energy response of a fibre-coupled beryllium oxide (BeO) ceramic dosimeter, named RL/OSL BeO FOD was investigated.
- Under response of both the RL and OSL signals observed for lower x-ray energies.
- The RL signal shows a constant response for x-ray energies above a 50 kVp SXR beam.
- The OSL signal differs from the RL at higher photon energies, and shows an over response.
- Different intrinsic energy response is observed for the RL and OSL.

ARTICLE INFO

Article history:
Received 25 September 2014
Received in revised form
5 December 2014
Accepted 6 December 2014
Available online 6 December 2014

Keywords:
Radioluminescence
Optically stimulated luminescence
Beryllium oxide (BeO)
Fibre optic dosimetry

ABSTRACT

Here we investigate the energy dependency of the radioluminescence (RL) and optically stimulated luminescence (OSL) of near water equivalent beryllium oxide (BeO) ceramics. The BeO ceramic is coupled to an optical fibre. We investigate the water equivalence of BeO ceramics by comparing the mass attenuation coefficients and mass stopping powers of BeO ceramic to those of water. We also compare the results to other common dosimeter materials; polyvinyl toluene (PVT) based plastic scintillators, lithium fluoride (LiF) and aluminium oxide (Al_2O_3:C). Results show that while PVT based plastic scintillators are the most water equivalent material investigated, the mass attenuation coefficients and mass stopping power ratios of BeO and water vary the least with energy. We also investigate the x-ray energy dependence of BeO ceramic for a range of energies produced by a superficial x-ray unit (SXR), an Iridium-192 source and a high energy linear accelerator. Results indicate a significant under response of the BeO ceramic RL and OSL signals for lower x-ray energies, up to 55% for the lower SXR beams. The RL signal from BeO ceramics shows a constant response for x-ray energies above a 50 kVp SXR beam.

1. Introduction

Since the 1950s there has been an interest in beryllium oxide (BeO) ceramics for dosimetry because of their near water equivalent effective atomic number, Z_{eff}, of ~7.1, compared to water, ~7.4 (Albrecht and Mandeville, 1956). BeO ceramics were initially investigated as a more water equivalent alternative to lithium fluoride (LiF, Z_{eff} ~ 8.2) as a thermoluminescent dosimeter (TLD) (Busuoli et al., 1977; Lembo et al., 1990; Scarpa, 1970; Tochilin et al., 1969). More recently being investigated as an alternative to aluminium oxide crystals (Al_2O_3:C, Z_{eff} ~ 11.1) as an optically stimulated luminescence (OSL) dosimeter chip (Bulur and Yeltik, 2010; Jahn et al., 2013; Sommer et al., 2007, 2008; Yukihara, 2011) and an OSL and radioluminescence (RL) optical fibre-coupled dosimeter (Santos et al., 2014, 2013).

While many studies have discussed BeO ceramics as tissue equivalent for dosimetric practice (Sommer et al., 2007, 2008), little has been studied in its energy dependency. Early studies has shown that the OSL signal from BeO ceramics weakly under responds to x-rays under 100 keV (Sommer et al., 2007; Sommer and Henniger, 2006). Recently it has been shown that the OSL from BeO ceramics has a continual reduction in response to low energy x-rays, with no significant constant region (Jahn et al., 2014, 2013). No

* Corresponding author. Department of Medical Physics, Royal Adelaide Hospital, Adelaide, South Australia, Australia.
E-mail address: alexandre.santos@adelaide.edu.au (A.M.C. Santos).

http://dx.doi.org/10.1016/j.radmeas.2014.12.006
1350-4487/

studies have investigated the energy dependency of the RL signal from BeO ceramics.

In this paper, we investigate the energy dependence of the OSL and RL from BeO ceramics in a fibre-coupled luminescence dosimeter (Santos et al., 2014). The overall energy dependence of a dosimeter response can be separated into two components: The intrinsic energy dependency and the absorbed-dose energy dependency (Rogers, 2009). The intrinsic energy dependency, $k_{bq}(Q)$, relates the detector's reading, $M_{det}(Q)$, to the average dose to the sensitive detecting material, $D_{det}(Q)$, for a specified beam quality, Q, i.e.,

$$D_{det}(Q) = k_{bq}(Q) M_{det}(Q). \tag{1}$$

While the absorbed-dose energy dependency, $f(Q)$, relates the dose to the detector material, $D_{det}(Q)$, to the dose to the medium, $D_{med}(Q)$, for a specified beam quality, Q, i.e.,

$$D_{med}(Q) = f(Q) D_{det}(Q). \tag{2}$$

It is this second component which the water equivalency of the material comes to play. For a photon detector, i.e. a detector which responds only to photons, $f(Q)$ is equal to the ratio of mass energy absorption coefficients of the medium to the detector (Nahum, 2009), i.e.,

$$\frac{1}{f(Q)} = \frac{D_{det}}{D_{med}} = \frac{\left(\frac{\overline{\mu}_{en}}{\rho}\right)_{det}}{\left(\frac{\overline{\mu}_{en}}{\rho}\right)_{med}}. \tag{3}$$

For an electron detector, i.e. a detector which responds only to electrons, $f(Q)$ can be approximated by the ratio of the mass collision stopping power of the medium to the detector (Nahum, 2009), i.e.,

$$\frac{1}{f(Q)} = \frac{D_{det}}{D_{med}} = \frac{\left(\frac{\overline{S}_{col}}{\rho}\right)_{det}}{\left(\frac{\overline{S}_{col}}{\rho}\right)_{med}}. \tag{4}$$

Both conditions must be evaluated as depending on the beam quality a detector can be either a photon detector, an electron detector, or a combination of the two. We investigate how $f(Q)$ varies with the beam quality, Q, in a water medium for BeO ceramics and other common discussed detector materials; LiF, Al_2O_3:C and polyvinyl toluene (PVT) based plastic scintillators.

We finally measure the overall energy dependency of a BeO ceramic fibre-coupled luminescence dosimeter by measuring the response for various x-ray beam qualities. Thus some conclusions can be made on the intrinsic energy dependency.

2. Materials and methods

2.1. Absorbed-dose energy dependency

Mass energy absorption coefficients for BeO ceramics, PVT based plastic scintillators, LiF, and Al_2O_3, were calculated by multiplying the mass fraction of each element by the corresponding mass energy absorption coefficient. Each elements mass energy absorption coefficient was collated from The National Institute of Standards and Technology (NIST) database (Hubbell and Seltzer, 2004). Mass stopping powers for the investigated detector materials were collated from the common materials on the ESTAR database (Berger et al., 2005). The composition, density and effective atomic number of each material can be found in Table 1. The effective atomic numbers were calculated utilizing a $Z^{2.94}$ dependency (McCullough and Holmes, 1985).

Since detectors are generally calibrated against a reference beam, a relative absorbed-dose factor, R, is investigated (Selvam and Keshavkumar, 2010). R is defined as:

$$R = \frac{(D_{det}/D_{med})_Q}{(D_{det}/D_{med})_{Qref}} = \frac{f\left(Q_{ref}\right)}{f(Q)}. \tag{5}$$

For the evaluation of R, a reference beam energy of 1.25 MeV was used as it is the effective energy of cobalt-60.

2.1.1. Burlin cavity theorem

The burlin cavity theory allows for an approximation of the dose to detector. In its simplest form it is defined as (Attix, 1986):

$$\frac{\overline{D_{det}}}{D_{med}} = d\frac{\left(\frac{\overline{S}_{col}}{\rho}\right)_{det}}{\left(\frac{\overline{S}_{col}}{\rho}\right)_{med}} + \left(1-d\right)\frac{\left(\frac{\overline{\mu}_{en}}{\rho}\right)_{det}}{\left(\frac{\overline{\mu}_{en}}{\rho}\right)_{med}}. \tag{6}$$

Where d is a weighting factor that varies between unity for small (or Bragg–Gray) cavities and zero for large cavities (or photon detectors). Burlin expressed d as:

$$d = \frac{1-e^{-\beta L}}{\beta L}, \tag{7}$$

where β is the effective absorption coefficient of the electrons in the cavity and L is the mean chord length across the volume. L is taken as $4V/S$, where V is the volume of the cavity and S is the surface area (Ogunleye, 1982).

Burlin suggested an expression for the evaluation of β:

$$e^{-\beta t_{max}} = 0.01, \tag{8}$$

where t_{max} is the maximum depth of electron penetration, which are obtained from the continuous-slowing down approximation (CSDA). The maximum depth of electron penetration was calculated for the maximum electron energy, which was assumed to be the monoenergetic photon energy. A value of 0.04 instead of 0.01 was used since it has been shown to improve the agreement with experimental results (Janssens et al., 1974). The d parameter was therefore calculated for a cylinder of size 1 mm diameter and 1 mm length. This was chosen because it is the dimensions of the BeO ceramic used in the experimental measurements.

2.2. BeO ceramic energy dependency

The energy dependency for the RL/OSL BeO FOD was evaluated for a range of x-ray energies using a superficial x-ray unit (SXR), an Iridium-192 source and a high energy linear accelerator. 1 Gy was

Table 1
The composition, density and effective atomic number of each of the materials.

Detector	Composition (Weight %)							Z_{eff}	<Z/A>	Density (g/cm^3)
	Be	O	H	Al	C	Li	F			
BeO	36	64	–	–	–	–	–	7.1	0.4798	2.85
LiF	–	–	–	–	–	26.8	73.2	8.2	0.4626	2.64
Al_2O_3	–	47.1	–	52.9	–	–	–	11.1	0.4904	3.97
PVT (C_9H_{10})	–	–	8.5	–	91.5	–	–	5.7	0.5463	1.03
Water	–	88.8	11.2	–	–	–	–	7.4	0.5551	1.00

Table 2
The effective energies used for the various beam qualities investigated.

Therapy unit	Beam quality	Effective energy (MeV)
Superficial X-ray unit	30 kVp – 0.2 mm Al HVL	0.014
	40 kVp – 0.5 mm Al HVL	0.019
	50 kVp – 1 mm Al HVL	0.024
	80 kVp – 2 mm Al HVL	0.029
	100 kVp – 3 mm Al HVL	0.035
	120 kVp – 5 mm Al HVL	0.043
	140 kVp – 8 mm Al HVL	0.055
	150 kVp – 0.5 mm Cu HVL	0.061
Afterloader	^{192}Ir	0.39
Linear accelerator	6 MV	2
	18 MV	6

delivered with the various x-ray sources. This was important since the OSL from BeO ceramic has been shown to not be linear over all doses (Santos et al., 2014). The measured x-ray energy responses are normalised to the response measured the highest superficial x-ray energy, and plotted against the effective energy of the x-ray beams shown in Table 2. The effective energy of the SXR energies was calculated based on their half value layers (HVL). The 1/3 rule of thumb was used for the high energy linac energies, and 0.39 MeV for the Iridium-192 source.

2.2.1. Dosimeter design

The RL/OSL BeO FOD consists of a 1.0 mm diameter cylinder of 1.0 mm in length BeO ceramic probe (Thermalox 995, Materion, USA). The BeO ceramic probe is butt-coupled to a silica/silica optical fibre using BC-600 optical cement (Bicron). The dosimetry system has been discussed in greater detail previously (Santos et al., 2014).

2.2.2. Superficial x-ray unit (SXR)

The response of the RL/OSL BeO FOD to low energy x-rays was evaluated using an SXR unit with tube voltages from 50 kVp to 150 kVp. The SXR unit was calibrated to dose to water based on the IPEMB code of practice (Klevenhagen et al., 1996). The RL/OSL BeO FOD was placed on the surface of a slab of solid water, oriented perpendicular to the beam. Calibrated doses of 1 Gy were delivered with the reference 5 cm cone.

2.2.3. Iridium – 192

An Iridium – 192 source from a microSelectron (Nucletron, Netherlands) high dose rate brachytherapy afterloader unit was used with a source strength of ~10 Ci to evaluate the response to intermediate energy x-rays. Both the source and the RL/OSL BeO FOD were inserted in 6F applicators and placed 1 cm away for each other. A custom perspex phantom submerged in water was used to secure the two needles. Calibrated doses of 1 Gy to water were delivered, and calculated based on AAPM TG-43 (Rivard et al., 2004) using Ocentra Brachy planning system (Nucletron, Netherlands).

2.2.4. Linear accelerator

The response to high energy x-rays was evaluated using 6 MV and 18 MV x-ray beams, delivered using a Varian Clinac iX linear accelerator (Varian Medical Systems, Inc., Palo Alto, USA). Dose to water was calibrated based on the IAEA code of practice (IAEA, 2000). To follow the absolute dosimetry protocol, the RL/OSL BeO FOD was placed at 10 cm depth in a solid water phantom and oriented perpendicular to the beam. The monitor units were corrected for the depth dose at 10 cm to deliver 1 Gy.

3. Results and discussion

3.1. Absorbed-dose energy dependence

3.1.1. Mass energy absorption coefficients

Fig. 1 a) shows the ratio of mass energy attenuation coefficients for material to water for; BeO, PVT, Al_2O_3 and LiF. It can be seen that PVT based plastic scintillators are the most water equivalent from an x-ray energy range of 100 keV to 10 MeV, as they are closest to unity for this range of x-ray energies. Over the entire investigated range, of 10 keV–20 MeV, BeO shows the least variation in its ratio. Al_2O_3 by far varies the most with energy and hence the least water equivalent of the investigated materials.

Fig. 1 b) shows the ratio of mass energy attenuation coefficients for material to water, normalised at the 1.25 MeV x-ray energy. It can be seen that BeO has the least varying ratio mass energy attenuation coefficients with water over the energy range. With the minimum and maximum relative absorbed-dose factor for BeO over the range of 10 keV–20 MeV being 87.0% and 101.2%, respectively. While PVT has a minimum and maximum of 37.8% and 100.4%, respectively.

3.1.2. Mass stopping power ratios

Fig. 2 a) shows the mass stopping power ratios for material to water for; BeO, PVT, Al_2O_3 and LiF. It can be seen that PVT based plastic scintillators are the most water equivalent as they are closest to unity for the range of electron energies. Again, Al_2O_3 has the

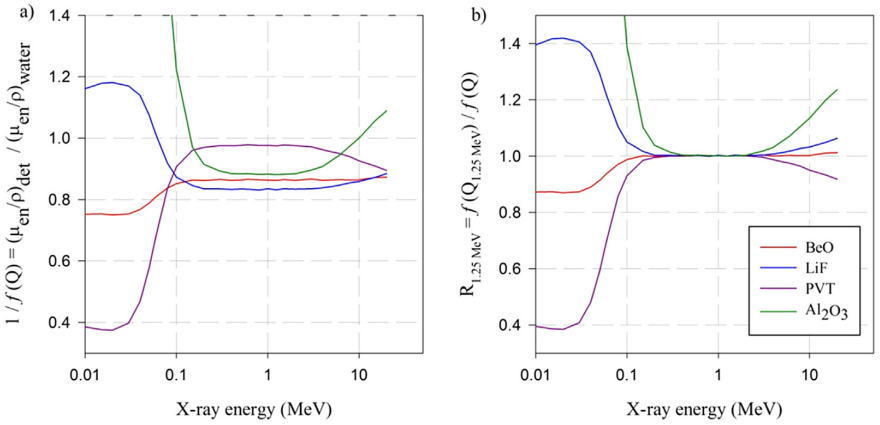

Fig. 1. a) the ratio of mass energy attenuation coefficients to water for BeO, (PVT), Al_2O_3 and LiF and b) the ratios normalised to 1.25 MeV for BeO, (PVT), Al_2O_3 and LiF.

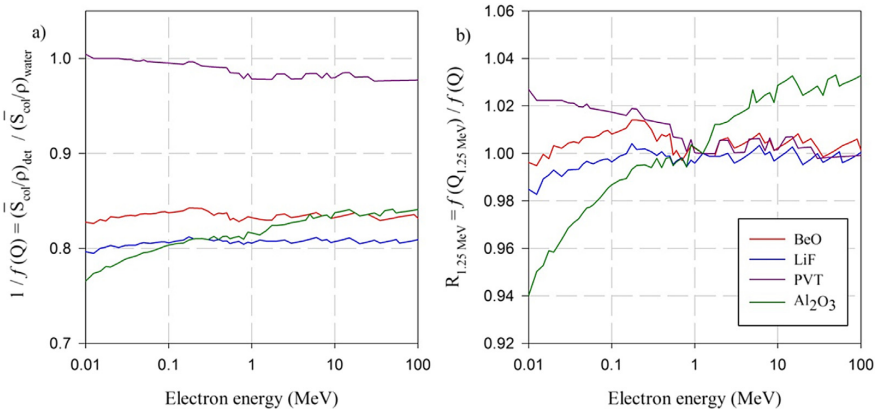

Fig. 2. a) the mass stopping power ratios to water for BeO, PVT based plastic scintillators, Al_2O_3 and LiF and b) the ratios normalised to 1.25 MeV for BeO, PVT based plastic scintillators, Al_2O_3 and LiF.

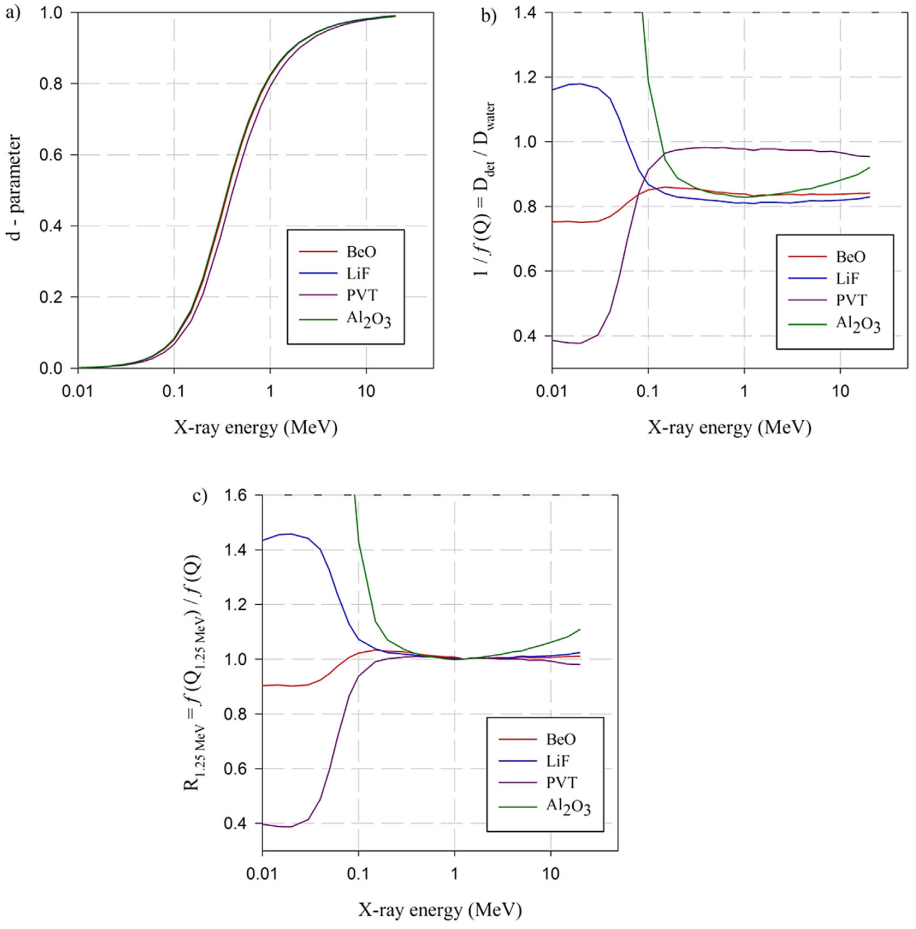

Fig. 3. a) the calculated d-parameter, b) the calculated Burlin cavity theory D_{det}/D_{water} and c) the *R* parameter normalised to 1.25 MeV normalised for BeO, PVT based plastic scintillators, Al_2O_3 and LiF.

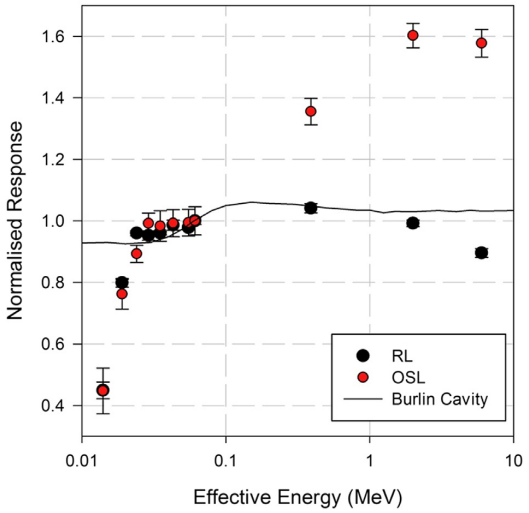

Fig. 4. The x-ray energy response of the OSL and RL signals for the RL/OSL BeO FOD, normalised to the highest SXR energy of effective energy 0.061 MeV. The burlin cavity theory calculated D_{det}/D_{med} for BeO normalised to 0.06 MeV has also been plotted.

greatest variation in its mass stopping power ratios.

Fig. 2 b) shows the mass stopping power ratios for material to water, normalised to 1.25 MeV. It can be seen that BeO and LiF have the least varying mass stopping power ratios with water over the energy range. Overall the mass stopping power ratios for the various materials do not vary with energy as much as the mass energy absorption coefficients.

3.1.3. Burlin cavity theory

Fig. 3 a) shows the calculated *d* parameter for the range of x-ray energies, for the 1 mm diameter, 1 mm long cylinder of detector material. It can be seen that the *d* parameter is quite similar for all the materials, each having a greater contribution on the mass energy absorption coefficients at low energies, and mass stopping powers at higher energies.

Fig. 3 b) shows the Burlin cavity theory D_{det}/D_{water} for BeO, PVT, Al_2O_3 and LiF. As expected Al_2O_3 show the greatest absorbed-dose energy dependency for the range of x-ray energies. In the x-ray energy range of 100 keV to 20 MeV, PVT is the least energy dependent, with the calculated D_{det}/D_{water} being almost unity. BeO does show the least variation of the entire range of x-ray energies investigated, from 10 keV to 20 MeV.

As discussed before, since a dosimeter is normally calibrated under some reference beam quality, the previously defined parameter *R* is of interest. Fig. 3 c) shows *R* for the range of x-ray energies, with reference beam energy of 1.25 MeV. As discussed BeO is the least varying of the entire energy range. For example at a low energy of 50 keV, the D_{det}/D_{water} for BeO is 95% of that at the reference beam energy, while it is 132% for LiF, 60% for PVT and 331% for Al_2O_3.

3.2. BeO ceramic overall energy dependency

Fig. 4 shows the measured energy response for the OSL and RL signals over the SXR, Ir-192 and linac energies, normalised to the highest superficial x-ray energy, with effective energy 0.061 MeV. The previously calculated burlin cavity D_{det}/D_{water} for BeO normalised to 0.06 MeV has also been plotted in Fig. 4. Each measurement shown was the mean from five readings, with the uncertainties corresponding to two standard deviations.

At the lowest superficial x-ray energy, both the RL and OSL under-respond by 55%. This under-response may be partly due to the self-absorption of the BeO ceramic. At the lower energies, there is no longer a uniform dose distribution within the detector volume. Therefore the self-absorption of the BeO ceramic will reduce the signal measured. Also the sources used are not mono-energetic but emit a broad energy spectrum, therefore the lower energy x-rays will lead to a reduced overall response.

It can then be seen that the OSL signal has a large energy response over the energy range, over-responding to the linac energies by a maximum of 160%. While the RL signal has little energy response beyond the 80 kVp superficial energy beam.

Fig. 5 shows the measured energy dependence from the RL/OSL BeO FOD and previously measured energy response of various other detector materials (Nunn et al., 2008; Reft, 2009; Williamson et al., 1999). All of the energy responses normalised to the highest

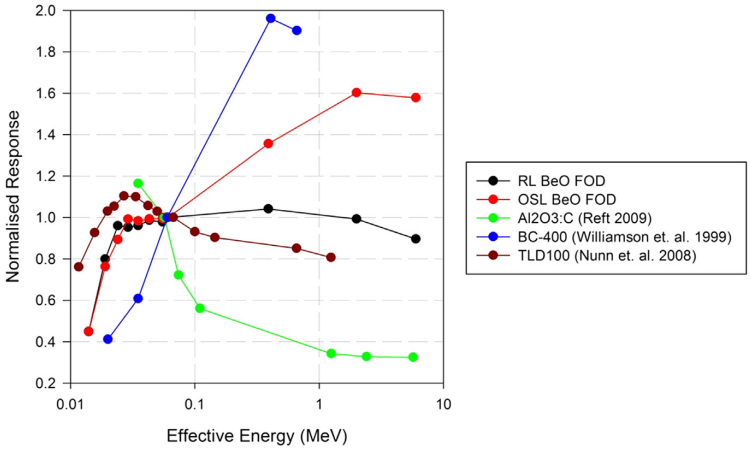

Fig. 5. The measured energy dependency of the RL and OSL from the RL/OSL BeO FOD compared to Al_2O_3:C OSLD, BC-400 plastic scintillator and LiF TLD100. All the measured energy responses have been normalised to a common effective energy of ~0.06 MeV.

effective energy which all measurements had in common, approximately 0.06 MeV. Of the detectors investigated, the RL/OSL BeO FOD and LiF (TLD-100), exhibit the least energy dependency.

4. Conclusion

Based on the mass energy attenuation coefficient and mass stopping power ratios to water, PVT based plastic scintillators are the most water equivalent materials, from those investigated. This has been previous shown (Beddar et al., 1992). Though when investigating the variation in the ratios with x-ray and electron energies, it can be seen that BeO shows the least variation. This indicates that based on the material composition that BeO is theoretically the most energy independent material of those investigated; therefore it has the least absorbed-dose energy response. This does not take into account any energy dependency in the mechanisms which these materials are measuring radiation dose, for this reason energy response investigations are of importance.

The OSL and RL x-ray energy response curves shown in Fig. 4, shows that the OSL is much more energy dependent than the RL. The OSL energy response matches that previously found in the BeOmax system (Jahn et al., 2013). No previous works have investigated the energy response of the RL in BeO ceramics. This indicates that the RL and OSL from BeO ceramic has two different intrinsic energy dependencies.

This finding indicates that the two radiation measurement mechanisms, the OSL and RL, may be independent of each other. This observation is supported by various previous studies. For instance, (Yukihara, 2011) found that the OSL and RL have different emission spectrums. Santos et al. (2014) found that the RL is insensitive to the accumulated dose in the BeO ceramic, which indicates that the RL and OSL are not competing. This is unlike other OSL materials such as Al_2O_3:C, where the RL response increases with accumulated dose due to the competition between RL and OSL (Edmund et al., 2006).

The energy dependency measurements show that there is a different energy response for the OSL and RL signals. The RL shows little energy dependency for x-ray energies above a superficial 50 kVp beam, while the OSL response differs from the RL response for x-ray energies above a superficial 150 kVp beam. The under-response observed for energies below the superficial 50 kVp beam may be due to the self-absorption of the BeO ceramics.

Future investigation of the difference between the RL and OSL response at higher x-ray energies is of interest.

Acknowledgements

The authors would like to thank Dr. Scott Penfold for the useful discussions and input into this study.

References

Albrecht, H.O., Mandeville, C.E., 1956. Storage of energy in beryllium oxide. Phys. Rev. 101, 1250.
Attix, F.H., 1986. Introduction to Radiological Physics and Radiation Dosimetry. Wiley.
Beddar, A.S., Mackie, T.R., Attix, F.H., 1992. Water-equivalent plastic scintillation detectors for high-energy beam dosimetry: I. Physical characteristics and theoretical consideration. Phys. Med. Biol. 37, 1883–1900.
Berger, M.J., Coursey, J.S., Zucker, M.A., Chang, J., 2005. ESTAR, PSTAR, and ASTAR: Computer Programs for Calculating Stopping-power and Range Tables for Electrons, Protons, and Helium Ions (version 1.2.3), (version 1.2.3) ed. National Institute of Standards and Technology, Gaithersburg, MD.
Bulur, E., Yeltik, A., 2010. Optically stimulated luminescence from BeO ceramics: an LM-OSL study. Radiat. Meas. 45, 29–34.
Busuoli, G., Sermenghi, I., Rimondi, O., Vicini, G., 1977. TL personnel dosimeter with BeO. Nucl. Instrum. Methods 140, 385–388.
Edmund, J.M., Andersen, C.E., Marckmann, C.J., Aznar, M.C., Akselrod, M.S., Botter-Jensen, L., 2006. CW-OSL measurement protocols using optical fibre Al2O3:C dosemeters. Radiat. Prot. Dosim. 119, 368–374.
Hubbell, J.H., Seltzer, S.M., 2004. Tables of X-Ray Mass Attenuation Coefficients and Mass Energy-Absorption Coefficients. Technology, N.I.o.S.a. (Ed.), (version 1.4) ed, Gaithersburg, MD.
IAEA, 2000. Absorbed Dose Determination in External Beam Radiotherapy. An International Code of Practice for Dosimetry Based on Standards of Absorbed Dose to Water. Technical Report Series No. 398, Vienna.
Jahn, A., Sommer, M., Henniger, J., 2014. OSL efficiency for BeO OSL dosimeters. Radiat. Meas. 71, 104–107.
Jahn, A., Sommer, M., Ullrich, W., Wickert, M., Henniger, J., 2013. The BeOmax system – dosimetry using OSL of BeO for several applications. Radiat. Meas. 56, 324–327.
Janssens, A., Eggermont, G., Jacobs, R., Thielens, G., 1974. Spectrum perturbation and energy deposition models for stopping power ratio calculations in general cavity theory. Phys. Med. Biol. 19, 619.
Klevenhagen, P.b.a.W.P.o.t.I.w.t.f.m.S.C., Aukett, R.J., Harrison, R.M., Moretti, C., Nahum, A.E., Rosser, K.E., 1996. The IPEMB code of practice for the determination of absorbed dose for x-rays below 300 kV generating potential (0.035 mm Al – 4 mm Cu HVL; 10-300 kV generating potential). Phys. Med. Biol. 41, 2605.
Lembo, L., Pimpinella, M., Mukherjee, B., 1990. Self optical attenuation coefficient of TL glow in BeO detectors. Radiat. Prot. Dosim. 33, 43–45.
McCullough, E.C., Holmes, T.W., 1985. Acceptance testing computerized radiation therapy treatment planning systems: direct utilization of CT scan data. Med. Phys. 12, 237–242.
Nahum, A.E., 2009. Cavity theory, stopping power ratios, correction factors. In: Rogers, D.W.O., Cygler, J.E. (Eds.), Clinical Dosimetry Measurements in Radiotherapy. Medical Physics Publishing, Madison.
Nunn, A.A., Davis, S.D., Micka, J.A., DeWerd, L.A., 2008. LiF: Mg,Ti TLD response as a function of photon energy for moderately filtered x-ray spectra in the range of 20-250 kVp relative to 60Co. Med. Phys. 35, 1859–1869.
Ogunleye, O.T., 1982. Influence of electron path length on the evaluation of Burlin's cavity theory. Br. J. Radiol. 55, 588–590.
Reft, C.S., 2009. The energy dependence and dose response of a commercial optically stimulated luminescent detector for kilovoltage photon, megavoltage photon, and electron, proton, and carbon beams. Med. Phys. 36, 1690–1699.
Rivard, M.J., Coursey, B.M., DeWerd, L.A., Hanson, W.F., Saiful Huq, M., Ibbott, G.S., Mitch, M.G., Nath, R., Williamson, J.F., 2004. Update of AAPM task group No. 43 Report: a revised AAPM protocol for brachytherapy dose calculations. Med. Phys. 31, 633–674.
Rogers, D.W.O., 2009. General characteristics of radiation dosimeters and a terminology to describe them. In: Rogers, D.W.O., Cygler, J.E. (Eds.), Clinical Dosimetry Measurements in Radiotherapy. Medical Physics Publishing, Madison, pp. 137–145.
Santos, A.M.C., Mohammadi, M., Afshar, V.,S., 2014. Investigation of a fibre-coupled beryllium oxide (BeO) ceramic luminescence dosimetry system. Radiat. Meas. 70, 52–58.
Santos, A.M.C., Mohammadi, M., Asp, J., Monro, T.M., Afshar, V.,S., 2013. Characterisation of a real-time fibre-coupled beryllium oxide (BeO) luminescence dosimeter in X-ray beams. Radiat. Meas. 53–54, 1–7.
Scarpa, G., 1970. The dosimetric use of beryllium oxide as a thermoluminescent material: a preliminary study. Phys. Med. Biol. 15, 667.
Selvam, T.P., Keshavkumar, B., 2010. Monte Carlo Investigation of Energy Response of Various Detector Materials in 125I and 169Yb Brachytherapy Dosimetry.
Sommer, M., Freudenberg, R., Henniger, J., 2007. New aspects of a BeO-based optically stimulated luminescence dosimeter. Radiat. Meas. 42, 617–620.
Sommer, M., Henniger, J., 2006. Investigation of a BeO-based optically stimulated luminescence dosemeter. Radiat. Prot. Dosim. 119, 394–397.
Sommer, M., Jahn, A., Henniger, J., 2008. Beryllium oxide as optically stimulated luminescence dosimeter. Radiat. Meas. 43, 353–356.
Tochilin, E., Goldstein, N., Miller, W.G., 1969. Beryllium oxide as a thermoluminescent dosimeter. Health Phys. 16, 1–7.
Williamson, J.F., Dempsey, J.F., Kirov, A.S., Monroe, J.I., Binns, W.R., Hedtjarn, H., 1999. Plastic scintillator response to low-energy photons. Phys. Med. Biol. 44, 857–871.
Yukihara, E.G., 2011. Luminescence properties of BeO optically stimulated luminescence (OSL) detectors. Radiat. Meas. 46, 580–587.

6.3 Discussion and Conclusion

The absorbed dose energy dependence was estimated using Burlin Cavity theory for BeO ceramic, polyvinyl toluene (PVT), LiF and Al_2O_3. It was found that while BeO ceramic is not the most water equivalent of the materials investigated, it had the least absorbed dose energy dependence. It was calculated that at a low energy of 50 keV, the D_{det}/D_{water} for BeO is 95% of that at the reference beam energy of 1.25 MeV, while it is 132% for LiF, 60% for PVT and 331% for Al2O3.

The overall energy dependence of the RL/OSL BeO FOD was experimentally measured with the use of a superficial x-ray unit, an ^{192}Ir source, and a high energy linear accelerator. A significantly different energy dependence was observed for the OSL and RL signals, indicating a different intrinsic energy dependence. At the lowest superficial x-ray energy, both the RL and OSL under-respond by 55%. The RL signal from BeO ceramics shows a constant response for x-ray energies above a 50 kVp SXR beam. Compared to the reported energy dependence of the other dosimetry systems, the RL was shown to be the least energy dependent.

Chapter 7

High dose rate brachytherapy dosimetry

The publication [P5] forms the basis of this chapter.

Alexandre M. C. Santos, Mohammad Mohammadi and Shahraam Afshar V., Evaluation of a real-time beryllium oxide (BeO) ceramic fibre-coupled luminescence dosimetry system for dose verification of high dose rate brachytherapy, *Medical Physics* 42 (11), 2015.

7.1 Development overview and motivation

The little energy dependence of the RL/OSL BeO FOD potentially makes this dosimetry system ideal for lower energy applications, such as brachytherapy dosimetry. Hence, in this chapter the RL/OSL BeO FOD is characterised for use in high dose rate brachytherapy. Due to its small size, the RL/OSL BeO FOD can be inserted into a 6F needle (Nucletron, Netherlands), as shown in figure 7.1. This allows the RL/OSL BeO FOD to be placed along side another 6F needle, which is connected to an ^{192}Ir afterloader (Nucletron, Netherlands).

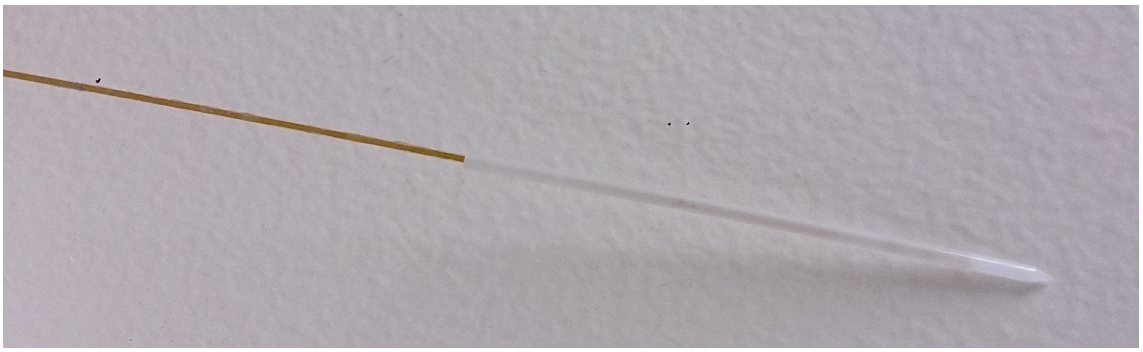

FIGURE 7.1: The RL/OSL BeO FOD inserted in a 6F needle, commonly used in HDR brachytherapy treatments.

7.2 Statement of Contribution

7.2.1 Conception

The idea to apply the BeO ceramic dosimetry system for the dose verification of high dose rate brachytherapy was conceptualised by Alexandre M. Caraça Santos.

7.2.2 Realisation

The experiments required for characterisation of the BeO ceramic dosimetry system for high dose rate brachytherapy was performed by Alexandre M. Caraça Santos.

7.2.3 Documentation

This paper was primarily written by Alexandre M. Caraça Santos. Editing was performed by all authors.

Statement of Authorship

Title of Paper	Evaluation of a real-time beryllium oxide (BeO) ceramic fibre-coupled luminescence dosimetry system for dose verification of high dose rate brachytherapy
Publication Status	☑ Published ☐ Accepted for Publication ☐ Submitted for Publication ☐ Publication Style
Publication Details	Alexandre M. C. Santos, Mohammad Mohammadi and Shahraam Afshar V., Evaluation of a real-time beryllium oxide (BeO) ceramic fibre-coupled luminescence dosimetry system for dose verification of high dose rate brachytherapy, Medical Physics, 42 (11), 2015.

Principal Author

Name of Principal Author (Candidate)	Alexandre Santos
Contribution to the Paper	Developed the final BeO ceramic probe, performed all of the experimental measurements, and wrote the manuscript and acted as corresponding author.
Overall percentage (%)	90%
Signature	Date 12/1/2016

Co-Author Contributions

By signing the Statement of Authorship, each author certifies that:

i. the candidate's stated contribution to the publication is accurate (as detailed above);
ii. permission is granted for the candidate in include the publication in the thesis; and
iii. the sum of all co-author contributions is equal to 100% less the candidate's stated contribution.

Name of Co-Author	Mohammad Mohammadi
Contribution to the Paper	Performed evaluation of the manuscript.
Signature	Date 12/01/2016

Name of Co-Author	Shahraam Afshar V.
Contribution to the Paper	Supervised development of work and manuscript evaluation.
Signature	Date 6/01/2016

Santos, A.M.C., Mohammadi, M. & Afshar Vahid, S. (2015). Evaluation of a real-time BeO ceramic fiber-coupled luminescence dosimetry system for dose verification of high dose rate brachytherapy.
Medical Physics, 42(11), 6349-6356.

7.3 Discussion and Conclusion

The favourable energy dependence observed for the RL/OSL BeO FOD, potentially make the dosimetry system ideal for brachytherapy applications. The RL/OSL BeO FOD was evaluated for dose verification of high dose rate (HDR) brachytherapy. The reproducibility, dose linearity, energy dependence, angular dependence and temperature dependence were evaluated for an ^{192}Ir HDR source. Based on the results shown in the publication [P5], the combined uncertainty was estimated to be 7.9% and 10.1% for the RL and OSL, respectively.

The RL/OSL BeO FOD was then applied to the commissioning of a 10 mm horizontal Leipzig applicator. Measured percentage depth doses were in agreement with reference Monte Carlo data to within 5%. The output for 1 Gy delivered at the prescription depth of 3 mm, was measured to be 0.99 ± 0.08 Gy and 1.01 ± 0.10 Gy for the RL and OSL, respectively.

Chapter 8

Conclusions and future work

8.1 Conclusion

The goal of this project was to develop a real-time dosimetry system for *in-vivo* dosimetry of high dose rate brachytherapy treatments. Primarily, this dosimeter needed to be of small size, such that it could be inserted into a brachytherapy needle or lumen catheter. It was also required that the dosimeter was sensitive enough for accurate and precise dose measurements. In order to be able to act promptly on an error occurring during the treatment the dosimeter also needed to capable of real-time dose rate measurement. Ideally, this dosimetry system would also have little energy dependence, such that it would be capable of dosimetry of low energy brachytherapy sources with few corrections.

In order to meet these requirements, a fibre-coupled luminescence dosimetry system was developed with a beryllium oxide (BeO) ceramic probe. This dosimetry system is capable of real-time dose rate measurements using the RL signal, and post exposure accumulated dose measurements using the OSL signal, from BeO ceramics. With the idea that the closely matched effective atomic number of BeO ceramic ($Z_{eff}\approx7.1$) to that of water ($Z_{eff}\approx7.4$) may result in little energy dependence.

In Chapter 3 a ray tracing model was developed in order to optimise the probe tip design. For BeO ceramic probe of 1 mm diameter, the model estimated that there would be no

increase in light collection beyond 1 mm length of BeO ceramic. This is because of the self optically attenuating properties of BeO ceramic.

In Chapter 4 a RL BeO ceramic fibre-coupled dosimeter was developed and characterised using a high energy 6 MV x-ray beam, and a superficial x-ray unit. The results obtained using the RL BeO FOD were promising, and provided confidence in continuing with the investigation of BeO ceramics as a probe material. The RL measurements led to an RL and OSL reader being developed in Chapter 5, named RL/OSL BeO FOD. The RL/OSL BeO FOD was characterised using a high energy 6 MV x-ray beam. The results obtained showed promise for the use of BeO ceramics.

In chapter 6 the energy dependence of the RL/OSL BeO ceramic is investigated. Little energy dependence was observed when compared to other similar dosimeters. Especially for the RL which was found to be fairly energy independence above 50 kVp x-rays. The little energy dependence observed led to the use of the RL/OSL BeO FOD for brachytherapy dosimetry, discussed in Chapter 7. The combined uncertainty was estimated to be 7.9% and 10.1% for the RL and OSL, respectively. These results are comparable to that previously reported for Al_2O_3:C crystal fibre-coupled luminescence dosimetry systems of 8% and 5% for the RL and OSL, respectively (Andersen et al., 2009a). While the estimated uncertainty of the RL/OSL BeO FOD for *in-vivo* dose verification can be considered high, it is still of interest for real-time detection of gross errors which can occur in brachytherapy treatments.

Therefore this thesis demonstrated the feasibility of using beryllium oxide ceramics as a near water-equivalent alternative to Al_2O_3:C crystals in fibre-coupled luminescence dosimetry systems. This work has shown that BeO ceramics have the potential to be a very useful material for dosimetry in radiotherapy. Especially for dosimetry in brachytherapy where its little energy dependency may be taken advantage of. However, with the current system using a background optical fibre for the stem effect correction, it is not able to be inserted into most needles for *in-vivo* dose verification.

8.2 Future work

Future work which could be done for this dosimetry system to be more effective, is further optimization of the probe tip and that of the reader system. Improved technique on the coupling of the BeO ceramic to the optical fibre and the use of other epoxies could improve the coupling efficiency, and therefore increase the light collection. Optimisation of the components in the reader, such as the use of different optical filters and beam splitter, could increase the sensitivity of the system. Also the mechanical removal of the optical filters during the measurement of the RL would significantly increase the RL sensitivity.

Further investigation is of interest into the underlying physics associated with the difference in energy dependence observed between the RL and OSL signals. Finally, an investigation into the use of alternative stem effect correction techniques is of interest such that the system could be practically applicable to *in-vivo* dose verification. Also, since only a single dosimeter was constructed, inter detector variability needs to be investigated. Therefore it would be of interest for a number a detectors to be constructed and compared to each other.

In order for the dosimetry system to be utilised for clinical *in-vivo* dose verification, further development is required such as:

- Fast and easy calibration procedures.
- How the detector will be used and localised, such as the development of rectal probes.
- The clinical impact of the dosimetry system, such as increase in total treatment time.
- Potential adaptation of reader to measure multiple fibre probes.

Future applications of this system may include the development of 2D and 3D arrays, where an optical switch could be utilised for readout.

Appendix A

Light collection modelling for a cladding coupled architecture

A.1 Maincode

```
%%%%%%%%%%%%%%%%%%%%%%%%%%%%%%%%%%%%%%%%%%%%%%%%%%%%%%%%%%%%%%%%%%%%%%%%%%%%%%%%
%   Main Geometric Optics Coupling Code!!!                                      %
%                                                                               %
%   this code works off 2D geometric optics, this should be a fair              %
%   assumption since the geometry is symetrical.                                %
%                                                                               %
%   only for "Cladding-Coupled" geometries!!                                    %
%%%%%%%%%%%%%%%%%%%%%%%%%%%%%%%%%%%%%%%%%%%%%%%%%%%%%%%%%%%%%%%%%%%%%%%%%%%%%%%%

clear all       %clear all variables
clc             %clears screen

tic        %For the Purpose of the time

matlabpool open 6       %Opens the threads
% matlabpool open       %Opens the threads

format long     %increases the precision of each value

%Defining some important variables

lambda=0.400;  %wavelength chosen
n_0=1.72753;    %refractive index of BeO at 400nm

l_s=100*10.^-3;      %length of OSL in meters
l_in=0.1*10.^-3;    %increaments along the length of the OSL in meters

r_co=0.4*10.^-3;   %radius of core in meters
r_cl=0.44*10.^-3;           %radius of cladding in meters, same as that of the OSL since
     "butt-coupled"

r_s=r_co;     % Outer radius of OSL in e-5 meters
r_in=10*10.^-6;    %increaments along the diameter of the OSL in meters
```

```
% n_co=sellPoly(lambda);  %refractive index of core
% n_cl=sellPMMA(lambda);  %refractive index of cladding
n_co=1.47;
NA=0.22;
n_cl=((n_co).^2 - (NA).^2).^0.5;


n_2=1;           %defining outer cladding [AIR ONLY TO BEGIN WITH !!!!!!!!!]

n_1=n_cl;    %refractive index of inner cladding
% r_11=[sqrt((r_co.^2)-((10*10.^-5).^2))];   %radius of n_1 and Inner radius of OSL in e
    -5 meters  **CHANGE THIS VARIABLE
r_11=2e-4;

I_0=1;              %the intensity of units [W m^-3 srad^-1] emitted by each source
% at_co=2.69e3;         %the optical attenuation coefficent of BeO ceramics [2.69+- 0.15
     mm^-1]
at_co=0;
%-------------------------------------------------------------------------%
%                                                                         %
%   Here we calculate the maxiumum acceptance angle in the core           %
%   Used in determining Bound rays
A=((n_co).^2 - (n_cl).^2);                                                %
B=A.^0.5;                                                                 %
Max_Theta=asin((1/n_0)*B);   %Maximum acceptance angle into the core      %
%
%                                                                         %
%-------------------------------------------------------------------------%

%-------------------------------------------------------------------------%
%                                                                         %
%   Here we calculate the Minimum total incident angle
%   Used in determining Refracted rays
Min_tot_inc=acos((1/n_0)*B);    %Minimum total incident angle
%
%                                                                         %
%-------------------------------------------------------------------------%

%-------------------------------------------------------------------------%
%   To Identify Possible errors in refractive indices                     %

if (n_1>n_2) & (n_1<n_0)
    disp ('we have right reflective indexs')
elseif (n_1<n_2)
    disp ('n_1<n_2 SHIT!')
elseif (n_1>n_0)
    disp ('n_1>n_0 SHIT!')
end

%                                                                         %
%-------------------------------------------------------------------------%



%Calculating the light collection efficiency for the different radii

matlabpool size
no_pools=ans;

parfor i=1:(no_pools)

    File_no=i;
    l_ssf=l_s*(i/no_pools)-l_in;
    l_ssi=l_s*((i-1)/no_pools);


    I_r_11=r_11;
    r_1=r_11;   %currently investigated n_1 radius

    %%When the source is beyond the radius of the core
```

```
    Scint_Coll=Scint_CE(File_no,l_ssf,l_ssi,l_in,r_s,r_in,Max_Theta,Min_tot_inc,r_co,I_0
    ,at_co,n_0,n_1,n_2,r_1,n_co,n_cl,I_r_11); %Outer_Coll_Eff(1) is sum of CE &
    Outer_Coll_Eff(2) is no. of sources


end

toc       %For the Purpose of the time

matlabpool close                %Closes the threads

disp('FINISHED !!!')

%% Plays some music to let you know that it is over
load handel
sound(y,Fs)
}
```

A.2 Ray path modelling

```
%%%%%%%%%%%%%%%%%%%%%%%%%%%%%%%%%%%%%%%%%%%%%%%%%%%%%%%%%%%%%%%%%%%%%%%%%%%%%%%
%   this code determines the capture efficiency from sources within the %
%   radius of the core !!!                                               %
%                                                                        %
%   FOR GRAPHING ONLY                                                    %
%                                                                        %
%   FOR Cladding Coupled                                                 %
%                                                                        %
%%%%%%%%%%%%%%%%%%%%%%%%%%%%%%%%%%%%%%%%%%%%%%%%%%%%%%%%%%%%%%%%%%%%%%%%%%%%%%%

function F=Scint_CE(File_no,l_ssf,l_ssi,l_in,r_s,r_in,Max_Theta,Min_tot_inc,r_co,I_0,
    at_co,n_0,n_1,n_2,r_1,n_co,n_cl,I_r_11)

format long

r_ss=r_s;



%%FOR THE POINT OF GRAPHING AT ONE POINT
l=[l_ssi:l_in:l_ssf];  %source points along the length of the OSL
r=[r_1:r_in:r_ss];  %source points radius!!
%%%%%%%%%%%%%%%%%%%%%%%%%%%%%%%%%%%%%%%%%%%%%%%%%%%%%%%%%%%%%%%%%%%%%%%%%%%%%%%



%%%%%%%%%%%%%%%%%%%%%%%%%%%%%%%%%%%%%%%%%%%%%%%%%%%%%%%%%%%%%%%%%%%%%%%%%%%%%%%
%
%   Defining both the propagation and azimuthal angles investigated

angle_p=[0:0.01:(pi/2)];      %Propagation Angle, which we are varying
angle_a=[0:0.01:pi];                  %Azimuthal angle, which we are varying
%%%%%%%%%%%%%%%%%%%%%%%%%%%%%%%%%%%%%%%%%%%%%%%%%%%%%%%%%%%%%%%%%%%%%%%%%%%%%%%

%-------------------------------------------------------------------------%
%   Defining Angles                                                       %

A=((n_co.^2) - (n_cl.^2)).^0.5;
theta_m1=sin((1/(n_1))*A);                          %maximum acceptance angle via n_1
Min_tot_inc1=acos((1/n_1)*A);    %Minimum total incident angle via n_1

theta_c_0=asin((1-((n_1.^2)/(n_0.^2))).^0.5);         %compliment of the critical angle
    between the n_1 and n_0
theta_c_2=asin((1-((n_2.^2)/(n_0.^2))).^0.5);         %compliment of the critical angle
    between the n_1 and n_2
```

```
theta_m2=acos((n_1/n_0)*cos(asin((1/(n_1))*A)));    %maximum acceptance angle from n_0
    via n_1

%                                                                              %
%------------------------------------------------------------------------------%



CE=0;
theta=0;
theta_1=0;
theta_2=0;
V_disc1=0;
path=0;
path_rad=0;

no_Sources=0;
no_core=0;
no_bound=0;
no_ref=0;
no_tun=0;
I_bound=0;
I_ref=0;
I_tun=0;
CE_bound=0;
CE_ref=0;
CE_tun=0;
total_No_Sources=0;
inc_core_no=0;
bound_No_Sources=0;
ref_No_Sources=0;
tun_No_Sources=0;


CE_bound1=0;
CE_ref1=0;
CE_tun1=0;

%Those via reflections from the scintillator wall
no=0;

no_core_s=0;
no_bound_s=0;
no_ref_s=0;
no_tun_s=0;
I_bound_s=0;
I_ref_s=0;
I_tun_s=0;
CE_bound_s=0;
CE_ref_s=0;
CE_tun_s=0;
total_No_Sources_s=0;
inc_core_no_s=0;
bound_No_Sources_s=0;
ref_No_Sources_s=0;
tun_No_Sources_s=0;

CE_bound1_s=0;
CE_ref1_s=0;
CE_tun1_s=0;

%Those via refractions from the scintillator into n_1

no_core_s1=0;
no_bound_s1=0;
no_ref_s1=0;
no_tun_s1=0;
I_bound_s1=0;
I_ref_s1=0;
I_tun_s1=0;
CE_bound_s1=0;
```

```
CE_ref_s1=0;
CE_tun_s1=0;
total_No_Sources_s1=0;
inc_core_no_s1=0;
bound_No_Sources_s1=0;
ref_No_Sources_s1=0;
tun_No_Sources_s1=0;

CE_bound1_s1=0;
CE_ref1_s1=0;
CE_tun1_s1=0;



a=0;
b=0;
theta_azi=0;


%-------------------------------------------------------------------------%
%   Checking Correct Angles                                               %

if (theta_m2>Max_Theta)
    disp ('all theta_m is accepted since theta_m2>Max_Theta')
else
    disp ('theta_m2<Max_Theta SHIT!')
end

if (theta_c_2>theta_m1)
    disp (' maximum light collection since theta_c_2>theta_m1')
else
    disp ('theta_c_2<theta_m1 SHIT!')
end

%                                                                         %
%-------------------------------------------------------------------------%


for i=1:length(l),

    a=l(i);      %current length along the OSL

    for j=1:length(r),

        b=abs(r(j));  %current radius along the OSL

        for w=1:length(angle_a),

            theta_a=angle_a(w);     %Currently investigated prop azimuthal
            angle_azi=(pi/2)-asin((b*sin(pi-theta_a))/r_ss);    %Current azimuthal angle


            for u=1:length(angle_p),

                no_Sources=no_Sources+1;

                angle_prop=angle_p(u);      %Current propagation angle

                angle_tot=acos(sin(abs(angle_prop))*sin(angle_azi));     %Total incident
     angle

                if (a~=0)        %Removing the dividing by zero!!!

                    path=a/cos(angle_prop);     %the pathlength the ray has travelled

                    path_x=path*cos(theta_a)*sin(angle_prop);     %pathlength in x
    direction
                    path_y=path*sin(theta_a)*sin(angle_prop);     %pathlength in y
    direction
```

```
                path_rad=(((b+path_x).^2)+((path_y).^2)).^(1/2);      %the radius of
 the ray from the optical axis when incident upon core


                if (path_rad<r_ss)&(path_rad>r_1)      %%Directly incident on the
fiber core

                    no_core=no_core+1;

                    if (abs(angle_prop)<Max_Theta)
                        no_bound=no_bound+1;
                        path_x=b+path_x;
                        I_bound=I_bound+I_0*exp(-at_co*path);

                    elseif (abs(angle_tot)<Min_tot_inc)
                        no_ref=no_ref+1;
                        path_x=b+path_x;
                        I_ref=I_ref+I_0*exp(-at_co*path);

                    else
                        no_tun=no_tun+1;
                        path_x=b+path_x;
                        I_tun=I_tun+I_0*exp(-at_co*path);
                    end



                    %
                    %   Determining Reflected rays off n_1 interface
                    %   wall
                    %
                elseif (abs(angle_prop)<theta_c_0)    %%Being reflected from the
scintillator wall
                    no_core_s=no_core_s+1;


                    if (abs(angle_prop)<Max_Theta)
                        no_bound_s=no_bound_s+1;
                        I_bound_s=I_bound_s+I_0*exp(-at_co*path);
                        theta_a=angle_a(w);
                    elseif (abs(angle_tot)<Min_tot_inc)&(abs(angle_prop)<theta_c_0)
                        no_ref_s=no_ref_s+1;
                        I_ref_s=I_ref_s+I_0*exp(-at_co*path);
                        theta_a=angle_a(w);
                    else
                        no_tun_s=no_tun_s+1;
                        I_tun_s=I_tun_s+I_0*exp(-at_co*path);
                        theta_a=angle_a(w);

                    end



                    %
                    %   Determining the refracted rays
                    %
                elseif (abs(angle_tot)<(pi/2-theta_c_0))
                    length_source=a;


                    %%Determine refracted Angles

                    angle_prop1=acos((n_0/n_1)*cos(angle_prop));        %Propagation
 angle in n_1
                    angle_azi1=acos(((n_0*sin(abs(angle_prop)))/(n_1*sin(abs(
angle_prop1))))*cos(angle_azi));     %Azimuthal angle in n_1


                    angle_tot1=asin((n_0/n_1)*sin(angle_tot));
                    angle_tot11=acos(sin(angle_prop1)*sin(angle_azi1));
```

```
                    if (abs(angle_tot1-angle_tot11)>1e-10)
                        angle_tot1-angle_tot11
                        angle_azi1
                    end


                    %Solve for pathlenth and ray tracing in n_1
                    rad_source=b;


                    no=no+1;
                    Ref_n1=Refracted(angle_prop,angle_azi,angle_prop1,angle_azi1,r_1
,r_ss,rad_source,length_source,theta_c_2,no,theta_a,theta_c_0,n_1,n_0,r_co);    %
Where Ref_n1(1) is path and Ref_n1(2) is q

                    path=Ref_n1(1);
                    q=Ref_n1(2);

                    if (q==0)   %Then ray reached core via n_0
                        no_core_s1=no_core_s1+1;

                        if (abs(angle_prop)<Max_Theta)
                            no_bound_s1=no_bound_s1+1;
                            I_bound_s1=I_bound_s1+I_0*exp(-at_co*path);
                            disp ('bound rays entering via n_0 BUT were refracted
through n_1')

                        elseif (abs(angle_tot)<Min_tot_inc)
                            no_ref_s1=no_ref_s1+1;
                            I_ref_s1=I_ref_s1+I_0*exp(-at_co*path);

                        else
                            no_tun_s1=no_tun_s1+1;
                            I_tun_s1=I_tun_s1+I_0*exp(-at_co*path);
                            disp ('tunneled rays entering via n_0 BUT were refracted
 through n_1')
                        end

                    elseif (q==1)   %Then ray reached core via n_1

                        no_core_s1=no_core_s1+1;

                        if (abs(angle_prop1)<theta_m1)
                            no_bound_s1=no_bound_s1+1;
                            I_bound_s1=I_bound_s1+I_0*exp(-at_co*path);

                        elseif (abs(angle_tot1)<Min_tot_inc1)
                            no_ref_s1=no_ref_s1+1;
                            I_ref_s1=I_ref_s1+I_0*exp(-at_co*path);

                        else
                            no_tun_s1=no_tun_s1+1;
                            I_tun_s1=I_tun_s1+I_0*exp(-at_co*path);
                        end

                    end


                end

            end
        end

    end

    t=l_in;
    R_1=b-(0.5*r_in);
    R_2=b+(0.5*r_in);
```

```
V_disc1=V_disc1 + (pi*t*(((R_2).^2)-((R_1).^2)));
V_disc=(pi*t*(((R_2).^2)-((R_1).^2)));

%%%%%%%%%%%%%%%%%%%%%%%%%%%%%%%%%%%%%%%%%%%%%%%%%%%%%%%%%%%%%%%%%%%%%%%
%
%       Determining Solid Angle and power of each class

if (no_bound>0)
    I_bound1=I_bound/no_bound;
    Sol_bound=(no_bound/no_Sources)*2*pi;
    CE_bound=CE_bound+I_bound1*((Sol_bound)*V_disc);
end

if (no_ref>0)
    I_ref1=I_ref/no_ref;
    Sol_ref=(no_ref/no_Sources)*2*pi;
    CE_ref=CE_ref+I_ref1*((Sol_ref)*V_disc);
end

if (no_tun>0)
    I_tun1=I_tun/no_tun;
    Sol_tun=(no_tun/no_Sources)*2*pi;
    CE_tun=CE_tun+I_tun1*((Sol_tun)*V_disc);
end


total_No_Sources=total_No_Sources+no_Sources;
inc_core_no=inc_core_no+no_core;
bound_No_Sources=bound_No_Sources+no_bound;
ref_No_Sources=ref_No_Sources+no_ref;
tun_No_Sources=tun_No_Sources+no_tun;

CE_bound1=CE_bound1+CE_bound;
CE_ref1=CE_ref1+CE_ref;
CE_tun1=CE_tun1+CE_tun;


%
%   Resetting the no.sources

no_core=0;
no_bound=0;
no_ref=0;
no_tun=0;
I_bound=0;
I_ref=0;
I_tun=0;
CE_bound=0;
CE_ref=0;
CE_tun=0;



%
%%For those from scintillator wall reflections
%
if (no_bound_s>0)
    I_bound1_s=I_bound_s/no_bound_s;
    Sol_bound_s=(no_bound_s/no_Sources)*2*pi;
    CE_bound_s=CE_bound_s+I_bound1_s*((Sol_bound_s)*V_disc);
end

if (no_ref_s>0)
    I_ref1_s=I_ref_s/no_ref_s;
    Sol_ref_s=(no_ref_s/no_Sources)*2*pi;
    CE_ref_s=CE_ref_s+I_ref1_s*((Sol_ref_s)*V_disc);
end

if (no_tun_s>0)
    I_tun1_s=I_tun_s/no_tun_s;
```

```
    Sol_tun_s=(no_tun_s/no_Sources)*2*pi;
    CE_tun_s=CE_tun_s+I_tun1_s*((Sol_tun_s)*V_disc);
end


total_No_Sources_s=total_No_Sources_s+no_Sources;
inc_core_no_s=inc_core_no_s+no_core_s;
bound_No_Sources_s=bound_No_Sources_s+no_bound_s;
ref_No_Sources_s=ref_No_Sources_s+no_ref_s;
tun_No_Sources_s=tun_No_Sources_s+no_tun_s;

CE_bound1_s=CE_bound1_s+CE_bound_s;
CE_ref1_s=CE_ref1_s+CE_ref_s;
CE_tun1_s=CE_tun1_s+CE_tun_s;


%
%   Resetting the no.sources


no_core_s=0;
no_bound_s=0;
no_ref_s=0;
no_tun_s=0;
I_bound_s=0;
I_ref_s=0;
I_tun_s=0;
CE_bound_s=0;
CE_ref_s=0;
CE_tun_s=0;



%
%%For those from scintillator wall refractions
%
if (no_bound_s1>0)
    I_bound1_s1=I_bound_s1/no_bound_s1;
    Sol_bound_s1=(no_bound_s1/no_Sources)*2*pi;
    CE_bound_s1=CE_bound_s1+I_bound1_s1*((Sol_bound_s1)*V_disc);
end

if (no_ref_s1>0)
    I_ref1_s1=I_ref_s1/no_ref_s1;
    Sol_ref_s1=(no_ref_s1/no_Sources)*2*pi;
    CE_ref_s1=CE_ref_s1+I_ref1_s1*((Sol_ref_s1)*V_disc);
end

if (no_tun_s1>0)
    I_tun1_s1=I_tun_s1/no_tun_s1;
    Sol_tun_s1=(no_tun_s1/no_Sources)*2*pi;
    CE_tun_s1=CE_tun_s1+I_tun1_s1*((Sol_tun_s1)*V_disc);
end


total_No_Sources_s1=total_No_Sources_s1+no_Sources;
inc_core_no_s1=inc_core_no_s1+no_core_s1;
bound_No_Sources_s1=bound_No_Sources_s1+no_bound_s1;
ref_No_Sources_s1=ref_No_Sources_s1+no_ref_s1;
tun_No_Sources_s1=tun_No_Sources_s1+no_tun_s1;

CE_bound1_s1=CE_bound1_s1+CE_bound_s1;
CE_ref1_s1=CE_ref1_s1+CE_ref_s1;
CE_tun1_s1=CE_tun1_s1+CE_tun_s1;


%
%   Resetting the no.sources

no_Sources=0;
```

```
        no_core_s1=0;
        no_bound_s1=0;
        no_ref_s1=0;
        no_tun_s1=0;
        I_bound_s1=0;
        I_ref_s1=0;
        I_tun_s1=0;
        CE_bound_s1=0;
        CE_ref_s1=0;
        CE_tun_s1=0;


        %
        %%%%%%%%%%%%%%%%%%%%%%%%%%%%%%%%%%%%%%%%%%%%%%%%%%%%%%%%%%%%%%%%%%%

    end

    i/length(l)

    Inner_Vdisc(i)=V_disc1;
    bound_CE(i)=CE_bound1;
    ref_CE(i)=CE_ref1;
    tun_CE(i)=CE_tun1;
    x_total_No_Sources(i)=total_No_Sources;
    x_inc_core_no(i)=inc_core_no;
    x_bound_No_Sources(i)=bound_No_Sources;
    x_ref_No_Sources(i)=ref_No_Sources;
    x_tun_No_Sources(i)=tun_No_Sources;

    %%From those refected from scintillator wall reflections
    bound_CE_s(i)=CE_bound1_s;
    ref_CE_s(i)=CE_ref1_s;
    tun_CE_s(i)=CE_tun1_s;
    x_inc_core_no_s(i)=inc_core_no_s;
    x_bound_No_Sources_s(i)=bound_No_Sources_s;
    x_ref_No_Sources_s(i)=ref_No_Sources_s;
    x_tun_No_Sources_s(i)=tun_No_Sources_s;

    %%From those refected from scintillator wall refractions
    bound_CE_s1(i)=CE_bound1_s1;
    ref_CE_s1(i)=CE_ref1_s1;
    tun_CE_s1(i)=CE_tun1_s1;
    x_inc_core_no_s1(i)=inc_core_no_s1;
    x_bound_No_Sources_s1(i)=bound_No_Sources_s1;
    x_ref_No_Sources_s1(i)=ref_No_Sources_s1;
    x_tun_No_Sources_s1(i)=tun_No_Sources_s1;

end

x_Inner=l;
y_Inner=r;


if (at_co==0)
    rootname1='_without_opt_att';
else
    rootname1='_with_opt_att';
end



rootname='OSL_Inner_r_';
extension='.mat';

filename=[rootname,int2str(I_r_11),rootname1,int2str(File_no),extension];

delete (filename)
```

```
save (filename, 'x_Inner', 'bound_CE','ref_CE','tun_CE', 'x_total_No_Sources','
    x_bound_No_Sources','x_ref_No_Sources','x_tun_No_Sources','y_Inner','Inner_Vdisc','
    x_bound_No_Sources_s','x_ref_No_Sources_s','x_tun_No_Sources_s','bound_CE_s','
    ref_CE_s','tun_CE_s','x_inc_core_no','x_inc_core_no_s','x_bound_No_Sources_s1','
    x_ref_No_Sources_s1','x_tun_No_Sources_s1','bound_CE_s1','ref_CE_s1','tun_CE_s1','
    x_inc_core_no_s1')     %Saves the variables y, x, x_CE and x_No_Sources


CEE=CE_bound;
Sources=no_Sources;
F=[CEE,Sources];
```

A.3 Refraction modelling

```
%%%%%%%%%%%%%%%%%%%%%%%%%%%%%%%%%%%%%%%%%%%%%%%%%%%%%%%%%%%%%%%%%%%%%%%%%%%%%%%
%
%   This code solves the ray paths when refracted into n_1
%   For the "Cladding Coupled" Geometry
%
%%%%%%%%%%%%%%%%%%%%%%%%%%%%%%%%%%%%%%%%%%%%%%%%%%%%%%%%%%%%%%%%%%%%%%%%%%%%%%%

function F=Refrated(angle_prop,angle_azi,angle_prop1,angle_azi1,r_1,r_ss,rad_source,
    length_source,theta_c_2,no,theta_a,theta_c_0,n_1,n_0,r_co)

format long


%
%   Making sure that we only look at positive propagation angles,
%   This is since we are varying the azimuthal angle
%
qq=0;
if (angle_prop<0)
    qq=5;
end

theta_a1=theta_a+(angle_azi-angle_azi1);



a=rad_source;     %Initial position of source in x
b=0;     %Initial position of source in y
g=0;
m=sqrt((a.^2)+(b.^2));      %Will be the current distance from optical axis
path=0;

%
% 1
%
%%Initial path in n_0

%
%%Determining Theta_a1


c=cos(theta_a)*sin(angle_prop);   %Variables in x
d=sin(theta_a)*sin(angle_prop);    %Variables in y
e=cos(angle_prop);           %Variables in z

%If ray reflected towards n_0
r_01=(-((2*a*c)+(2*b*d))+sqrt((((2*a*c)+(2*b*d)).^2)-(4*((c.^2)+(d.^2))*((a.^2)+(b.^2)
    -((r_1).^2)))))/(2*((c.^2)+(d.^2)));     %plus
r_02=(-((2*a*c)+(2*b*d))-sqrt((((2*a*c)+(2*b*d)).^2)-(4*((c.^2)+(d.^2))*((a.^2)+(b.^2)
    -((r_1).^2)))))/(2*((c.^2)+(d.^2)));     %minus
%If ray reflected kept in n_1
```

```
r_11=(-((2*a*c)+(2*b*d))+sqrt((((2*a*c)+(2*b*d)).^2)-(4*((c.^2)+(d.^2))*((a.^2)+(b.^2)
    -((r_ss).^2)))))/(2*((c.^2)+(d.^2)));      %plus


if (isreal(r_01)==1)&(isreal(r_02==1))

    if (r_02>0)
        if (r_01>r_02)
            r_0=r_02;
        elseif (r_01<=0)
            r_0=r_02;
        else
            r_0=r_1;
        end
    else
        r_0=r_01;
    end
elseif (isreal(r_01)==1)&(isreal(r_02)==0)
    r_0=r_01;
elseif (isreal(r_01)==0)&(isreal(r_02)==1)
    r_0=r_02;
else
    r_0=r_01;
end

q=0;

if (isreal(r_0)==1)&(isreal(r_11)==1)       %If both are real

    if (r_11<=0)&(r_0>0)
        x=r_0*c;
        y=r_0*d;
        z=r_0*e;


        a=a+x;
        b=b+y;
        g=g+z;
        m=sqrt((a.^2)+(b.^2));

        q=0;



        if (g<length_source)        %Still hasnt reached the optical fiber and is now
    refracted into n_1

            %%Need to re-calculate azimuthal in n_1

            path=path + r_0;     %pathlenth travelled in n_0

            %
            %%Ensuring the corrent azimuthal angle
            x_1=a;
            x_0=a-x;
            y_1=b;
            y_0=b-y;
            length=sqrt(((x_1-x_0).^2)+((y_1-y_0).^2));
            azi1=acos(((length.^2)+(sqrt(((x_0).^2)+((y_0).^2)).^2)-(r_1.^2))/(2*length*
    sqrt(((x_0).^2)+((y_0).^2))))-(pi/2);
            azi1=abs(azi1);
            if (rad_source==0)
                azi1=pi/2;
            end

            %   Determining new azimuthal angles

            angle_azi1=acos(((n_0*sin(abs(angle_prop)))/(n_1*sin(abs(angle_prop1))))*cos
    (azi1));
            angle_azi=acos(((n_1*sin(abs(angle_prop1)))/(n_0*sin(abs(angle_prop))))*cos(
    angle_azi1));
```

```
        theta_a1=theta_a+(azi1-angle_azi1);
        theta_a=theta_a1+(angle_azi-angle_azi1);


        if (angle_azi>pi/2)
            disp ('wtf with azi0')
        end

        q=1;        %letting know that now in n_1

        c=cos(theta_a1)*sin(angle_prop1);   %Variables in x
        d=sin(theta_a1)*sin(angle_prop1);    %Variables in y
        e=cos(angle_prop1);           %Variables in z for n_1


        %
        %%Determining path of ray
        r_r1=(-((2*a*c)+(2*b*d))+sqrt((((2*a*c)+(2*b*d)).^2)-(4*((c.^2)+(d.^2))*((a
.^2)+(b.^2)-((r_1).^2)))))/(2*((c.^2)+(d.^2)));  %plus
        r_r2=(-((2*a*c)+(2*b*d))-sqrt((((2*a*c)+(2*b*d)).^2)-(4*((c.^2)+(d.^2))*((a
.^2)+(b.^2)-((r_1).^2)))))/(2*((c.^2)+(d.^2)));  %minus

        if (isreal(r_r1)==1)&(isreal(r_r2==1))
            if (r_r2>0)
                if (r_r1>r_r2)
                    r=r_r1;
                else
                    r=r_r2;
                end
            else
                r=r_r1;
            end


        elseif (isreal(r_r1)==1)&(isreal(r_r2)==0)
            r=r_r1;
        elseif (isreal(r_r1)==0)&(isreal(r_r2)==1)
            r=r_r2;
        else
            r=r_r1;
        end



        x=r*c;
        y=r*d;
        z=r*e;

        a=a+x;
        b=b+y;
        g=g+z;
        m=sqrt((a.^2)+(b.^2));



    else
        disp('something wrong with initial calcs')
        1

    end

elseif (r_0<r_11)&(r_0>0)  %then ray travelling to n_1
    x=r_0*c;
    y=r_0*d;
    z=r_0*e;


    a=a+x;
    b=b+y;
    g=g+z;
```

```
    m=sqrt((a.^2)+(b.^2));

    q=0;


    if (g<length_source)        %Still hasnt reached the optical fiber and is now
refracted into n_0


        %%Need to re-calculate azimuthal in n_1
        path=path + r_0;     %pathlenth travelled in n_0

        %
        %%Ensuring the corrent azimuthal angle
        x_1=a;
        x_0=a-x;
        y_1=b;
        y_0=b-y;
        length=sqrt(((x_1-x_0).^2)+((y_1-y_0).^2));
        azi1=acos(((length.^2)+(sqrt(((x_0).^2)+((y_0).^2)).^2)-(r_1.^2))/(2*length*
sqrt(((x_0).^2)+((y_0).^2))))-(pi/2);
        azi1=abs(azi1);
        if (rad_source==0)
            azi1=pi/2;
        end

        %   Determining new azimuthal angles
        angle_azi1=acos(((n_0*sin(abs(angle_prop)))/(n_1*sin(abs(angle_prop1))))*cos
(azi1));
        angle_azi=acos(((n_1*sin(abs(angle_prop1)))/(n_0*sin(abs(angle_prop))))*cos(
angle_azi1));

        theta_a1=theta_a+(azi1-angle_azi1);
        theta_a=theta_a1+(angle_azi-angle_azi1);

        if (angle_azi>pi/2)
            disp ('wtf with azi0')
        end

        q=1;        %letting know that now in n_1

        c=cos(theta_a1)*sin(angle_prop1);   %Variables in x
        d=sin(theta_a1)*sin(angle_prop1);    %Variables in y
        e=cos(angle_prop1);           %Variables in z for n_1


        %
        %%Determining path of ray
        r_r1=(-((2*a*c)+(2*b*d))+sqrt((((2*a*c)+(2*b*d)).^2)-(4*((c.^2)+(d.^2))*((a
.^2)+(b.^2)-((r_1).^2)))))/(2*((c.^2)+(d.^2)));  %plus
        r_r2=(-((2*a*c)+(2*b*d))-sqrt((((2*a*c)+(2*b*d)).^2)-(4*((c.^2)+(d.^2))*((a
.^2)+(b.^2)-((r_1).^2)))))/(2*((c.^2)+(d.^2)));  %minus


        if (isreal(r_r1)==1)&(isreal(r_r2==1))
            if (r_r2>0)
                if (r_r1>r_r2)
                    r=r_r1;
                else
                    r=r_r2;
                end
            else
                r=r_r1;
            end


        elseif (isreal(r_r1)==1)&(isreal(r_r2)==0)
            r=r_r1;
        elseif (isreal(r_r1)==0)&(isreal(r_r2)==1)
            r=r_r2;
```

```
            else
                r=r_r1;
            end



            x=r*c;
            y=r*d;
            z=r*e;

            a=a+x;
            b=b+y;
            g=g+z;
            m=sqrt((a.^2)+(b.^2));



        else
%             disp('something wrong with initial calcs')
%             2

        end

    elseif (r_0<=0)&(r_11>0)

        x=r_11*c;
        y=r_11*d;
        z=r_11*e;

        a=a+x;
        b=b+y;
        g=g+z;
        m=sqrt((a.^2)+(b.^2));

        q=0;



        if (g<length_source)
            path=path + r_11;     %pathlenth travelled in n_0
            q=0;

        else
            disp('something wrong with initial calcs')
            3

        end

    elseif (r_11<r_0)&(r_11>0)      %then ray was reflected to n_1 again travelling
    through n_1
        x=r_11*c;
        y=r_11*d;
        z=r_11*e;

        a=a+x;
        b=b+y;
        g=g+z;
        m=sqrt((a.^2)+(b.^2));

        q=0;



        if (g<length_source)
            path=path + r_11;     %pathlenth travelled in n_0
            q=0;

        else
            disp('something wrong with initial calcs')
            4
```

```
        end

    else
        q=2;
    end

elseif (isreal(r_0)==1)&(isreal(r_11)==0)  %then ray was reflected to n_0 since only
    real option
    x=r_0*c;
    y=r_0*d;
    z=r_0*e;

    a=a+x;
    b=b+y;
    g=g+z;
    m=sqrt((a.^2)+(b.^2));

    q=0;



    if (g<length_source)        %Still hasnt reached the optical fiber and is now
    refracted into n_0

        %%Need to re-calculate azimuthal in n_1
        path=path + r_0;     %pathlenth travelled in n_0

        %
        %%Ensuring the corrent azimuthal angle
        x_1=a;
        x_0=a-x;
        y_1=b;
        y_0=b-y;
        length=sqrt(((x_1-x_0).^2)+((y_1-y_0).^2));
        azi1=acos(((length.^2)+(sqrt(((x_0).^2)+((y_0).^2)).^2)-(r_1.^2))/(2*length*sqrt
    (((x_0).^2)+((y_0).^2))))-(pi/2);
        azi1=abs(azi1);
        if (rad_source==0)
            azi1=pi/2;
        end

        %   Determining new azimuthal angles
        angle_azi1=acos(((n_0*sin(abs(angle_prop)))/(n_1*sin(abs(angle_prop1))))*cos(
    azi1));
        angle_azi=acos(((n_1*sin(abs(angle_prop1)))/(n_0*sin(abs(angle_prop))))*cos(
    angle_azi1));

        theta_a1=theta_a+(azi1-angle_azi1);
        theta_a=theta_a1+(angle_azi-angle_azi1);

        if (angle_azi>pi/2)
            disp ('wtf with azi0')
        end


        q=1;        %letting know that now in n_1

        c=cos(theta_a1)*sin(angle_prop1);   %Variables in x
        d=sin(theta_a1)*sin(angle_prop1);    %Variables in y
        e=cos(angle_prop1);           %Variables in z

        %
        %%determines path of ray
        r_r1=(-((2*a*c)+(2*b*d))+sqrt((((2*a*c)+(2*b*d)).^2)-(4*((c.^2)+(d.^2))*((a.^2)
    +(b.^2)-((r_1).^2)))))/(2*((c.^2)+(d.^2)));  %plus
        r_r2=(-((2*a*c)+(2*b*d))-sqrt((((2*a*c)+(2*b*d)).^2)-(4*((c.^2)+(d.^2))*((a.^2)
    +(b.^2)-((r_1).^2)))))/(2*((c.^2)+(d.^2)));  %minus

        if (isreal(r_r1)==1)&(isreal(r_r2==1))
            if (r_r2>0)
                if (r_r1>r_r2)
```

```
                    r=r_r1;
                else
                    r=r_r2;
                end
            else
                r=r_r1;
            end


        elseif (isreal(r_r1)==1)&(isreal(r_r2)==0)
            r=r_r1;
        elseif (isreal(r_r1)==0)&(isreal(r_r2)==1)
            r=r_r2;
        else
            r=r_r1;
        end




        x=r*c;
        y=r*d;
        z=r*e;

        a=a+x;
        b=b+y;
        g=g+z;
        m=sqrt((a.^2)+(b.^2));



    else
        disp('something wrong with initial calcs')
        6

    end

elseif (isreal(r_11)==1)&(isreal(r_0)==0)      %then ray travels to n_1 since it is only
     real option
    x=r_11*c;
    y=r_11*d;
    z=r_11*e;

    a=a+x;
    b=b+y;
    g=g+z;
    m=sqrt((a.^2)+(b.^2));

    q=0;



    if (g<length_source)

        path=path + r_11;     %pathlenth travelled in n_0
        q=0;

    else
        disp('something wrong with initial calcs')
        7

    end
elseif (isreal(r_11)==0) & (isreal(r_0)==0)     %if neither are possible, there must be
    something wrong in angles
    disp('angles not right since both r_11 and r_0 are complex')

end
```

```
while (g<length_source)        %If still hasnt reached the optical fiber, then now
    refracted in n_1

    %
    %% Removes any negative progagation angle
    if (qq==5)
        q=5;

        break
    end

    %
    % 2
    %
    %% If ray is exiting n_1 and entering n_0
    if (q==1)       %hence ray in n_1 and entering n_0

        c=cos(theta_a)*sin(angle_prop);      %Variables in x for n_1
        d=sin(theta_a)*sin(angle_prop);      %Variables in y for n_1
        e=cos(angle_prop);           %Variables in z for n_1

        %
        %%Determining ray path
        r_r1=(-((2*a*c)+(2*b*d))+sqrt((((2*a*c)+(2*b*d)).^2)-(4*((c.^2)+(d.^2))*((a.^2)
    +(b.^2)-((r_ss).^2)))))/(2*((c.^2)+(d.^2)));     %plus
        r_r2=(-((2*a*c)+(2*b*d))-sqrt((((2*a*c)+(2*b*d)).^2)-(4*((c.^2)+(d.^2))*((a.^2)
    +(b.^2)-((r_ss).^2)))))/(2*((c.^2)+(d.^2)));     %minus

        if (isreal(r_r1)==1)&(isreal(r_r2==1))
            if (r_r2>0)
                if (r_r1>r_r2)
                    r=r_r2;
                else
                    r=r_r1;
                end
            else
                r=r_r1;
            end
        elseif (isreal(r_r1)==1)&(isreal(r_r2)==0)
            r=r_r1;
        elseif (isreal(r_r1)==0)&(isreal(r_r2)==1)
            r=r_r2;
        else
            r=r_r1;
        end


        x=r*c;
        y=r*d;
        z=r*e;

        a=a+x;
        b=b+y;
        g=g+z;

        q=0;    %letting know that now in n_0
        m=sqrt((a.^2)+(b.^2));



        %Checking if ray going beyond core
        %If so need to correct to get position at core
        if (g>length_source)

            a=a-x;
            b=b-y;
            g=g-z;
```

```
            z=length_source-g;
            r_0=z/e;

            x=r_0*c;
            y=r_0*d;

            a=a+x;
            b=b+y;
            g=g+z;

            q=0;

            path=path + r_0;     %pathlenth travelled in n_0



            break

        end


        path=path + r;     %pathlenth travelled in n_0


    end

    %
    % 3
    %
    %% If ray reflects from the n_0 and n_2 interface
    if (abs(angle_prop1)<theta_c_2)&(q==0)    %Will reflect from n_1 and n_2 interface



        %Determining the reflected azimuthal angle

        theta_a=theta_a+(2*angle_azi);




        c=cos(theta_a)*sin(angle_prop);      %Variables in x for n_1
        d=sin(theta_a)*sin(angle_prop);     %Variables in y for n_1
        e=cos(angle_prop);           %Variables in z for n_1


        %%Once reflected ray may travel to n_0 or n_1 interface

        %If ray reflected towards n_0
        r_01=(-((2*a*c)+(2*b*d))+sqrt((((2*a*c)+(2*b*d)).^2)-(4*((c.^2)+(d.^2))*((a.^2)
    +(b.^2)-((r_1).^2)))))/(2*((c.^2)+(d.^2)));     %plus
        r_02=(-((2*a*c)+(2*b*d))-sqrt((((2*a*c)+(2*b*d)).^2)-(4*((c.^2)+(d.^2))*((a.^2)
    +(b.^2)-((r_1).^2)))))/(2*((c.^2)+(d.^2)));     %minus
        %If ray reflected kept in n_1
        r_11=(-((2*a*c)+(2*b*d))+sqrt((((2*a*c)+(2*b*d)).^2)-(4*((c.^2)+(d.^2))*((a.^2)
    +(b.^2)-((r_ss).^2)))))/(2*((c.^2)+(d.^2)));     %plus


        if (isreal(r_01)==1)&(isreal(r_02==1))

            if (r_02>0)
                if (r_01>r_02)
                    r_0=r_02;
                elseif (r_01<=0)
                    r_0=r_02;
                else
                    r_0=r_1;
                end
```

```
        else
            r_0=r_01;
        end
    elseif (isreal(r_01)==1)&(isreal(r_02)==0)
        r_0=r_01;
    elseif (isreal(r_01)==0)&(isreal(r_02)==1)
        r_0=r_02;
    else
        r_0=r_01;
    end


    if (isreal(r_0)==1)&(isreal(r_11)==1)       %If both are real and possible

        if (r_11<=0)&(r_0>0)
            x=r_0*c;
            y=r_0*d;
            z=r_0*e;


            a=a+x;
            b=b+y;
            g=g+z;
            m=sqrt((a.^2)+(b.^2));

            fprintf(file_7, '%1.12f \t %1.12f \t %1.12f \t %i \t %1.12f \t %1.12f \t
 %1.12f \t %1.12f \t %1.12f \t %1.12f \t %1.12f \n', a,b,g,q,m,theta_a,theta_a1,
angle_azi,angle_azi1,angle_prop,angle_prop1);    %Putting in positions x,y,z

            if (g<length_source)        %Still hasnt reached the optical fiber and
is now refracted into n_0

                %%Need to re-calculate azimuthal in n_1
                path=path + r_0;     %pathlenth travelled in n_0

                %
                %%Ensuring the corrent azimuthal angle
                x_1=a;
                x_0=a-x;
                y_1=b;
                y_0=b-y;
                length=sqrt(((x_1-x_0).^2)+((y_1-y_0).^2));
                azi1=acos(((length.^2)+(r_ss.^2)-(r_1.^2))/(2*length*r_ss))-(pi/2);
                azi1=abs(azi1);
                if (rad_source==0)
                    azi1=pi/2;
                end

                %   Determining new azimuthal angles
                angle_azi1=acos(((n_0*sin(abs(angle_prop)))/(n_1*sin(abs(angle_prop1
))))*cos(azi1));
                angle_azi=acos(((n_1*sin(abs(angle_prop1)))/(n_0*sin(abs(angle_prop)
)))*cos(angle_azi1));

                theta_a1=theta_a+(azi1-angle_azi1);
                theta_a=theta_a1+(angle_azi-angle_azi1);

                if (angle_azi>pi/2)
                    disp ('wtf with azi0')
                end

                q=1;        %letting know that now in n_1

                c=cos(theta_a1)*sin(angle_prop1);   %Variables in x
                d=sin(theta_a1)*sin(angle_prop1);    %Variables in y
                e=cos(angle_prop1);           %Variables in z for n_1


                %
                %%Determining path of ray
```

```
                r_r1=(-((2*a*c)+(2*b*d))+sqrt((((2*a*c)+(2*b*d)).^2)-(4*((c.^2)+(d
.^2))*((a.^2)+(b.^2)-((r_1).^2)))))/(2*((c.^2)+(d.^2)));  %plus
                r_r2=(-((2*a*c)+(2*b*d))-sqrt((((2*a*c)+(2*b*d)).^2)-(4*((c.^2)+(d
.^2))*((a.^2)+(b.^2)-((r_1).^2)))))/(2*((c.^2)+(d.^2)));  %minus

                if (isreal(r_r1)==1)&(isreal(r_r2==1))
                    if (r_r2>0)
                        if (r_r1>r_r2)
                            r=r_r1;
                        else
                            r=r_r2;
                        end
                    else
                        r=r_r1;
                    end


                elseif (isreal(r_r1)==1)&(isreal(r_r2)==0)
                    r=r_r1;
                elseif (isreal(r_r1)==0)&(isreal(r_r2)==1)
                    r=r_r2;
                else
                    r=r_r1;
                end



                x=r*c;
                y=r*d;
                z=r*e;

                a=a+x;
                b=b+y;
                g=g+z;
                m=sqrt((a.^2)+(b.^2));



            else
                a=a-x;
                b=b-y;
                g=g-z;

                z=length_source-g;
                r_0=z/e;

                x=r_0*c;
                y=r_0*d;

                a=a+x;
                b=b+y;
                g=g+z;

                path=path + r_0;     %pathlenth travelled in n_0


                break

            end

        elseif (r_0<r_11)&(r_0>0)  %then ray was reflected to n_0
            x=r_0*c;
            y=r_0*d;
            z=r_0*e;


            a=a+x;
            b=b+y;
            g=g+z;
            m=sqrt((a.^2)+(b.^2));
```

```
            if (g<length_source)        %Still hasnt reached the optical fiber and
is now refracted into n_0

                path=path + r_0;     %pathlenth travelled in n_0

                %%Need to re-calculate azimuthal in n_0


                %
                %%Ensuring the corrent azimuthal angle
                x_1=a;
                x_0=a-x;
                y_1=b;
                y_0=b-y;
                length=sqrt(((x_1-x_0).^2)+((y_1-y_0).^2));
                azi1=acos(((length.^2)+(r_ss.^2)-(r_1.^2))/(2*length*r_ss))-(pi/2);
                azi1=abs(azi1);
                if (rad_source==0)
                    azi1=pi/2;
                end

                %   Determining new azimuthal angles
                angle_azi1=acos(((n_0*sin(abs(angle_prop)))/(n_1*sin(abs(angle_prop1
))))*cos(azi1));
                angle_azi=acos(((n_1*sin(abs(angle_prop1)))/(n_0*sin(abs(angle_prop)
)))*cos(angle_azi1));

                theta_a1=theta_a+(azi1-angle_azi1);
                theta_a=theta_a1+(angle_azi-angle_azi1);

                if (angle_azi>(pi/2+0.00000001))
                    disp ('wtf with azi0')
                end


                q=1;        %letting know that now in n_1

                c=cos(theta_a1)*sin(angle_prop1);   %Variables in x
                d=sin(theta_a1)*sin(angle_prop1);    %Variables in y
                e=cos(angle_prop1);           %Variables in z for n_1


                %
                %%Determining path of ray
                r_r1=(-((2*a*c)+(2*b*d))+sqrt((((2*a*c)+(2*b*d)).^2)-(4*((c.^2)+(d
.^2))*((a.^2)+(b.^2)-((r_1).^2)))))/(2*((c.^2)+(d.^2)));  %plus
                r_r2=(-((2*a*c)+(2*b*d))-sqrt((((2*a*c)+(2*b*d)).^2)-(4*((c.^2)+(d
.^2))*((a.^2)+(b.^2)-((r_1).^2)))))/(2*((c.^2)+(d.^2)));  %minus


                if (isreal(r_r1)==1)&(isreal(r_r2==1))
                    if (r_r2>0)
                        if (r_r1>r_r2)
                            r=r_r1;
                        else
                            r=r_r2;
                        end
                    else
                        r=r_r1;
                    end


                elseif (isreal(r_r1)==1)&(isreal(r_r2)==0)
                    r=r_r1;
                elseif (isreal(r_r1)==0)&(isreal(r_r2)==1)
                    r=r_r2;
                else
                    r=r_r1;
                end
```

```
            x=r*c;
            y=r*d;
            z=r*e;

            a=a+x;
            b=b+y;
            g=g+z;
            m=sqrt((a.^2)+(b.^2));


        else
            a=a-x;
            b=b-y;
            g=g-z;

            z=length_source-g;
            r_0=z/e;

            x=r_0*c;
            y=r_0*d;

            a=a+x;
            b=b+y;
            g=g+z;

            path=path + r_0;     %pathlenth travelled in n_0


            break

        end

    elseif (r_0<=0)&(r_11>0)

        x=r_11*c;
        y=r_11*d;
        z=r_11*e;

        a=a+x;
        b=b+y;
        g=g+z;
        m=sqrt((a.^2)+(b.^2));


        if (g<length_source)
            path=path + r_11;     %pathlenth travelled in n_0
            q=0;

        else
            a=a-x;
            b=b-y;
            g=g-z;

            z=length_source-g;
            r_11=z/e;

            x=r_11*c;
            y=r_11*d;

            a=a+x;
            b=b+y;
            g=g+z;

            path=path + r_11;     %pathlenth travelled in n_0
```

```
                break

            end

        elseif (r_11<r_0)&(r_11>0)      %then ray was reflected to n_1 again
travelling through n_1
            x=r_11*c;
            y=r_11*d;
            z=r_11*e;

            a=a+x;
            b=b+y;
            g=g+z;
            m=sqrt((a.^2)+(b.^2));



            if (g<length_source)
                path=path + r_11;     %pathlenth travelled in n_0
                q=0;

            else
                a=a-x;
                b=b-y;
                g=g-z;

                z=length_source-g;
                r_11=z/e;

                x=r_11*c;
                y=r_11*d;

                a=a+x;
                b=b+y;
                g=g+z;

                path=path + r_11;     %pathlenth travelled in n_0


                break

            end

        else
            q=2;

            break
        end

    elseif (isreal(r_0)==1)&(isreal(r_11)==0)  %then ray was reflected to n_0 since
only real option
        x=r_0*c;
        y=r_0*d;
        z=r_0*e;

        a=a+x;
        b=b+y;
        g=g+z;
        m=sqrt((a.^2)+(b.^2));



        if (g<length_source)        %Still hasnt reached the optical fiber and is
now refracted into n_0

            path=path + r_0;     %pathlenth travelled in n_0

            %%Need to re-calculate azimuthal in n_0

            %
            %%Ensuring the corrent azimuthal angle
```

```
            x_1=a;
            x_0=a-x;
            y_1=b;
            y_0=b-y;
            length=sqrt(((x_1-x_0).^2)+((y_1-y_0).^2));
            azi1=acos(((length.^2)+(r_ss.^2)-(r_1.^2))/(2*length*r_ss))-(pi/2);
            azi1=abs(azi1);
            if (rad_source==0)
                azi1=pi/2;
            end

            %   Determining new azimuthal angles
            angle_azi1=acos(((n_0*sin(abs(angle_prop)))/(n_1*sin(abs(angle_prop1))))
*cos(azi1));
            angle_azi=acos(((n_1*sin(abs(angle_prop1)))/(n_0*sin(abs(angle_prop))))*
cos(angle_azi1));

            theta_a1=theta_a+(azi1-angle_azi1);
            theta_a=theta_a1+(angle_azi-angle_azi1);

            if (angle_azi>pi/2)
                disp ('wtf with azi0')
            end



            q=1;        %letting know that now in n_1

            c=cos(theta_a1)*sin(angle_prop1);   %Variables in x
            d=sin(theta_a1)*sin(angle_prop1);    %Variables in y
            e=cos(angle_prop1);           %Variables in z

            %
            %%determines path of ray
            r_r1=(-((2*a*c)+(2*b*d))+sqrt((((2*a*c)+(2*b*d)).^2)-(4*((c.^2)+(d.^2))
*((a.^2)+(b.^2)-((r_1).^2)))))/(2*((c.^2)+(d.^2)));  %plus
            r_r2=(-((2*a*c)+(2*b*d))-sqrt((((2*a*c)+(2*b*d)).^2)-(4*((c.^2)+(d.^2))
*((a.^2)+(b.^2)-((r_1).^2)))))/(2*((c.^2)+(d.^2)));  %minus

            if (isreal(r_r1)==1)&(isreal(r_r2==1))
                if (r_r2>0)
                    if (r_r1>r_r2)
                        r=r_r1;
                    else
                        r=r_r2;
                    end
                else
                    r=r_r1;
                end


            elseif (isreal(r_r1)==1)&(isreal(r_r2)==0)
                r=r_r1;
            elseif (isreal(r_r1)==0)&(isreal(r_r2)==1)
                r=r_r2;
            else
                r=r_r1;
            end




            x=r*c;
            y=r*d;
            z=r*e;

            a=a+x;
            b=b+y;
            g=g+z;
            m=sqrt((a.^2)+(b.^2));
```

```
        else
            a=a-x;
            b=b-y;
            g=g-z;

            z=length_source-g;
            r_0=z/e;

            x=r_0*c;
            y=r_0*d;

            a=a+x;
            b=b+y;
            g=g+z;

            path=path + r_0;     %pathlenth travelled in n_0


            break

        end

    elseif (isreal(r_11)==1)&(isreal(r_0)==0)      %then ray was reflected to n_1
since it is only real option
        x=r_11*c;
        y=r_11*d;
        z=r_11*e;

        a=a+x;
        b=b+y;
        g=g+z;
        m=sqrt((a.^2)+(b.^2));



        if (g<length_source)
            path=path + r_11;     %pathlenth travelled in n_0
            q=0;

        else
            a=a-x;
            b=b-y;
            g=g-z;

            z=length_source-g;
            r_11=z/e;

            x=r_11*c;
            y=r_11*d;

            path=path + r_11;     %pathlenth travelled in n_0

            a=a+x;
            b=b+y;
            g=g+z;

            break

        end
    elseif (isreal(r_11)==0) & (isreal(r_0)==0)     %if neither are possible, there
must be something wrong in angles
        q=3;
        %disp('angles not right since both r_11 and r_0 are complex')

        break

    end
```

```
    elseif (q==0)&(abs(angle_prop1)>theta_c_2)          %Ray is refracted out
        q=4;

        break

    end

    if (q==2)
        break
    end

end


if (g>(length_source+0.001))
    if (q~=2)&(q~=3)&(q~=4)&(q~=1)
        disp ('rays at the end going beyond the core of the fiber')
    end

end

%
%   Since still getting some imaginary paths
%   NEED TO FIX
%
if (isreal(path)==0)
    path=real(path);
end

path_final=path;
q_final=q;


F=[path_final,q_final];
```

Appendix B

Water equivalence and energy dependence

These codes were used to model the water equivalence and energy dependence of various detector materials.

B.1 Effective atomic number

```
%
%%  Calculation of effective atomic numbers
%%  Through various methods

clear all
clc

N0=6.022*10.^23;        %   Avogadro Constant

% m=3.5;       % Equation factor from Johns and Cunningham
m=2.94;       % Equation factor from (McCullough and Holmes, 1985).

%
%%  Water

%   Oxygen
n_1=1;                          %       Number of element in compound
z_1=8;                          %       Atomic number of element
a_1=15.999;                     %       Atomic mass of element

%   Hydrogen
n_2=2;
z_2=1;
a_2=1.008;

w_1=(n_1*a_1)/(((n_1*a_1)+(n_2*a_2)));
N_1=N0*z_1*w_1/a_1;
w_2=(n_2*a_2)/(((n_1*a_1)+(n_2*a_2)));
N_2=N0*z_2*w_2/a_2;

a_11=N_1/(N_1+N_2);
a_21=N_2/(N_1+N_2);
```

```
z_water_1=(a_11*(z_1^m))+(a_21*(z_2^m));
z_water=nthroot(z_water_1,m)

%
%%  Beryllium Oxide

%   Beryllium
n_1=1;
z_1=4;
a_1=9.012182;

%   Oxygen
n_2=1;
z_2=8;
a_2=15.999;

w_1=(n_1*a_1)/(((n_1*a_1)+(n_2*a_2)));
N_1=N0*z_1*w_1/a_1;
w_2=(n_2*a_2)/(((n_1*a_1)+(n_2*a_2)));
N_2=N0*z_2*w_2/a_2;

a_11=N_1/(N_1+N_2);
a_21=N_2/(N_1+N_2);

z_beo_1=(a_11*(z_1^m))+(a_21*(z_2^m));
z_beo=nthroot(z_beo_1,m)

% Aliox(Al2O3:C)

%   Aluminium
n_1=2;
z_1=13;
a_1=26.981;

%   Oxygen
n_2=3;
z_2=8;
a_2=15.999;

w_1=(n_1*a_1)/(((n_1*a_1)+(n_2*a_2)));
N_1=N0*z_1*w_1/a_1;
w_2=(n_2*a_2)/(((n_1*a_1)+(n_2*a_2)));
N_2=N0*z_2*w_2/a_2;

a_11=N_1/(N_1+N_2);
a_21=N_2/(N_1+N_2);

z_al2o3_1=(a_11*(z_1^m))+(a_21*(z_2^m));
z_al2o3=nthroot(z_al2o3_1,m)

% Lithium Fluoride

%   Lithium
n_1=1;
z_1=3;
a_1=6.94;

%   Fluorine
n_2=1;
z_2=9;
a_2=18.998;

w_1=(n_1*a_1)/(((n_1*a_1)+(n_2*a_2)));
N_1=N0*z_1*w_1/a_1;
w_2=(n_2*a_2)/(((n_1*a_1)+(n_2*a_2)));
N_2=N0*z_2*w_2/a_2;

a_11=N_1/(N_1+N_2);
a_21=N_2/(N_1+N_2);

z_LiF_1=(a_11*(z_1^m))+(a_21*(z_2^m));
```

```
z_LiF=nthroot(z_LiF_1,m)

%   BC-400 PS [Polyvinyltoluene base (C9H10)]

%   Carbon
n_1=9;
z_1=6;
a_1=12.0107;

%   Hydrogen
n_2=10;
z_2=1;
a_2=1.00794;

w_1=(n_1*a_1)/(((n_1*a_1)+(n_2*a_2)));
N_1=N0*z_1*w_1/a_1;
w_2=(n_2*a_2)/(((n_1*a_1)+(n_2*a_2)));
N_2=N0*z_2*w_2/a_2;

a_11=N_1/(N_1+N_2);
a_21=N_2/(N_1+N_2);

z_BC400_1=(a_11*(z_1^m))+(a_21*(z_2^m));
z_BC400=nthroot(z_BC400_1,m)

%   Polystyrene base (C8H8)

%   Carbon
n_1=8;
z_1=6;
a_1=12.0107;

%   Hydrogen
n_2=8;
z_2=1;
a_2=1.00794;

w_1=(n_1*a_1)/(((n_1*a_1)+(n_2*a_2)));
N_1=N0*z_1*w_1/a_1;
w_2=(n_2*a_2)/(((n_1*a_1)+(n_2*a_2)));
N_2=N0*z_2*w_2/a_2;

a_11=N_1/(N_1+N_2);
a_21=N_2/(N_1+N_2);

z_PS_1=(a_11*(z_1^m))+(a_21*(z_2^m));
z_PS=nthroot(z_PS_1,m)

%   Hexance Example (C6H14)

%   Carbon
n_1=6;
z_1=6;
a_1=12.0107;

%   Hydrogen
n_2=14;
z_2=1;
a_2=1.00794;

w_1=(n_1*a_1)/(((n_1*a_1)+(n_2*a_2)));
N_1=N0*z_1*w_1/a_1;
w_2=(n_2*a_2)/(((n_1*a_1)+(n_2*a_2)));
N_2=N0*z_2*w_2/a_2;

a_11=N_1/(N_1+N_2);
a_21=N_2/(N_1+N_2);

z_Hexane_1=(a_11*(z_1^m))+(a_21*(z_2^m));
z_Hexane=nthroot(z_Hexane_1,m)
```

B.2 Burlin Cavity Theory

```
%
%%  Calculates the burlin cavity theorem

clear all
clc

%
%%      Determine stopping power ratios
NIST_e_data
NIST_CSDA_data

for i=1:length(nist_e)
    sp_e(i)=nist_e(i);
    sp_ratio_BeO(i)=nist_BeO(i)/nist_water(i);
    sp_ratio_BC400(i)=nist_BC400(i)/nist_water(i);
    sp_ratio_LiF(i)=nist_LiF(i)/nist_water(i);
    sp_ratio_Al2O3(i)=nist_Al2O3(i)/nist_water(i);
end

%
%%  Determine mass energy absorption coefficents

clear nist_e
clear nist_BeO
clear nist_BC400
clear nist_LiF
clear nist_Al2O3
clear nist_water

NIST_mu_ab_data
nist_e=nist_O_e;

%
%%  BeO

%   Beryllium
n_1=1;
z_1=4;
a_1=9.012182;

%   Oxygen
n_2=1;
z_2=8;
a_2=15.999;

w_1=(n_1*a_1)/(((n_1*a_1)+(n_2*a_2)));
w_2=(n_2*a_2)/(((n_1*a_1)+(n_2*a_2)));

for i=1:length(nist_e)
    mu_BeO(i)=(w_1*(nist_Be(i)))+(w_2*(nist_O(i)));
end

%   BC-400 PS [Polyvinyltoluene base (C8H10)]

%   Carbon
n_1=9;
z_1=6;
a_1=12.0107;

%   Hydrogen
n_2=10;
z_2=1;
a_2=1.00794;

w_1=(n_1*a_1)/(((n_1*a_1)+(n_2*a_2)));
w_2=(n_2*a_2)/(((n_1*a_1)+(n_2*a_2)));

for i=1:length(nist_e)
```

```
    mu_BC400(i)=(w_1*(nist_C(i)))+(w_2*(nist_H(i)));
end

% Aliox(Al2O3:C)
%   Aluminium
n_1=2;
z_1=13;
a_1=26.981;

%   Oxygen
n_2=3;
z_2=8;
a_2=15.999;

w_1=(n_1*a_1)/(((n_1*a_1)+(n_2*a_2)));
w_2=(n_2*a_2)/(((n_1*a_1)+(n_2*a_2)));

for i=1:length(nist_e)
    mu_Al2O3(i)=(w_1*(nist_Al(i)))+(w_2*(nist_O(i)));
end

% Lithium Fluoride
%   Lithium
n_1=1;
z_1=3;
a_1=6.94;

%   Fluorine
n_2=1;
z_2=9;
a_2=18.998;

w_1=(n_1*a_1)/(((n_1*a_1)+(n_2*a_2)));
w_2=(n_2*a_2)/(((n_1*a_1)+(n_2*a_2)));

for i=1:length(nist_e)
    mu_LiF(i)=(w_1*(nist_Li(i)))+(w_2*(nist_F(i)));
end

for i=1:length(nist_e)
    mab_e(i)=nist_e(i);
    mab_ratio_BeO(i)=mu_BeO(i)/nist_H2O(i);
    mab_ratio_BC400(i)=mu_BC400(i)/nist_H2O(i);
    mab_ratio_LiF(i)=mu_LiF(i)/nist_H2O(i);
    mab_ratio_Al2O3(i)=mu_Al2O3(i)/nist_H2O(i);
end

figure (1)
p1=plot(mab_e,mab_ratio_BeO,'r')
hold
p2=plot(sp_e(1:53),sp_ratio_BeO(1:53),'r--')
p3=plot(mab_e,mab_ratio_BC400,'b')
p4=plot(sp_e(1:53),sp_ratio_BC400(1:53),'b--')
p5=plot(mab_e,mab_ratio_LiF,'k')
p6=plot(sp_e(1:53),sp_ratio_LiF(1:53),'k--')
p7=plot(mab_e,mab_ratio_Al2O3,'m')
p8=plot(sp_e(1:53),sp_ratio_Al2O3(1:53),'m--')
legend([p1;p2;p3;p4;p5;p6;p7;p8],'BeO d=0','BeO d=1','BC400 d=0','BC400 d=1','LiF d=0','
    LiF d=1','Al2O3 d=0','Al2O3 d=1')
title ('Burlin Cavity theory calculated Dose_{det} / Dose_{water}')
xlabel ('x-ray energy (MeV)')
ylabel ('D_{det}/D_{water}')

%
%%      Calculating the burlin cavit theorem

r_cyl=0.05;      % the radius of the cylinder in [cm]
h_cyl=0.1;       % the height of the cylinder in [cm]
V_cyl=pi*(r_cyl^2)*h_cyl;       % the volume of the cylinder in [cm3]
S_cyl=(2*pi*(r_cyl^2))+(2*pi*r_cyl*h_cyl);      %the surface area of the cylinder
L_cyl=(4*V_cyl)/S_cyl;          %the mean chord leangth across the cylinder in [cm]
```

```
a=0;
for i=1:length(mab_e)
    if (mab_e(i)>=0.01)
        a=a+1;
        bc_e(a)=mab_e(i);

        %
        %%  Find the corresponding electron energy
        for j=1:length(sp_e)

            if (sp_e(j)==mab_e(i))
                bc_sp_loc(a)=j;
                bc_mab_loc(a)=i;

            elseif (sp_e(j)>mab_e(i))&(sp_e(j-1)<mab_e(i))
                disp('Have to interpolate!!')
                pause
            end

        end
    end
end

for i=1:length(bc_sp_loc)

    t_max_BeO(i)=nist_CSDA_BeO(bc_sp_loc(i));
    t_max_BC400(i)=nist_CSDA_BC400(bc_sp_loc(i));
    t_max_LiF(i)=nist_CSDA_LiF(bc_sp_loc(i));
    t_max_Al2O3(i)=nist_CSDA_Al2O3(bc_sp_loc(i));
end

beta_BeO=-log(0.04)./t_max_BeO;
beta_BC400=-log(0.04)./t_max_BC400;
beta_LiF=-log(0.04)./t_max_LiF;
beta_Al2O3=-log(0.04)./t_max_Al2O3;

for i=1:length(bc_e)

    d_BeO(i)=(1-exp(-beta_BeO(i)*L_cyl))/(beta_BeO(i)*L_cyl);
    d_BC400(i)=(1-exp(-beta_BC400(i)*L_cyl))/(beta_BC400(i)*L_cyl);
    d_LiF(i)=(1-exp(-beta_LiF(i)*L_cyl))/(beta_LiF(i)*L_cyl);
    d_Al2O3(i)=(1-exp(-beta_Al2O3(i)*L_cyl))/(beta_Al2O3(i)*L_cyl);

end

figure (2)
p1=semilogx(bc_e,d_BeO,'r')
hold
p2=semilogx(bc_e,d_BC400,'b')
p3=semilogx(bc_e,d_LiF,'k')
p4=semilogx(bc_e,d_Al2O3,'m')
legend([p1;p2;p3;p4],'BeO','BC400','LiF','Al2O3')
title ('Burlin Cavity theory calculated d parameter')
xlabel ('x-ray energy (MeV)')
ylabel ('d')

%
%%  Calculating the Burlin Cavity
for i=1:length(bc_e)

    D_BeO_D_H2O(i)=(d_BeO(i)*sp_ratio_BeO(bc_sp_loc(i)))+((1-d_BeO(i))*mab_ratio_BeO(
    bc_mab_loc(i)));
    D_BC400_D_H2O(i)=(d_BC400(i)*sp_ratio_BC400(bc_sp_loc(i)))+((1-d_BC400(i))*
    mab_ratio_BC400(bc_mab_loc(i)));
    D_LiF_D_H2O(i)=(d_LiF(i)*sp_ratio_LiF(bc_sp_loc(i)))+((1-d_LiF(i))*mab_ratio_LiF(
    bc_mab_loc(i)));
    D_Al2O3_D_H2O(i)=(d_Al2O3(i)*sp_ratio_Al2O3(bc_sp_loc(i)))+((1-d_Al2O3(i))*
    mab_ratio_Al2O3(bc_mab_loc(i)));
end
```

```
figure (3)
p1=semilogx(bc_e,D_BeO_D_H2O,'r')
hold
p2=semilogx(bc_e,D_BC400_D_H2O,'b')
p3=semilogx(bc_e,D_LiF_D_H2O,'k')
p4=semilogx(bc_e,D_Al2O3_D_H2O,'m')
legend([p1;p2;p3;p4],'BeO','BC400','LiF','Al2O3')
title ('Burlin Cavity theory calculated Dose_{det} / Dose_{water}')
xlabel ('x-ray energy (MeV)')
ylabel ('D_{det}/D_{water}')


% %
% %%  Normalised ratio to 1.25 MeV energy
% norm_BeO=D_BeO_D_H2O/D_BeO_D_H2O(18);
% norm_BC400=D_BC400_D_H2O/D_BC400_D_H2O(18);
% norm_Al2O3=D_Al2O3_D_H2O/D_Al2O3_D_H2O(18);
% norm_LiF=D_LiF_D_H2O/D_LiF_D_H2O(18);

%
%%  Normalised ratio to 0.06 MeV energy
norm_BeO=D_BeO_D_H2O/D_BeO_D_H2O(7);
norm_BC400=D_BC400_D_H2O/D_BC400_D_H2O(7);
norm_Al2O3=D_Al2O3_D_H2O/D_Al2O3_D_H2O(7);
norm_LiF=D_LiF_D_H2O/D_LiF_D_H2O(7);

figure (4)
p1=semilogx(bc_e,norm_BeO,'r')
hold
p2=semilogx(bc_e,norm_BC400,'b')
p3=semilogx(bc_e,norm_LiF,'k')
p4=semilogx(bc_e,norm_Al2O3,'m')
legend([p1;p2;p3;p4],'BeO','BC400','LiF','Al2O3')
title ('Burlin Cavity theory calculated R')
xlabel ('x-ray energy (MeV)')
ylabel ('R=(Dose_{det}/Dose_{water})/(Dose_{det}/Dose_{water})_{10MeV}')
```

Bibliography

Albrecht, H. O. and Mandeville, C. E. (1956). Storage of energy in beryllium oxide. *Phys. Rev.*, 101:1250–1252.

Aldelaijan, S., Mohammed, H., Tomic, N., Liang, L.-H., DeBlois, F., Sarfehnia, A., Abdel-Rahman, W., Seuntjens, J., and Devic, S. (2011). Radiochromic film dosimetry of hdr 192ir source radiation fields. *Medical Physics*, 38(11):6074–6083.

Alecu, R. and Alecu, M. (1999). In-vivo rectal dose measurements with diodes to avoid misadministrations during intracavitary high dose rate brachytherapy for carcinoma of the cervix. *Medical Physics*, 26(5):768–770.

Anagnostopoulos, G., Baltas, D., Geretschlaeger, A., Martin, T., Papagiannis, P., Tselis, N., and Zamboglou, N. (2003). In vivo thermoluminescence dosimetry dose verification of transperineal 192ir high-dose-rate brachytherapy using ct-based planning for the treatment of prostate cancer. *International Journal of Radiation Oncology*Biology*Physics*, 57(4):1183 – 1191.

Andersen, C., Damkjær, S., Kertzscher, G., Greilich, S., and Aznar, M. (2011). Fiber-coupled radioluminescence dosimetry with saturated al2o3:c crystals: Characterization in 6 and 18 mv photon beams. *Radiation Measurements*, 46(10):1090 – 1098.

Andersen, C. E., Aznar, M. C., Bøtter-Jensen, L., Back, S. A., Mattsson, S., and Medin, J. (2003). Development of optical fibre luminescence techniques for real time in vivo dosimetry in radiotherapy. *Int. Symp. on Standards and Code of Practice in Medical Radiation Dosimetry (Vienna: IAEA)*.

Andersen, C. E., Marckmann, C. J., Aznar, M. C., Bøtter-Jensen, L., Kjær-Kristoffersen, F., and Medin, J. (September 2006). An algorithm for real-time dosimetry in intensity-modulated radiation therapy using the radioluminescence signal from Al2O3:C. *Radiation Protection Dosimetry*, 120(1-4):7–13.

Andersen, C. E., ren Kynde Nielsen, S., Greilich, S., Helt-Hansen, J., Lindegaard, J. C., and Tanderup, K. (2009a). Characterization of a fiber-coupled al[sub 2]o[sub 3]:c luminescence dosimetry system for online in vivo dose verification during [sup 192]ir brachytherapy. *Medical Physics*, 36(3):708–718.

Andersen, C. E., ren Kynde Nielsen, S., Lindegaard, J. C., and Tanderup, K. (2009b). Time-resolved in vivo luminescence dosimetry for online error detection in pulsed dose-rate brachytherapy. *Medical Physics*, 36(11):5033–5043.

Anton, M., Hackel, T., Zink, K., von Voigts-Rhetz, P., and Selbach, H.-J. (2015). Response of the alanine/esr dosimeter to radiation from an ir-192 hdr brachytherapy source. *Physics in Medicine and Biology*, 60(1):175.

Anton, M., Wagner, D., Selbach, H.-J., Hackel, T., Hermann, R. M., Hess, C. F., and Vorwerk, H. (2009). In vivo dosimetry in the urethra using alanine/esr during 192 ir hdr brachytherapy of prostate cancer—a phantom study. *Physics in Medicine and Biology*, 54(9):2915.

Archambault, L., Beddar, A. S., Gingras, L., Lacroix, F., Roy, R., and Beaulieu, L. (2007). Water-equivalent dosimeter array for small-field external beam radiotherapy. *Medical Physics*, 34(5):1583–1592.

Archambault, L., Beddar, A. S., Gingras, L., Roy, R., and Beaulieu, L. (2006). Measurement accuracy and cerenkov removal for high performance, high spatial resolution scintillation dosimetry. *Medical Physics*, 33(1):128–135.

Archambault, L., Therriault-Proulx, F., Beddar, S., and Beaulieu, L. (2012). A mathematical formalism for hyperspectral, multipoint plastic scintillation detectors. *Physics in Medicine and Biology*, 57(21):7133.

Australian Institute of Health and Welfare (2014). *Australian Cancer Incidence and Mortality (ACIM) books: All cancers combined*. Canberra: AIHW.

Aznar, M. C., Andersen, C. E., Bøtter-Jensen, L., Bäck, S. . J., Mattsson, S., Kjær-Kristoffersen, F., and Medin, J. (2004). Real-time optical-fibre luminescence dosimetry for radiotherapy: physical characteristics and applications in photon beams. *Physics in Medicine and Biology*, 49(9):1655.

Aznar, M. C., Hemdal, B., Medin, J., Marckmann, C. J., Andersen, C. E., Botter-Jensen, L., Andersson, I., and Mattsson, S. (2005). In vivo absorbed dose measurements in mammography using a new real-time luminescence technique. *Br J Radiol*, 78(928):328–334.

Baskar, R., Lee, K. A., Yeo, R., and Yeoh, K.-W. (2012). Cancer and radiation therapy: Current advances and future directions. *International Journal of Medical Sciences*, 9(3):193–199.

Beddar, A., Kinsella, K., Ikhlef, A., and Sibata, C. (2001). A miniature ldquo;scintillator-fiberoptic-pmt rdquo; detector system for the dosimetry of small fields in stereotactic radiosurgery. *Nuclear Science, IEEE Transactions on*, 48(3):924–928.

Beddar, A. S., Law, S., Suchowerska, N., and Mackie, T. R. (2003). Plastic scintillation dosimetry: optimization of light collection efficiency. *Physics in Medicine and Biology*, 48(9):1141.

Beddar, A. S., Mackie, T. R., and Attix, F. H. (1992a). Water-equivalent plastic scintillation detectors for high-energy beam dosimetry: I. physical characteristics and theoretical considerations. *Physics in Medicine and Biology*, 37(10):1883.

Beddar, A. S., Mackie, T. R., and Attix, F. H. (1992b). Water-equivalent plastic scintillation detectors for high-energy beam dosimetry: Ii. properties and measurements. *Physics in Medicine and Biology*, 37(10):1901.

Benoit, D., Garcia, P., Matias-Vaille, S., Ravotti, F., Vaille, J., Glaser, M., Brichard, B., Fernandez, A., Chatry, C., and Dusseau, L. (2008a). Real-time fibered optically stimulated luminescence dosimeter based on srs:ce,sm phosphor. *Nuclear Science, IEEE Transactions on*, 55(4):2154–2160.

Benoit, D., Vaille, J.-R., Lautissier, J., Matias-Vaille, S., Isturiz, J., Garcia, P., Brichard, B., and Dusseau, L. (2008b). Feasibility of fibered monitoring system for pulsed dose-rate facilities based on radioluminescence of srs:ce,sm phosphor. *Nuclear Science, IEEE Transactions on*, 55(6):3421–3427.

Birks, J., editor (1964). *The Theory and Practice of Scintillation Counting*. International Series of Monographs in Electronics and Instrumentation. Pergamon.

Brezovich, I. A., Duan, J., Pareek, P. N., Fiveash, J., and Ezekiel, M. (2000). In vivo urethral dose measurements: A method to verify high dose rate prostate treatments. *Medical Physics*, 27(10):2297–2301.

Bøtter-Jensen, L., McKeever, S., and Wintle, A., editors (2003). *Optically Stimulated Luminescence Dosimetry*. Elsevier, Amsterdam.

Bulur, E. (2014). More on the tr-osl signal from beo ceramics. *Radiation Measurements*, 66:12 – 20.

Bulur, E., Bøtter-Jensen, L., and Murray, A. (2001a). Frequency modulated pulsed stimulation in optically stimulated luminescence. *Nuclear Instruments and Methods in Physics Research Section B: Beam Interactions with Materials and Atoms*, 179(1):151 – 159.

Bulur, E., Bøtter-Jensen, L., and Murray, A. (2001b). Lm-osl signals from some insulators: an analysis of the dependency of the detrapping probability on stimulation light intensity. *Radiation Measurements*, 33(5):715 – 719. Proceedings of the International Symposium on Luminescent Detecto rs and Transformers of Ionizing Radiation.

Bulur, E. and Göksu, H. (1998). {OSL} from beo ceramics: new observations from an old material. *Radiation Measurements*, 29(6):639 – 650.

Bulur, E. and Yeltik, A. (2010). Optically stimulated luminescence from beo ceramics: An lm-osl study. *Radiation Measurements*, 45(1):29 – 34.

Busuoli, G., Lembo, L., Nanni, R., and Sermenghi, I. (1983). Use of beo in routine personnel dosimetry. *Radiation Protection Dosimetry*, 6(1-4):317–320.

Busuoli, G., Sermenghi, I., Rimondi, O., and Vicini, G. (1977). {TL} personnel dosimeter with beo. *Nuclear Instruments and Methods*, 140(2):385 – 388.

C. Polf, J., W. S. McKeever, S., S. Akselrod, M., and Holmstrom, S. (2002). A real-time, fibre optic dosimetry system using al2o3 fibres. *Radiation Protection Dosimetry*, 100(1-4):301–304.

Caretto, N., Chiodini, N., Moretti, F., Origgi, D., Tosi, G., and Vedda, A. (2010). Feasibility of dose assessment in radiological diagnostic equipments using ce-doped radioluminescent optical fibers. *Nuclear Instruments and Methods in Physics Research Section A: Accelerators, Spectrometers, Detectors and Associated Equipment*, 612(2):407 – 411.

Carrara, M., Cavatorta, C., Borroni, M., Tenconi, C., Cerrotta, A., Fallai, C., Gambarini, G., Vedda, A., and Pignoli, E. (2013). Characterization of a ce3+ doped sio2 optical dosimeter for dose measurements in {HDR} brachytherapy. *Radiation Measurements*, 56:312 – 315. Proceedings of the 8th International Conference on Luminescent Detectors and Transformers of Ionizing Radiation (LUMDETR 2012).

Carrara, M., Tenconi, C., Guilizzoni, R., Borroni, M., Cavatorta, C., Cerrotta, A., Fallai, C., Gambarini, G., Vedda, A., and Pignoli, E. (2014a). Stem effect of a ce3+ doped sio2 optical dosimeter irradiated with a 192ir {HDR} brachytherapy source. *Radiation Physics and Chemistry*, 104(0):175 – 179. 1st International Conference on Dosimetry and its Applications.

Carrara, M., Tenconi, C., Rossi, G., Guilizzoni, R., Borroni, M., Cerrotta, A., Fallai, C., Gambarini, G., Vedda, A., and Pignoli, E. (2014b). Temperature dependence of a ce3+ doped sio2 radioluminescent dosimeter for in vivo dose measurements in {HDR} brachytherapy. *Radiation Measurements*, 71(0):324 – 328. Proceedings of the 17th Solid State Dosimetry Conference (SSD17).

Cartwright, L. E., Suchowerska, N., Yin, Y., Lambert, J., Haque, M., and McKenzie, D. R. (2010). Dose mapping of the rectal wall during brachytherapy with an array of scintillation dosimeters. *Medical Physics*, 37(5):2247–2255.

Chiu-Tsao, S.-T., de la Zerda, A., Lin, J., and Kim, J. H. (1994). High-sensitivity gafchromic film dosimetry for 125i seed. *Medical Physics*, 21(5):651–657.

Chiu-Tsao, S.-T., Medich, D., and Munro, J. (2008). The use of new gafchromic® ebt film for i125 seed dosimetry in solid water® phantom. *Medical Physics*, 35(8):3787–3799.

Clift, M. A., Johnston, P. N., and Webb, D. V. (2002). A temporal method of avoiding the cerenkov radiation generated in organic scintillator dosimeters by pulsed mega-voltage electron and photon beams. *Physics in Medicine and Biology*, 47(8):1421.

Clift, M. A., Sutton, R. A., and Webb, D. V. (2000). Dealing with cerenkov radiation generated in organic scintillator dosimeters by bremsstrahlung beams. *Physics in Medicine and Biology*, 45(5):1165.

Committee on Beryllium Alloy Exposures, Committee on Toxicology, N. R. C. (2008). *Managing Health Effects of Beryllium Exposure*. The National Academies Press, Washington, DC.

Cygler, J. E., Saoudi, A., Perry, G., Morash, C., and E, C. (2006). Feasibility study of using {MOSFET} detectors for in vivo dosimetry during permanent low-dose-rate prostate implants. *Radiotherapy and Oncology*, 80(3):296 – 301.

Damkjaer, S., Andersen, C., and Aznar, M. (2008). Improved real-time dosimetry using the radioluminescence signal from al2o3:c. *Radiation Measurements*, 43(2-6):893 – 897. Proceedings of the 15th Solid State Dosimetry (SSD15).

Das, R., Toye, W., Kron, T., Williams, S., and Duchesne, G. (2007). Thermoluminescence dosimetry for in-vivo verification of high dose rate brachytherapy for prostate cancer. *Australasian Physics & Engineering Sciences in Medicine*, 30(3):178–184.

de Boer, S. F., Beddar, A. S., and Rawlinson, J. A. (1993). Optical filtering and spectral measurements of radiation-induced light in plastic scintillation dosimetry. *Physics in Medicine and Biology*, 38(7):945.

Edmund, J. M., Andersen, C. E., Marckmann, C. J., Aznar, M. C., Akselrod, M. S., and Bøtter-Jensen, L. (September 2006). CW-OSL measurement protocols using optical fibre Al2O3:C dosemeters. *Radiation Protection Dosimetry*, 119(1-4):368–374.

Elsey, J., McKenzie, D. R., Lambert, J., Suchowerska, N., Law, S. L., and Fleming, S. C. (2007). Optimal coupling of light from a cylindrical scintillator into an optical fiber. *Appl. Opt.*, 46(3):397–404.

Erfurt, G. and R. Krbetschek, M. (2002). A radioluminescence study of spectral and dose characteristics of common luminophors. *Radiation Protection Dosimetry*, 100(1-4):403–406.

Espinoza, A., Beeksma, B., Petasecca, M., Fuduli, I., Porumb, C., Cutajar, D., Corde, S., Jackson, M., Lerch, M. L. F., and Rosenfeld, A. B. (2013). The feasibility study and characterization of a two-dimensional diode array in "magic phantom" for high dose rate brachytherapy quality assurance. *Medical Physics*, 40(11).

Espinoza, A., Petasecca, M., Fuduli, I., Howie, A., Bucci, J., Corde, S., Jackson, M., F. Lerch, M. L., and Rosenfeld, A. B. (2015). The evaluation of a 2d diode array in "magic phantom" for use in high dose rate brachytherapy pretreatment quality assurance. *Medical Physics*, 42(2):663–673.

Fontbonne, J., Iltis, G., Ban, G., Battala, A., Vernhes, J., Tillier, J., Bellaize, N., Le Brun, C., Tamain, B., Mercier, K., and Motin, J. (2002). Scintillating fiber dosimeter for radiation therapy accelerator. *Nuclear Science, IEEE Transactions on*, 49(5):2223 – 2227.

Gambarini, G., Borroni, M., Grisotto, S., Maucione, A., Cerrotta, A., Fallai, C., and Carrara, M. (2012). Solid state {TL} detectors for in vivo dosimetry in brachytherapy. *Applied Radiation and Isotopes*, 71, Supplement(0):48 – 51. {XII} International Symposium on Solid State Dosimetry.

Gambarini, G., Carrara, M., Negri, A., Invernizzi, M., Tenconi, C., Scotti, A., Pirola, L., Borroni, M., Tomatis, S., and Fallai, C. (2010). Dosimetry in hdr brachytherapy with fricke-gel layers and fricke-gel catheters. *Journal of Physics: Conference Series*, 250(1):012089.

Gambarini, G., Carrara, M., Tenconi, C., Mantaut, N., Borroni, M., Cutajar, D., Petasecca, M., Fuduli, I., Lerch, M., Pignoli, E., and Rosenfeld, A. (2014). Online in vivo dosimetry in high dose rate prostate brchytherapy with {MOSkin} detectors: In phantom feasibility study. *Applied Radiation and Isotopes*, 83, Part C(0):222 – 226. Proceedings of the {XIII} International Symposium. {XXIII} National Congress on Solid State Dosimetry. Ocoyoacac, Mexico, October 15 – 19, 2012.

Gaza, R. and McKeever, S. W. S. (2006). A real-time, high-resolution optical fibre dosemeter based on optically stimulated luminescence (osl) of kbr:eu, for potential use during the radiotherapy of cancer. *Radiation Protection Dosimetry*, 120(1-4):14–19.

Hardcastle, N., Cutajar, D. L., Metcalfe, P. E., Lerch, M. L. F., Perevertaylo, V. L., Tomé, W. A., and Rosenfeld, A. B. (2010). In vivo real-time rectal wall dosimetry for prostate radiotherapy. *Physics in Medicine and Biology*, 55(13):3859.

Hsu, S.-M., Yeh, C.-Y., Yeh, T.-C., Hong, J.-H., Tipton, A. Y. H., Chen, W.-L., Sun, S.-S., and Huang, D. Y. C. (2008). Clinical application of radiophotoluminescent glass dosimeter for dose verification of prostate hdr procedure. *Medical Physics*, 35(12):5558–5564.

Ismail, A., Giraud, J.-Y., Lu, G., Sihanath, R., Pittet, P., Galvan, J., and Balosso, J. (2009). Radiotherapy quality insurance by individualized in vivo dosimetry: State of the art. *Cancer/Radiothérapie*, 13(3):182 – 189.

Ismail, A., Pittet, P., Lu, G., Galvan, J., Giraud, J., and Balosso, J. (2011). In vivo dosimetric system based on gallium nitride radioluminescence. *Radiation Measurements*, 46(12):1960 – 1962. Proceedings of the 16th Solid State Dosimetry Conference , September 19-24 , Sydney , Australia.

Jahn, A., Sommer, M., and Henniger, J. (2010). 2d-osl-dosimetry with beryllium oxide. *Radiation Measurements*, 45(3–6):674 – 676. Proceedings of the 7th European Conference on Luminescent Detectors and Transformers of Ionizing Radiation (LUMDETR 2009).

Jahn, A., Sommer, M., and Henniger, J. (2014). {OSL} efficiency for beo {OSL} dosimeters. *Radiation Measurements*, 71:104 – 107. Proceedings of the 17th Solid State Dosimetry Conference (SSD17).

Jahn, A., Sommer, M., Liebmann, M., and Henniger, J. (2011). Progress in 2d-osl-dosimetry with beryllium oxide. *Radiation Measurements*, 46(12):1908 – 1911. Proceedings of the 16th Solid State Dosimetry Conference , September 19-24 , Sydney , Australia.

Jahn, A., Sommer, M., Ullrich, W., Wickert, M., and Henniger, J. (2013). The beomax system – dosimetry using {OSL} of beo for several applications. *Radiation Measurements*, 56:324 – 327. Proceedings of the 8th International Conference on Luminescent Detectors and Transformers of Ionizing Radiation (LUMDETR 2012).

Kapp, K. S., Stuecklschweiger, G. F., Kapp, D. S., and Hackl, A. G. (1992). Dosimetry of intracavitary placements for uterine and cervical carcinoma: results of orthogonal film, tld, and ct-assisted techniques. *Radiotherapy and Oncology*, 24(3):137 – 146.

Kertzscher, G., Andersen, C. E., Siebert, F.-A., Nielsen, S. K., Lindegaard, J. C., and Tanderup, K. (2011). Identifying afterloading {PDR} and {HDR} brachytherapy errors using real-time fiber-coupled al2o3:c dosimetry and a novel statistical error decision criterion. *Radiotherapy and Oncology*, 100(3):456 – 462. Special Issue on Medical Physics and Brachytherapy.

Kertzscher, G., Rosenfeld, A., Beddar, S., Tanderup, K., and Cygler, J. E. (2014). In vivo dosimetry: trends and prospects for brachytherapy. *The British Journal of Radiology*, 87(1041):20140206.

Kirisits, C., Rivard, M. J., Baltas, D., Ballester, F., Brabandere, M. D., van der Laarse, R., Niatsetski, Y., Papagiannis, P., Hellebust, T. P., Perez-Calatayud, J., Tanderup, K., Venselaar, J. L., and Siebert, F.-A. (2014). Review of clinical brachytherapy uncertainties: Analysis guidelines of gec-estro and the aapm. *Radiotherapy and Oncology*.

Klawikowski, S. J., Zeringue, C., Wootton, L. S., Ibbott, G. S., and Beddar, S. (2014). Preliminary evaluation of the dosimetric accuracy of the in vivo plastic scintillation detector oartrac system for prostate cancer treatments. *Physics in Medicine and Biology*, 59(9):N27.

Klein, D. and McKeever, S. (2008). Optically stimulated luminescence from kbr:eu as a near-real-time dosimetry system. *Radiation Measurements*, 43(2–6):883 – 887. Proceedings of the 15th Solid State Dosimetry (SSD15).

Klein, D., Peakheart, D. W., and McKeever, S. W. (2010a). Performance of a near-real-time kbr:eu dosimetry system under computed tomography x-rays. *Radiation Measurements*, 45(3–6):663 – 667. Proceedings of the 7th European Conference on Luminescent Detectors and Transformers of Ionizing Radiation (LUMDETR 2009).

Klein, D. M., Tailor, R. C., Archambault, L., Wang, L., Therriault-Proulx, F., and Beddar, A. S. (2010b). Measuring output factors of small fields formed by collimator jaws and multileaf collimator using plastic scintillation detectors. *Medical Physics*, 37(10):5541–5549.

Knoll, G. F. (2000). *Radiation detection and measurement / Glenn F. Knoll*. New York : J. Wiley, 3rd ed edition.

Lambert, J., McKenzie, D. R., Law, S., Elsey, J., and Suchowerska, N. (2006). A plastic scintillation dosimeter for high dose rate brachytherapy. *Physics in Medicine and Biology*, 51(21):5505.

Lambert, J., Nakano, T., Law, S., Elsey, J., McKenzie, D. R., and Suchowerska, N. (2007). In vivo dosimeters for hdr brachytherapy: A comparison of a diamond detector, mosfet, tld, and scintillation detector. *Medical Physics*, 34(5):1759–1765.

Lambert, J., Yin, Y., McKenzie, D. R., Law, S., and Suchowerska, N. (2008). Cerenkov-free scintillation dosimetry in external beam radiotherapy with an air core light guide. *Physics in Medicine and Biology*, 53(11):3071.

Lambert, J., Yin, Y., McKenzie, D. R., Law, S. H., Ralston, A., and Suchowerska, N. (2010). A prototype scintillation dosimeter customized for small and dynamic megavoltage radiation fields. *Physics in Medicine and Biology*, 55(4):1115.

Leroy, C. and Rancoita, P. G. (2009). *Principles of radiation interaction in matter and detection / Claude Leroy, Pier-Giorgio Rancoita*. Singapore ; London : World Scientific, 2nd ed edition.

Liu, P. Z. Y., Suchowerska, N., Lambert, J., Abolfathi, P., and McKenzie, D. R. (2011). Plastic scintillation dosimetry: comparison of three solutions for the cerenkov challenge. *Physics in Medicine and Biology*, 56(18):5805.

Liu, P. Z. Y., Suchowerska, N., and McKenzie, D. R. (2013). Twisted pair of optic fibers for background removal in radiation fields. *Appl. Opt.*, 52(22):5500–5507.

Létourneau, D., Pouliot, J., and Roy, R. (1999). Miniature scintillating detector for small field radiation therapy. *Medical Physics*, 26(12):2555–2561.

Magne, S., Auger, L., Bordy, J. M., de Carlan, L., Isambert, A., Bridier, A., Ferdinand, P., and Barthe, J. (2008). Multichannel dosemeter and Al2O3:C optically stimulated luminescence fibre sensors for use in radiation therapy: evaluation with electron beams. *Radiation Protection Dosimetry*, 131(1):93–99.

Marcazzó, J., Henniger, J., Khaidukov, N. M., Makhov, V. N., Caselli, E., and Santiago, M. (2007). Efficient crystal radiation detectors based on tb 3+ -doped fluorides for radioluminescence dosimetry. *Journal of Physics D: Applied Physics*, 40(17):5055.

Marckmann, C. J., Andersen, C. E., Aznar, M. C., and Bøtter-Jensen, L. (September 2006). Optical fibre dosemeter systems for clinical applications based on radioluminescence and optically stimulated luminescence from Al2O3:C. *Radiation Protection Dosimetry*, 120(1-4):28–32.

Mayles, P., Nahum, A., and Rosenwald, J. (2007). *Handbook of Radiotherapy Physics: Theory and Practice*. Taylor & Francis.

McKeever, S. (1988). *Thermoluminescence of Solids*. Cambridge Solid State Science Series. Cambridge University Press.

Molina, P., Sommer, M., Kattner, F., and Henniger, J. (2013). Response characterization of an y2o3:eu-based radioluminescence probe under 60co irradiation. *Radiation Measurements*, 56:338 – 341. Proceedings of the 8th International Conference on Luminescent Detectors and Transformers of Ionizing Radiation (LUMDETR 2012).

Nakano, T., Suchowerska, N., Bilek, M. M., McKenzie, D. R., Ng, N., and Kron, T. (2003). High dose-rate brachytherapy source localization: positional resolution using a diamond detector. *Physics in Medicine and Biology*, 48(14):2133.

Nath, R., Anderson, L. L., Luxton, G., Weaver, K. A., Williamson, J. F., and Meigooni, A. S. (1995). Dosimetry of interstitial brachytherapy sources: Recommendations of the aapm radiation therapy committee task group no. 43. *Medical Physics*, 22(2):209–234.

Nose, T., Koizumi, M., Yoshida, K., Nishiyama, K., Sasaki, J., Ohnishi, T., Kozuka, T., Gomi, K., Oguchi, M., Sumida, I., Takahashi, Y., Ito, A., and Yamashita, T. (2008). In vivo dosimetry of high-dose-rate interstitial brachytherapy in the pelvic region: Use of a radiophotoluminescence glass dosimeter for measurement of 1004 points in 66 patients with pelvic malignancy. *International Journal of Radiation Oncology*Biology*Physics*, 70(2):626 – 633.

Nose, T., Koizumi, M., Yoshida, K., Nishiyama, K., Sasaki, J., Ohnishi, T., and Peiffert, D. (2005). In vivo dosimetry of high-dose-rate brachytherapy: Study on 61 head-and-neck cancer patients using radiophotoluminescence glass dosimeter. *International Journal of Radiation Oncology*Biology*Physics*, 61(3):945 – 953.

Nowotny, R. (2007). Radioluminescence of some optical fibres. *Physics in Medicine and Biology*, 52(4):N67.

Nowotny, R. and Taubeck, A. (2009). A method for the production of composite scintillators for dosimetry in diagnostic radiology. *Physics in Medicine and Biology*, 54(6):1457.

Pai, S., Reinstein, L. E., Gluckman, G., Xu, Z., and Weiss, T. (1998). The use of improved radiochromic film for in vivo quality assurance of high dose rate brachytherapy. *Medical Physics*, 25(7):1217–1221.

Palmer, A. L., Di Pietro, P., Alobaidli, S., Issa, F., Doran, S., Bradley, D., and Nisbet, A. (2013a). Comparison of methods for the measurement of radiation dose distributions in high dose rate (hdr) brachytherapy: Ge-doped optical fiber, ebt3 gafchromic film, and presage® radiochromic plastic. *Medical Physics*, 40(6).

Palmer, A. L., Nisbet, A., and Bradley, D. (2013b). Verification of high dose rate brachytherapy dose distributions with ebt3 gafchromic film quality control techniques. *Physics in Medicine and Biology*, 58(3):497.

Piermattei, A., Azario, L., Monaco, G., Soriani, A., and Arcovito, G. (1995). p-type silicon detector for brachytherapy dosimetry. *Medical Physics*, 22(6):835–839.

Pittet, P., Jalade, P., Balosso, J., Gindraux, L., Guiral, P., Wang, R., Chaikh, A., Gaudu, A., Ribouton, J., Rousseau, J., Galvan, J.-M., Rivoire, A., Giraud, J.-Y., and Lu, G.-N. (2015). Dosimetry systems based on gallium nitride probe for radiotherapy, brachytherapy and interventional radiology. {*IRBM*}, 36(2):92 – 100. {ANR} {TECSAN} 2015.

Podgoršak, E. and Agency, I. A. E. (2005). *Radiation Oncology Physics: A Handbook for Teachers and Students*. International Atomic Energy Agency.

Polf, J. C., Yukihara, E. G., Akselrod, M. S., and McKeever, S. W. S. (2004). Real-time luminescence from al2o3 fiber dosimeters. *Radiation Measurements*, 38(2):227 – 240.

Poon, E., Reniers, B., Devic, S., Vuong, T., and Verhaegen, F. (2006). Dosimetric characterization of a novel intracavitary mold applicator for ir192 high dose rate endorectal brachytherapy treatment. *Medical Physics*, 33(12):4515–4526.

Pradhan, A. S., Lee, J. I., and Kim, J. L. (2008). Recent developments of optically stimulated luminescence materials and techniques for radiation dosimetry and clinical applications. *Journal of Medical Physics / Association of Medical Physicists of India*, 33.

Qi, Z.-Y., Deng, X.-W., Cao, X.-p., Huang, S.-M., Lerch, M., and Rosenfeld, A. (2012). A real-time in vivo dosimetric verification method for high-dose rate intracavitary brachytherapy of nasopharyngeal carcinoma. *Medical Physics*, 39(11):6757–6763.

Raffi, J. A., Davis, S. D., Hammer, C. G., Micka, J. A., Kunugi, K. A., Musgrove, J. E., Winston, J. W., Ricci-Ott, T. J., and DeWerd, L. A. (2010). Determination of exit skin dose for i192r intracavitary accelerated partial breast irradiation with thermoluminescent dosimeters. *Medical Physics*, 37(6):2693–2702.

Reniers, B., Landry, G., Eichner, R., Hallil, A., and Verhaegen, F. (2012). In vivo dosimetry for gynaecological brachytherapy using a novel position sensitive radiation detector: Feasibility study. *Medical Physics*, 39(4):1925–1935.

Rhyner, C. R. and Miller, W. G. (1970). Radiation dosimetry by optically-stimulated luminescence of beo. *Health Physics*, 18(6).

Rivard, M. J., Coursey, B. M., DeWerd, L. A., Hanson, W. F., Saiful Huq, M., Ibbott, G. S., Mitch, M. G., Nath, R., and Williamson, J. F. (2004). Update of aapm task group no. 43 report: A revised aapm protocol for brachytherapy dose calculations. *Medical Physics*, 31(3):633–674.

Rustgi, S. N. (1998). Application of a diamond detector to brachytherapy dosimetry. *Physics in Medicine and Biology*, 43(8):2085.

Safavi-Naeini, M., Han, Z., Cutajar, D., Guatelli, S., Petasecca, M., Lerch, M. L. F., Franklin, D. R., Jakubek, J., Pospisil, S., Bucci, J., Zaider, M., and Rosenfeld, A. B. (2013). Brachyview, a novel inbody imaging system for hdr prostate brachytherapy: Design and monte carlo feasibility study. *Medical Physics*, 40(7):–.

Scarpa, G. (1970). The dosimetric use of beryllium oxide as a thermoluminescent material: A preliminary study. *Physics in Medicine and Biology*, 15(4):667.

Schultka, K., Ciesielski, B., Serkies, K., Sawicki, T., Tarnawska, Z., and Jassem, J. (2006). Epr/alanine dosimetry in ldr brachytherapy—a feasibility study. *Radiation Protection Dosimetry*, 120(1-4):171–175.

Seymour, E. L., Downes, S. J., Fogarty, G. B., Izard, M. A., and Metcalfe, P. (2011). In vivo real-time dosimetric verification in high dose rate prostate brachytherapy. *Medical Physics*, 38(8):4785–4794.

Smith, R. L., Taylor, M. L., McDermott, L. N., Haworth, A., Millar, J. L., and Franich, R. D. (2013). Source position verification and dosimetry in hdr brachytherapy using an epid. *Medical Physics*, 40(11):–.

Sommer, M., Freudenberg, R., and Henniger, J. (2007). New aspects of a beo-based optically stimulated luminescence dosimeter. *Radiation Measurements*, 42(4–5):617 – 620. Proceedings of the 6th European Conference on Luminescent Detectors and Transformers of Ionizing Radiation (LUMDETR 2006).

Sommer, M. and Henniger, J. (2006). Investigation of a beo-based optically stimulated luminescence dosemeter. *Radiation Protection Dosimetry*, 119(1-4):394–397.

Sommer, M., Jahn, A., and Henniger, J. (2008). Beryllium oxide as optically stimulated luminescence dosimeter. *Radiation Measurements*, 43(2–6):353 – 356. Proceedings of the 15th Solid State Dosimetry (SSD15).

Suchowerska, N., Jackson, M., Lambert, J., Yin, Y. B., Hruby, G., and McKenzie, D. R. (2011). Clinical trials of a urethral dose measurement system in brachytherapy using scintillation detectors. *International Journal of Radiation Oncology*Biology*Physics*, 79(2):609 – 615.

Tanderup, K., Beddar, S., Andersen, C. E., Kertzscher, G., and Cygler, J. E. (2013). In vivo dosimetry in brachytherapy. *Medical Physics*, 40(7):–.

Tenconi, C., Carrara, M., Borroni, M., Cerrotta, A., Cutajar, D., Petasecca, M., Lerch, M., Bucci, J., Gambarini, G., Pignoli, E., and Rosenfeld, A. (2014). Trus-probe integrated {MOSkin} detectors for rectal wall in vivo dosimetry in {HDR} brachytherapy: In phantom feasibility study. *Radiation Measurements*, 71(0):379 – 383. Proceedings of the 17th Solid State Dosimetry Conference (SSD17).

Therriault-Proulx, F., Archambault, L., Beaulieu, L., and Beddar, S. (2012). Development of a novel multi-point plastic scintillation detector with a single optical transmission line for radiation dose measurement. *Physics in Medicine and Biology*, 57(21):7147.

Therriault-Proulx, F., Beddar, S., and Beaulieu, L. (2013). On the use of a single-fiber multipoint plastic scintillation detector for 192ir high-dose-rate brachytherapy. *Medical Physics*, 40(6).

Tochilin, E., Goldstein, N., and Miller, W. (1969). Beryllium oxide as a thermoluminescent dosimeter. *Health Physics*, 16(1).

Toye, W., Das, R., Kron, T., Franich, R., Johnston, P., and Duchesne, G. (2009). An in vivo investigative protocol for {HDR} prostate brachytherapy using urethral and rectal thermoluminescence dosimetry. *Radiotherapy and Oncology*, 91(2):243 – 248.

Vidovic, A. K., Juang, T., Meltsner, S., Adamovics, J., Chino, J., Steffey, B., Craciunescu, O., and Oldham, M. (2014). An investigation of a presage in vivo dosimeter for brachytherapy. *Physics in Medicine and Biology*, 59(14):3893.

Waldeland, E., Hole, E. O., Sagstuen, E., and Malinen, E. (2010). The energy dependence of lithium formate and alanine epr dosimeters for medium energy x rays. *Medical Physics*, 37(7):3569–3575.

Waldhäusl, C., Wambersie, A., Pötter, R., and Georg, D. (2005). In-vivo dosimetry for gynaecological brachytherapy: Physical and clinical considerations. *Radiotherapy and Oncology*, 77(3):310 – 317.

Walsh, K. and Vidal, E. (2009). *Beryllium Chemistry and Processing*. ASM International.

Wang, R., Ribouton, J., Pittet, P., Guiral, P., Jalade, P., and Lu, G. (2014). Implementation of gan based real-time source position monitoring in {HDR} brachytherapy. *Radiation Measurements*, 71(0):293 – 296. Proceedings of the 17th Solid State Dosimetry Conference (SSD17).

Williamson, J. F., Dempsey, J. F., Kirov, A. S., Monroe, J. I., Binns, W. R., and Hedtjärn, H. (1999). Plastic scintillator response to low-energy photons. *Physics in Medicine and Biology*, 44(4):857.

Wootton, L., Kudchadker, R., Lee, A., and Beddar, S. (2014). Real-time in vivo rectal wall dosimetry using plastic scintillation detectors for patients with prostate cancer. *Physics in Medicine and Biology*, 59(3):647.

Yukihara, E. G. (2011). Luminescence properties of beo optically stimulated luminescence (osl) detectors. *Radiation Measurements*, 46(6–7):580 – 587.

Yukihara, E. G., McKeever, S. W., and Akselrod, M. S. (2014). State of art: Optically stimulated luminescence dosimetry – frontiers of future research. *Radiation Measurements*, 71(0):15 – 24. Proceedings of the 17th Solid State Dosimetry Conference (SSD17).

Yukihara, E. G. and McKeever, S. W. S. (2011). *Optically Stimulated Luminescence*. John Wiley and Sons, Ltd.

Zaman, Z., Ung, N., Malik, R., Ho, G., Phua, V., Jamalludin, Z., Baharuldin, M., and Ng, K. (2014). Comparison of planned and measured rectal dose in-vivo during high dose rate cobalt-60 brachytherapy of cervical cancer. *Physica Medica*, 30(8):980 – 984.